British Geological Survey
NATURAL ENVIRONMENT RESEARCH COUNCIL

A gravity interpretation of the Central North Sea

Energy and Marine Geoscience Programme
Commissioned Report CR/15/119

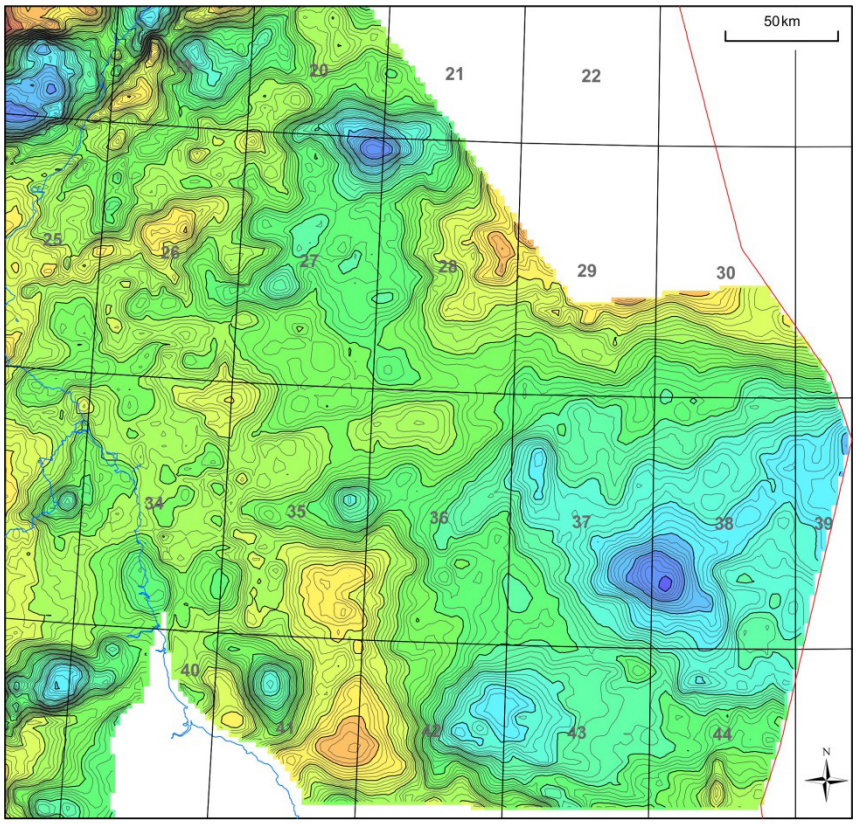

BRITISH GEOLOGICAL SURVEY

ENERGY AND MARINE GEOSCIENCE PROGRAMME

COMMISSIONED REPORT CR/15/119

A gravity interpretation of the Central North Sea

G S Kimbell and J P Williamson

Keywords

Gravity; interpretation; modelling; Central North Sea; Palaeozoic; magnetic.

Front cover

Contour map of the stripped gravity field. The gravity effect of the Zechstein and younger sequence and a regional trend have been subtracted from the observed gravity field.

Bibliographical reference

KIMBELL, G S, WILLIAMSON, J P. 2015. A gravity interpretation of the Central North Sea. *British Geological Survey Commissioned Report*, CR/15/119. 75pp.

Keyworth, Nottingham British Geological Survey 2015

BRITISH GEOLOGICAL SURVEY

The full range of our publications is available from BGS shops at Nottingham, Edinburgh, London and Cardiff (Welsh publications only) see contact details below or shop online at www.geologyshop.com

The London Information Office also maintains a reference collection of BGS publications, including maps, for consultation.

We publish an annual catalogue of our maps and other publications; this catalogue is available online or from any of the BGS shops.

The British Geological Survey carries out the geological survey of Great Britain and Northern Ireland (the latter as an agency service for the government of Northern Ireland), and of the surrounding continental shelf, as well as basic research projects. It also undertakes programmes of technical aid in geology in developing countries.

The British Geological Survey is a component body of the Natural Environment Research Council.

British Geological Survey offices

BGS Central Enquiries Desk

Tel 0115 936 3143 Fax 0115 936 3276

email enquiries@bgs.ac.uk

Environmental Science Centre, Keyworth, Nottingham NG12 5GG

Tel 0115 936 3241 Fax 0115 936 3488

email sales@bgs.ac.uk

Murchison House, West Mains Road, Edinburgh EH9 3LA

Tel 0131 667 1000 Fax 0131 668 2683

email scotsales@bgs.ac.uk

Natural History Museum, Cromwell Road, London SW7 5BD

Tel 020 7589 4090 Fax 020 7584 8270

Tel 020 7942 5344/45 email bgslondon@bgs.ac.uk

Columbus House, Greenmeadow Springs, Tongwynlais, Cardiff CF15 7NE

Tel 029 2052 1962 Fax 029 2052 1963

Maclean Building, Crowmarsh Gifford, Wallingford OX10 8BB

Tel 01491 838800 Fax 01491 692345

Geological Survey of Northern Ireland, Department of Enterprise, Trade & Investment, Dundonald House, Upper Newtownards Road, Ballymiscaw, Belfast, BT4 3SB

Tel 028 9038 8462 Fax 028 9038 8461

www.bgs.ac.uk/gsni/

Parent Body

Natural Environment Research Council, Polaris House, North Star Avenue, Swindon SN2 1EU

Tel 01793 411500 Fax 01793 411501

www.nerc.ac.uk

Website www.bgs.ac.uk

Shop online at www.geologyshop.com

Requests and enquiries should be addressed to Alison Monaghan, 21CXRM Palaeozoic Project Leader, als@bgs.ac.uk.

Foreword and acknowledgements

This report is a published product of the 21st Century Exploration Road Map (21CXRM) Palaeozoic project. This joint industry-Government-BGS project comprised a regional petroleum systems analysis of the offshore Devonian and Carboniferous in the North Sea and Irish Sea.

TOTAL E&P UK Ltd and Richard Milton-Worssell (Oil and Gas Authority) are thanked for technical review of this report and associated digital data.

Contents

FIGURES

Summary

A gravity investigation of the Central North Sea has been undertaken with the aim of supplementing a parallel seismic investigation (Arsenikos et al., 2015) by targeting those areas where the seismic information was sparse or of poor quality. By stripping the gravity effect of the Zechstein and younger sequence it was hoped that concealed Upper Palaeozoic basins could be identified in the residual gravity signatures and distinguished from anomalies associated with Late Caledonian granitic plutons.

Density logs from a set of wells across the region were compiled and used to calibrate a density model for the cover sequence. This model employed a combination of compaction trends and burial anomalies in the post-Zechstein units and a relationship between overall thickness and average density in the Zechstein unit. It was used, together with a depth-converted structural model from the seismic interpretation, to calculate the gravity effect down to base Zechstein. This, along with a long-wavelength background field, was subtracted from the observations to leave a residual gravity anomaly that was inverted to produce a 3D model of variations in the thickness of a pre-Zechstein layer that incorporated the effects of both basins and granites. The modelling results were analysed in combination with magnetic imaging and available mapping of intra-Upper Palaeozoic seismic reflectors. Granites were often easy to identify on the basis of a low in the gravity inversion surface that coincided with a structural high defined seismically and, in some cases, a magnetic signature. There are, however, some more ambiguous features that cannot be confidently classified without further information. Relatively low density rocks within the Lower Palaeozoic basement and zones of high density basement or pervasive high density intrusive rocks introduce distortion into the model, and the identification and separation of these influences requires more detailed combined seismic, gravity and magnetic modelling.

Potential targets (areas of pre-Zechstein sedimentary thickening) were identified in Quads 19-20, Quads 26-28, and just to the north of an 150 km offshore extrapolation of the line which forms the southern margin of the Tweed Basin in the onshore area (the Pressen-Flodden-Ford faults). Geophysical anomalies in the Q36-37 area suggest a complex interplay between sedimentary and igneous features and would also benefit from further investigation. A ‘ramp’ in the gravity inversion surface appears to be linked, at least in part, to lateral density variations associated with overcompaction along the Sole Pit axis. The geophysical feature extends beyond previous mapping of that axis and is overlain by the Breagh gas field, so is an appropriate target for more detailed study (which could address the possibility of a basement influence on the observed anomalies). The results obtained indicate that gravity/magnetic interpretation provides a useful supplement to seismic reflection surveys, even where the latter form the primary exploration method. There are, for example, features at the southern margin of the Forth Approaches Basin and possible intra-basinal structures within the North Dogger Basin that could add to our understanding of those areas.

The new government-funded seismic/gravity/magnetic surveys over the Central North Sea, which were conducted in 2015 and will be released in 2016, will provide the ideal resource with which to follow up the results of this investigation.

1 Introduction

The 21CXRM Palaeozoic Project aimed to stimulate exploration of the Devonian and Carboniferous plays of the Central North Sea - Mid North Sea High, Moray Firth - East Orkney Basin and in the Irish Sea area. The objectives of the project included regional analysis of the plays and building of consistent digital datasets, working collaboratively with the OGA, Oil and Gas UK and industry.

The project results are delivered as a series of reports and as digital datasets for each area. This report describes the interpretation of gravity data in the Central North Sea area. Gravity and magnetic data were compiled and imaged over a region spanning the original study area and 3D gravity modelling was conducted within a smaller rectangle, based on the availability of seismic constraints (Figure 1). The particular emphasis of the project was to investigate the possibility that pre-Zechstein source rock basins occur within areas that were poorly imaged by the currently available seismic data.

2 Gravity and magnetic data

2.1 DATA SOURCES

This study has employed BGS gravity and magnetic data. The gravity compilation (Figure 2) comprised marine tracklines to the east and onshore gravity stations to the west. The marine surveys were mainly acquired digitally, but some lines in the northern part of the study area are based on analogue data which were subsequently digitised. The data come from the BGS 'adjusted' marine gravity database, which does not include all available survey lines (some segments have been removed because of noise or crossover errors). The magnetic compilation (Figure 2) was based on marine tracklines in the east and the national aeromagnetic survey (flown in 1955-1965) in the west. There is alternative aeromagnetic coverage of the North Sea (originally flown by Aeroservice Corporation), which has been used in BGS published geophysical maps. Those maps informed the present study but the digital data were not employed.

The gravity and magnetic survey data were imported into Geosoft (Oasis Montaj) databases for detailed examination and gridding. They were interpolated onto regular grids with a 1 km node spacing and these were used in the generation of a range of georeferenced geophysical images including the Bouguer gravity anomaly, residual Bouguer anomaly, total magnetic intensity, reduced-to-pole magnetic field, and residual reduced-to-pole magnetic field shown in Figures 4-8 respectively. The full set of images provided in the digital deliverables is described in Appendix 1.

2.2 QUALITATIVE DESCRIPTION OF GRAVITY FEATURES

Figure 9 is an annotated version of a residual gravity image which has been labelled with some key features. The image highlights a series of conspicuous gravity lows which are caused by Late Caledonian granites. It has long been recognised (e.g. Bott, 1967) that the Carboniferous basins of north-east England are separated by relatively uplifted blocks (the Cheviot Block, Alston Block, Askrigg Block and Market Weighton Block) which are underpinned by granite masses (the Cheviot, North Pennine (Weardale), Askrigg and Market Weighton granites respectively; Figure 9). Further possible granites have been identified from gravity data in the offshore area, where seismic data have been used to constrain the gravity effect of the overlying sedimentary sequence. These include the Farne, Teeside and Dogger granites (Donato et al., 1983), the Amethyst Granite (Donato and Megson, 1990) and the Cleaver Bank Granite (Donato,

1993) (Figure 9). The other strong control on basin formation is the grain inherited from the underlying basement, which was developed during continental convergence in the Lower Palaeozoic (closure of the Iapetus and Tornquist oceans) and subsequent Acadian deformation (e.g. Chadwick and Holliday, 1991). In the north-west part of the study area, an east-north-east (Iapetus) trend dominates the gravity signatures. Towards the east, north-westward trends are evident, and are inferred to be inherited from structures created during the closure of the Tornquist Ocean.

There is a strong gravity gradient across a major fault system that forms the southern margin of the Upper Palaeozoic half-graben underlying the Forth Approaches Basin (Cartwright et al., 2001; Granby Enterprises and TGS, 2008). Silurian rocks are proved by well 26/14-1 to the south of this fault zone and in the intervening area there is a north-east-trending magnetic anomaly. This may be caused by highly magnetic metasedimentary rocks of the Ordovician Marchburn Formation, part of the Tappins Group which forms the northernmost tracts of the Southern Upland terrane (Floyd and Kimbell, 1995; Barron et al., 2004). The magnetisation is due to ophiolitic fragments presumed to be derived from lateral equivalents of the Ballantrae Complex in SW Scotland. If this hypothesis is correct, it implies that the fault system which forms the basin margin beneath the Forth Approaches is a reactivation of the Southern Upland Fault and that the latter fault is offset in the offshore area, possibly by a north-north-east-trending early structure. Other explanations are possible (e.g. lateral variability in the magnetic properties of the Southern Uplands units), but the gravity data do indicate that a structure which trends north-north-east from the Dunbar area has influenced the subsequent evolution of the western margin of the Forth Approaches Basin (Dunbar lineament in Figure 9).

Distinct gravity signatures are observed over the Lower Palaeozoic outcrop of the Southern Uplands terrane. These include: (i) short-wavelength effects associated with density differences between the steeply dipping tracts; (ii) effects associated with variations in the depth and/or density of an underlying basement; and (iii) possible concealed, late Caledonian intrusions (in particular the Tweeddale batholith) (Floyd, 1999; Akhurst et al., 2001; Lagios and Hipkin, 1979). These observations invite caution when interpreting gravity anomalies over the offshore extension of the Southern Uplands terrane in terms of Upper Palaeozoic basins, although there are features in that area that would be worth closer examination. For example, a pronounced gravity low in the immediate offshore area has been interpreted by Lagios (1983) to be an extension of the Oldhamstocks Basin. Inspection of the details of the onshore gravity field confirms that there is a decrease associated with the Upper Palaeozoic sedimentary rocks, but that there is some overlap between this and a gravity gradient aligned with the Laurieston Fault within the Southern Uplands Lower Palaeozoic sequence. This fault was fomerly identified as the boundary the Gala and Hawick Groups in south-east Scotland (Akhurst et al., 2001), but the southernmost Gala Group tracts in this area have now been assigned to the newly-defined Riccarton Group (Stone and McMillan, 2013). It follows that the offshore Oldhamstocks anomaly may reflect the combined effect of both Upper and Lower Palaeozoic low density rocks.

There is an east-north-east-trending gravity lineament just to the south of the structural high on the southern side of the Forth Approaches Basin and a zone of generally lower gravity values between this and a further ENE-trending lineament which crosses the southern parts of Quads 25-27. There is the possibility of an igneous contribution to the latter gravity feature, because wide Permo-Carboniferous quartz-dolerite dykes underlie the area immediately south of the lineament (Smythe, 1994), although the limited seismic imaging available does provide hints of northward sedimentary thickening across the lineament (see Section 5).

Farther south an east-north-east gravity trend extends offshore from the Cheviot area. This has been identified as the Pressen-Flodden-Ford (PFF) trend in Figure 9, named after the fault system which forms the southern boundary of the Tweed Basin in the onshore area, a boundary which Chadwick and Holliday (1991) identified offshore on the NEC seismic profile (see also

Freeman et al., 1988). The gravity imaging suggests that this lineament may continue for at least 150 km east of the coastline.

The east-north-east-trending grain in the gravity images discussed above extends as far as a line which extends in an east-south-east direction from the SW corner of Quad 19 to the edge of the study area (Figure 9). This bears similarities to 'lineament A' of Lyngsie et al. (2006) and Lyngsie and Thybo (2007). It lies up to 40 km to the SW of the latter feature in the north, but converges with it south-eastward. Lyngsie et al. (2006) and Lyngsie and Thybo (2007) regarded their feature as marking the lower crustal suture between Eastern Avalonia and Baltica in the south-east and between Laurentia and Baltica in the north-west, with the implication that the deep crustal expression of the Iapetus Suture does not extend north-east of this line. This is compatible with the observation that upper crustal structures which have inherited the Iapetus 'grain' generally appear to terminate at this line. Lyngsie and Thybo (2007) linked lineament A to the Elbe Line, a long-lived line of crustal weakness (Scheck et al., 2002).

There is a gravity low over the offshore extension of the Northumberland Trough, a half graben with a southern margin formed by the Stublick – Ninety Fathom fault system (Bott, 1967; Kimbell et al., 1989; Chadwick et al., 1995). The gravity low can only be traced about 40 km offshore; the basin appears relatively deep in an area spanning the southern part of the boundary between Quads 34 and 35, but is then truncated at a north- to north-north-west-trending gravity high. There is evidence of noise in the gravity survey data over this lineament and a c. 10 km data gap along a nearshore strip (Figure 2) which causes blurring of the gravity signatures. The truncation of the Northumberland Trough is likely to be part of the 'block and basin' configuration described above, and probably relates to buttressing of the area to the east by granite plutons (the Farne Granite and its possible subsidiary granite pluton beneath the west side of Quad 35).

The Stainmore Trough is associated with a gravity low, with a gravity gradient over its northern margin at the Butterknowle Fault (Figure 9). The gravity data suggest that there is only a very limited offshore extension of this basin, which is truncated by a block underlain by the Teeside Granite.

2.3 SOURCES OF MAGNETIC ANOMALIES

A brief overview of magnetic sources in the region is provided here. Further discussion of specific magnetic features in the modelled area is provided in Section 5.

- Higher magnetic field values over north-west Scotland are associated with Laurentian magnetic crystalline basement. Magnetic Palaeoproterozoic (Rhins terrane) rocks just to the north-west of the study area have been accreted against Archaean (Lewisian) magnetic basement farther north (Rollin, 2009). The low magnetic field values in the north-west part of the study area relates to less magnetic crust underlying the southern part of the Grampian terrane. The higher magnetic field in the south-west part of the study area is likely to relate to an underlying Avalonian (Neoproterozoic) basement (Kimbell and Quirk, 1999; Kimbell et al., 2006). Magnetic Precambrian crystalline rocks also form the basement beneath Baltica to the east of the study area (Banka et al., 2002; Williamson et al., 1995).
- Longer wavelength magnetic anomalies over the Midland Valley Terrane (Figure 7) may be associated with the Ordovician arc complex that underpins it (Bluck, 2013), and it is possible that magnetic anomalies offshore Stonehaven (southern parts of Quads 19 and 20) have similar explanations. Magnetic anomalies are also associated with Ordovician ophiolitic rocks at the margins of the Midland Valley terrane and magnetic sedimentary rocks derived from them (e.g. the Tappins Group – see above).
- Ordovician magmatism associated with south-eastward subduction of the Tornquist Ocean may explain north-west-trending magnetic anomalies on the north-east side of the Midlands Microcraton (Pharaoh et al., 1993).

- Magnetic anomalies are associated with a number of known or inferred late Caledonian intrusions. Amongst these are a distinct anomaly over the Dogger Granite and a subtle one over the Farne Granite (compare Figures 8 and 9). These features, together with a granite intersected in Dutch well A17-1, lie along a WNW-ESE alignment that has a local expression spanning the coastline in the Borders area. A series of local magnetic anomalies along this trend can be correlated with three late Caledonian dioritic intrusions in the onshore area (Lammer Law, Priestlaw and Cockburn Law) and three further inferred dioritic intrusions offshore (Kimbell et al., 2006). A north-north-east-trending magnetic anomaly in the north-east part of Quad 36 lies between the Farne and Dogger granites and might have a plutonic origin, although correlations with seismic mapping suggest a possible alternative (extrusive) interpretation (see Section 5). Not all the late Caledonian intrusions in the region have a positive magnetic expression. The North Pennine (Weardale) granite batholith in particular is non-magnetic and there is a magnetic low associated with its interaction with magnetic basement (Kimbell et al., 2006, 2010). In the offshore area, the Teeside Granite also appears to have a relatively low magnetisation,
- Devonian and Carboniferous magmatism in the Midland Valley is associated with conspicuous short-wavelength magnetic anomalies, and may be implicated in longer wavelength features if there are underlying, deep-seated intrusive bodies of this age.
- Magnetic anomalies associated with Permo-Carboniferous quartz-dolerite dykes cross the Midland Valley in a west-east direction and can be traced offshore along an arcuate trend for up to 180 km (Figure 8). A particularly conspicuous group of dykes crosses the coast close to Dunbar (Smythe, 1994). Magmatism of this age also has a magnetic expression over the Whin Sill and associated dykes in Northern England and is likely to be a source of magnetic anomalies at the eastern extremity of the mapped area (Inge Volcanic Formation).
- Magnetic anomalies are associated with the Jurassic Forties Volcanic Province just to the north of the north-east corner of the study area.
- Reversely magnetised Palaeogene dykes are responsible for narrow, linear negative magnetic anomalies which trend east-southeast across the study area. These include the Acklington Dyke (which crosses Quads 34-36; Figure 8), the Blyth Dyke (visible at the southern edge of Quad 35) and the Cleveland-Armathwaite Dyke (which meets the coast in the central part of Quad 41, but is difficult to trace offshore in the current data compilation). In the offshore area, magnetic anomalies associated with Palaeogene dykes tend to form a series of local minima as a result of aliasing between widely-spaced survey lines, although there are also genuine gaps in the shallow magnetic expressions of the dykes.

3 Rock densities

3.1 GEOPHYSICAL LOG DATA

Digital logs from 146 wells (Figure 1) were used to investigate rock densities in the Central North Sea area. The well logs were corrected to depth below seabed so that they could be compared with published compaction trends for different lithologies (Sclater and Christie, 1980). An example log is provided in Figure 10, and a set of such plots is included in the supplementary material (see Appendix 2). The latter includes most of the wells analysed but a subset is excluded for confidentiality reasons.

Figures 11 to 15 merge the compiled density data within the units used in the seismic interpretation and gravity modelling (Arsenikos et al., 2015; Section 4), colour-coding these according to Quad. Available logs through the post-Chalk sequence typically indicate densities between 1.8 and 2.3 Mg/m^3 and show a general compaction trend (Figure 11), although this does not closely match any of those defined by Sclater and Christie (1980). A summary plot for the measured Chalk densities (Figure 12) shows clear evidence of a compaction trend similar to that predicted for this lithology by Sclater and Christie (1980), although there are departures

associated with burial anomalies (see Section 3.2). Density measurements of the pre-Chalk – post-Zechstein layer are more heterogeneous, although there is still a broad compaction trend (Figure 13). The Zechstein density logs reveal a broad range of densities due to the presence of low density (c. 2.1 Mg/m^3) halite and high density (c. 2.9 Mg/m^3) anhydrite as well as limestones and dolomites with densities of around 2.7 Mg/m^3 (Figure 14).

The overall average density of the pre-Zechstein rocks in the sampled sections is 2.557 Mg/m^3, and the average densities within individual wells range from 2.29 Mg/m^3 to 2.71 Mg/m^3. There is evidence of a compaction trend in the longer logged sections, although this is less obvious in the merged plot (Figure 15) than it is with the younger sedimentary strata.

One approach to incorporating the density information derived from well logs would be to use simple averages or to interpolate/extrapolate from the well locations using geostatistical methods (kriging). Examples of the results obtained using the latter approach are included in a supplementary document (Appendix 2). There are several problems with this approach:

(i) The well logs do not necessarily sample the whole of the unit in question, leading to bias in the nominal averages.
(ii) The distribution of data points is not adequate to simulate lateral density variations across the modelled area without further control.
(iii) Individual well logs may contain noise, miscalibration and erroneous segments. A degree of filtering was provided by only employing data for which the density correction log indicated a value of less than 0.1 Mg/m^3 and by some editing of grossly erroneous segments, but it nonetheless remains the case that a density model that relied too heavily on individual logs might be susceptible to distortion.

The density modelling has therefore adopted a predictive approach which employed additional control. This was obtained from an understanding of compaction trends and burial anomalies in the sedimentary rocks, and the relationship between thickness and average density in the evaporitic Zechstein sequence.

3.2 CONSTRUCTION OF A DENSITY MODEL FOR THE CENTRAL NORTH SEA AREA

The results of studies by Japsen (1998, 1999, 2000) have been used to inform compaction models for the Central North Sea area. These studies defined departures from normal compaction trends on the basis of seismic velocities observed in geophysical well logs, which provide a larger database than was available for the density analysis conducted for the present study. Overcompaction is observed in areas where uplift and erosion has removed some of the cover sequence such that the rocks that remain have velocities that would, in normally compacted rocks, be characteristic of greater depth of burial. Undercompaction can result when rocks are buried rapidly and fluid cannot escape, such that its overpressure reduces velocities to values that would be characteristic of shallower depth of burial in normally compacted rocks. Burial anomalies should affect rock densities in a similar fashion to their velocities, a prediction that was tested by seeing how well the anomalies inferred by Japsen (1998, 1999, 2000) simulated the available density observations when applied to the normal compaction trends of Sclater and Christie (1980). The sections below describe how a density model was constructed for each of the layers in the cover sequence model defined by seismic interpretation (Arsenikos et al, 2015; see Section 4.1.1 below).

3.2.1 Post-Chalk density model

Japsen (1999) observed undercompaction (overpressure) in post-Chalk rocks below the Mid-Miocene unconformity in the central part of the North Sea and related this to the rapid burial and sealing quality of the strata below this unconformity. Towards the west, increasing amounts of overcompaction were observed in this sequence and were interpreted to be the result of Neogene

erosion. Rocks above the Mid-Miocene unconformity displayed properties more characteristic of normal compaction. Very few of the available density logs span this unconformity, but there is evidence in the logs from wells 30/23A-3 and 38/16-1 of a reduction of density with depth likely to be due to undercompaction of the rocks beneath the unconformity. A detailed map of the Mid-Miocene unconformity was not interpreted within the present project, but its influence on modelled densities is subtle, and allowed the use a generalized representation of this interface, based on other sources, without significant loss of accuracy. A density model was constructed which split the Cenozoic sequence using this generalised interface and predicted densities in the lower part using a combination of the shale compaction curve of Sclater and Christie (1980) and the burial anomalies of Japsen (1999, fig. 9c). An empirically defined undercompaction threshold equivalent to a burial anomaly of 300 m was applied (the fit to the observations was degraded when greater amounts of undercompaction were applied). The sequence above the Mid-Miocene unconformity was assigned an average density of 2.0-2.1 Mg/m^3 on the basis of the available density logging in wells 30/16-9, 30/23A-3, 44/23-7, 44/26-2, 44/26-4 and 44/28-4. These are relatively high values for areas which have not undergone recent denudation, and might reflect a sampling bias in the available well data, although it is possible that compaction associated with grounded ice sheets might have influenced superficial densities (cf. Graham et al., 2010, 2011). The current density model for the layer below the Mid-Miocene unconformity applies a simple westward extrapolation of the Japsen (1999) burial anomalies in the gap between that model and the coast, and this is likely to have led to an underestimate of superficial densities there. The effect on the gravity calculations is small, because of the thin post-Chalk sequence in that area, but this is something that could be improved in future iterations. Figure 16 shows the density model adopted for the post-Chalk sequence, together with a comparison of observed and calculated average densities in the limited sections for which well measurements were available, illustrating the reduction in scatter resulting from application of the published burial anomalies.

3.2.2 Chalk density model

Burial anomalies within the Chalk have been published by Japsen (1998, 2000). These showed a similar pattern to the post-Chalk trends, with undercompaction in the central part of the North Sea and the increasing overcompaction in a westward direction. The later study refined the normal Chalk compaction trend relative to which the burial anomalies were estimated (Japsen, 2000; his Appendix B). A burial anomaly grid for the Chalk was derived from these results, with the values estimated by Japsen (1998) corrected to account for the later modification to the baseline. Values based on these anomalies, combined the chalk compaction curve of Sclater and Christie (1980), provide a better agreement with the observations in overcompacted areas but diverge where undercompaction is predicted (Figure 17). The reason for the contrasting influence of overpressure on the velocity and density of the Chalk is not known, but for the purposes of gravity modelling a correction was applied that allowed for overcompaction but simply used the normal compaction curve in overpressured areas (Figure 17).

3.2.3 Pre-Chalk – post Zechstein density model

The pre-Chalk – post-Zechstein sequence contains heterogeneous lithologies and has a highly variable density. For example, Triassic evaporites have densities that are both much less (halite) and much greater (anhydrite) than the sedimentary rocks. This made it a particularly difficult unit to simulate. A preliminary model for this sequence was derived by assuming the shale compaction trend of Sclater and Christie (1980) and the burial anomalies assumed for the overlying Chalk (Figure 18). As with the overlying unit, applying corrections for overcompaction led to an improvement in the agreement with measured values but there was divergence when undercompaction corrections were applied. Japsen (2000) compared burial anomalies in the Chalk and the Triassic Bunter Shale and detected enhanced overcompaction in the pre-Chalk sequence along the Sole Pit axis, associated with inversion along this axis prior to deposition of the Chalk. The area where the pre-Chalk burial anomaly was inferred to exceed the

Chalk burial anomaly is shown in Figure 18. This effect was not explicitly incorporated in the current gravity model: the alternative approach was taken of analysing the model residuals for evidence that would provide an independent view of its extent.

3.2.4 Zechstein density model

Examination of the density logs through the Zechstein Group revealed that the logging frequently commenced near the base of this unit and that, in these cases, anhydrite was sampled preferentially whereas halite tended to dominate in the unlogged sections. For this reason the estimates of average density for the Zechstein sequence were based on a set of 70 logs which sampled at least 60% of its thickness. A cross-plot of average density against thickness shows an inverse relationship, with average density increasing as thickness decreases (Figure 19b), reflecting the greater proportion of halite in the thick evaporitic sequences. This fact was used in predicting the average Zechstein density by regression kriging using the well values as the primary variable and the relationship between thickness and density as external drift. A floor value of 2.1 Mg/m^3 was applied to avoid 'overshoot' in very thick sequences. The resulting density model is shown in Figure 19a.

3.2.5 Pre-Zechstein density model

Figure 20 illustrates a map based on the average densities of the pre-Zechstein rocks derived by kriging of values measured in geophysical well logs at the sites indicated. It was not considered appropriate to use this interpolation as the basis for modelling this sequence, however, as it is based on samples from the upper part of the sequence and is unlikely to reflect the average density over its full depth. Instead, a highly generalised model of the density of the pre-Zechstein Upper Palaeozoic rocks was employed in the gravity modelling. This was guided by the logged wells with the thickest intersections and assumed a uniform average value of 2.55 Mg/m^3 over most of the modelled area, increasing to 2.65 Mg/m^3 at its southern edge.

3.2.6 Basement densities

The geological basement beneath the region comprises metamorphosed Lower Palaeozoic rocks and underlying crystalline basement and is intruded by Devonian granites. Information on the densities of Lower Palaeozoic rocks in the onshore region is summarised by Kimbell et al. (2006) and has been supplemented by further unpublished BGS density measurements in the Southern Uplands. The average density of the Southern Uplands units is about 2.72 Mg/m^3 but ranges from around 2.70 Mg/m^3 in the quartz-rich units to 2.75 Mg/m^3 in denser lithologies. In northern England, average densities range from about 2.72 Mg/m^3 in the Silurian rocks to 2.78 Mg/m^3 in the Ordovician (Kimbell et al., 2006 and references therein). The density of the underlying crystalline rocks is difficult to estimate and likely to include lateral variability. In particular, relatively high seismic velocities beneath the Midland Valley of Scotland (Bamford, 1979; Barton, 1992) and the central part of the North Sea (Barton and Wood, 1984) suggest that higher densities may apply there. In the former case this could relate to igneous rocks associated with the origin of the Midland Valley as an Ordovician arc terrane, together with subsequent igneous additions; in the latter case the higher velocities appear to relate to basement derived from Baltica.

The gravity modelling presented here assumes a simple average density of 2.75 Mg/m^3 for the basement, and the possible role of intra-basement density contrasts is considered in the analysis of the modelling results.

4 Gravity modelling

The gravity modelling involved the construction of a forward model of the gravity effect of the sequence down to base Zechstein and the use of gravity inversion to infer structures at greater depth.

4.1 STRUCTURAL INPUTS

4.1.1 Seismic reflection data

The following depth-converted structural horizons were employed in the gravity modelling and were a product of the seismic interpretation carried out in the companion study (Arsenikos et al., 2015):

- Seabed
- Base Cenozoic (Top Chalk)
- Base Chalk
- Base Mesozoic (Top Zechstein)
- Base Zechstein
- Top Cementstone Formation
- Top Kyle Limestone

Seismic horizons were also picked at the top of the Scremerston Formation and the top of the Fell Sandstone, but these were not used directly in the gravity modelling. The Zechstein and later horizons covered most of the offshore part of the study area, but the top Cementstone and Top Kyle horizons had more restricted coverage (Figure 21).

The time constraints were such that it was necessary to use working versions of the depth-converted seismic horizons in the gravity modelling, rather than the final versions delivered by the seismic interpretation project (Arsenikos et al., 2015). Over most of the area this does not affect the outcome, but there are localities where inaccuracies in the thickness of the Zechstein sequence in the earlier version are sufficient to have a significant impact on the gravity modelling; these are shown as model distortions on Figure 21 and discussed in Section 5. The discrepancy in Quad 44 took the form of an overestimate of Zechstein thickness in the version used in the gravity modelling whereas the Quad 42 and Quad 28-29 areas included both overestimates and underestimates. Note that, even with improvements in depth-conversion, the coarse structural grids employed will not resolve all the detail in areas with complex salt geometries.

4.1.2 Seismic refraction data

Barton and Wood (1984) report the results of a seismic refraction experiment which extended from close to the UK mainland across the Central Graben. The western third of the profile lies within the present study area (Figure 21). The shallow part of the velocity model for this profile (down to base Zechstein) was based on other data sources and no intracrustal refractors were identified in the underlying crust, which was modelled using continuous velocity gradients (Barton and Wood, 1984). Although relatively high (5.5-5.9 km/s) sub-Zechstein P-wave velocities in the resulting model (Barton and Wood, 1984, fig. 11) appear to rule out a significant thickness of Carboniferous and/or Devonian sedimentary rocks, this part of the model is poorly resolved as a result of the source-receiver distribution. The receivers were concentrated over the Central Graben (spanning from Quad 29 to Quad 23), and this will have limited the ability to resolve shallow structure farther west (see the raypaths in fig. 10 of Barton and Wood, 1984).What this profile does detect is a distinct eastward increase in lower crustal velocity which commences beneath Quad 28, coinciding with the ESE-trending lineament which truncates features with ‘Iapetus’ trends. This offers support for the hypothesis of Lyngsie et al. (2006) and

Lyngsie and Thybo (2007), potentially extending lower crust with Baltica affinity even further to the SW than they proposed.

The SWABS (Seismic Wide-Angle and Broadband Survey) experiment involved coincident normal-incidence and wide-angle seismic data acquisition (Singh et al. 1998; McCaughey et al., 2000). A velocity model was produced by traveltime inversion, and the upper part of this resolves an eastward thickening layer with velocities of 3.2-3.8 km/s, which is likely to comprise Permian and younger sedimentary rocks (McCaughey et al., 2000, fig. 5). The layer immediately beneath this, with velocities ranging upward from just under 4.5 km/s, was interpreted by McCaughey et al. (2000) as crystalline crust but is considered more likely to include Palaeozoic sedimentary rocks in its upper part. On the basis of comparison with onshore geology and geophysics there is likely to be a Lower Carboniferous sequence with a velocity of around 4-4.5 km/s underlain by Lower Palaeozoic metamorphic basement with a velocity of 5.5-5.7 km/s, which is in turn underlain by crystalline crust with a velocity of $\geq$6 km/s. The interpretation of an expanding spread profile (ESP) reported by Singh et al. (1998) is broadly compatible with this scheme, although the velocity variation in that model is characterised by gradients rather than 'steps'. The first arrivals at offsets of 10-30 km in the stacked ESP data shown in fig. 4 of Singh et al. (1998) are compatible with a 5.7 km/s refractor in a simple velocity model. A preliminary examination of this evidence suggests that about 1 km of Carboniferous rocks may be present beneath the SWABS profile at the site of the ESP, although more detailed modelling of the results of this experiment is recommended.

The Caledonian Suture Seismic Project (CSSP) involved a long refraction line extending from the Irish Sea to the Mid North Sea High (Bott et al., 1985). The upper crustal structure beneath the eastern part of the profile has been considered by Green (1984) who identified Upper Carboniferous (P-wave velocity of 3.7 km/s), Lower Carboniferous/Devonian (4.3-4.5 km/s) and Lower Palaeozoic (5.6 km/s) refractors beneath the North Sea segment of the profile. Probable crystalline basement with a higher velocity (6.17 km/s) was traced about 40 km offshore, but not further to the east. The top Lower Palaeozoic refractor lay at a depth of 2 km beneath Quad 34, shallowing to 1.2 km beneath the western side of Quad 35 and then deepening to 3 km from the eastern side of Quad 35 eastwards.

The available seismic refraction data have low resolution, but the SWABS and CSSP results did provide information on depth to basement that was employed during the modelling.

4.2 GRAVITY MODELLING PROCEDURE

The gravity calculations were made using GM-SYS 3D routines within the Geosoft Oasis Montaj software package. Structural grids with a 5 km node spacing were used as the basis for the initial modelling, but the final gravity inversion resampled these at 2.5 km intervals, and employed an observed gravity field that incorporated the wavelengths available with this closer sampling. This admits slightly higher resolution in the gravity inversion where the overlying structure was smoothly varying (i.e. adequately reproduced by the 5 km grid) but obviously does not circumvent the resolution limits that apply where that structure contains short wavelengths. The model explicitly included the seawater layer (with a density of 1.03 Mg/m^3) and thus simulates free-air gravity anomalies in the offshore area. The input field (Figure 22) was based on free-air gravity anomalies offshore and Bouguer anomalies onshore and the gravity calculation surface was at the datum level in both the offshore and onshore areas. The onshore part of the model was thus treated in an approximate fashion (using the variable density Bouguer reduction to simulate the effect of rocks above datum), but this area was not the focus for the investigation so such an approach was considered acceptable.

An initial forward gravity calculation (Figure 23) was based on a model with horizons at seabed, top Chalk, base Chalk, top Zechstein and base Zechstein, together with the density models described in Section 4 applied to the units between these horizons. Further forward gravity models were calculated down to the Top Cementstone and the Top Kyle horizons where these

were present. The wavenumber domain modelling method employed requires continuous grids, so the mapped structures were interpolated and extrapolated to fill the full model rectangle prior to calculation and masked back to the relevant limits after calculation. There is thus potential for edge-effects in the modelling results. There is no evidence of substantial artefacts ('ringing') in the results, but more subtle distortion associated with the influence of unmapped structures outside the modelled areas is inevitable, particularly in the case of the deeper (Carboniferous and Devonian) horizons with limited mapped extent. The calculations relating to the deeper horizons were, however, only used for guiding the construction of a background field, as described in the following paragraph, and as part of that process calculations made close to the edges of seismically-mapped areas were given less weight than those away from such boundaries.

When the calculated field (Figure 23) is subtracted from the observed field (Figure 22) the resultant is dominated by a regional gradient due primarily to a reduction in the depth to Moho and increase in crustal density towards the central part of the North Sea. It is necessary to remove this long-wavelength effect so that the signatures due to shallower structure can be isolated and modelled. In some modelling schemes this is done by an explicitly modelled Moho (e.g. Kimbell et al. 2004; Milton-Worssell et al., 2010). If a simple crustal density model is assumed, this apparent Moho also absorbs gravity variations associated with deep intra-crustal density variations. Lateral variations in crustal density are likely to occur beneath the area (see Section 3.2.6), and incorporating them explicitly is difficult, given the sparsity of the available deep seismic velocity control. An alternative approach was therefore adopted in which the deeper effects were simulated using a 'background' field. Constraints were identified where the deeper Palaeozoic horizons were mapped, where seismic refraction data resolved the basement, from well and outcrop data, and on the basis that the residual field would be dominated by negative anomalies (i.e. explicable in terms of underlying low-density units). A background field was then defined by a 4^{th} order polynomial (Figure 24) based on these constraints. The use of such a smooth surface is a major simplification (and means that nominal control points were not necessarily honoured), but was considered the best option for the initial modelling exercise, given the limitations of the available constraints and the regional scale of the model. Inspection of the gravity field over areas of exposed basement (e.g. the Southern Uplands) show that there is local density variation in the upper crustal basement which generates shorter wavelength variations in the background field, but the separation and modelling of these in the offshore area is a topic for more detailed investigations.

After forward calculation of the gravity effect to base Zechstein and removal of the background field, the residual anomalies (Figure 25) were inverted by varying the thickness of a sub-Zechstein layer with the density structure shown in Figure 20b. The GM-SYS 3D inversion routines failed to converge satisfactorily despite a range of trials in which the key parameters (e.g. the low-pass filter applied) were varied. An alternative optimisation sequence was therefore employed in which modification to the inverted surface was achieved by iteratively scaling the residual gravity anomalies using a 'Bouguer slab' calculation. The modified surface was low-pass filtered (using a Butterworth filter with a central wavelength of 10 km) after each iteration and prior to recalculation of the gravity anomalies. The depth to the final inverted horizon is shown in Figure 26 and the thickness between this horizon and the base Zechstein surface is shown in Figure 27. Contours from the latter display are superimposed on a residual magnetic map in Figure 28. The calculated field for the full model is shown in Figure 29 and residual anomalies after this and the background field have been subtracted from the observed field are shown in Figure 30.

The customised inversion procedure proved effective, with residual anomalies generally less than 1 mGal and an RMS residual anomaly which reduced to 1.02 mGal after 4 iterations (Figure 30). The largest positive anomalies are associated with the Grampian basic rocks in the north-western corner of the area and the largest negative anomalies occur over granites, neither of which were intended for accurate simulation. There is an area of larger residuals in the southern parts of Quads 41-43, which is likely to relate to a combination of inaccuracies in the cover

sequence model combined with the difficulty of accommodating short-wavelength effects by modification of a deep horizon.

The depth grid produced by the gravity inversion was converted into two-way travel time, assuming an average velocity of 4.069 km/s between base Zechstein and the intra Palaeozoic seismic picks (as in the initial seismic depth-conversion). The time horizon was then imported into the seismic workstation environment so that it could be superimposed on the seismic displays and inform the interpretation process.

4.3 GUIDANCE ON VIEWING AND USING THE GRAVITY INVERSION RESULTS

It is important to explain the context of the gravity inversion results so that they can be used effectively. Some illustrations and comments are provided in this report but it is hoped that users will import the digital outputs into their own interpretation platforms and extract more information from them.

It is well-known that gravity inversion is non-unique – i.e. an observed gravity anomaly can be explained by a range of subsurface density structures. The process of gravity interpretation involves constraining parts of the density structure using other sources in order to make the problem more tractable. This has been done in the present example by using seismic modelling and density predictions to remove a part of the cover sequence from the inversion problem. The removal of the background field represents another step in the isolation of a gravity signal that is suitable for inversion. Any inaccuracies in these processes will be carried through into the inversion results.

A key target is the depth to geological basement beneath the Upper Palaeozoic sequence, and in parts of the study area the gravity inversion will represent a response to variations in that depth. When analysing the results it needs to be borne in mind that: (i) the density contrast at this basement surface is poorly calibrated, leading to inaccuracies in the resolution of its topography; and, importantly, (ii) intra-basement density contrasts are also simulated by the inversion horizon.

The granites that underlie the area are key intra-basement features that are simulated in the inversion, and the form taken by the inversion surface will not simulate their geometries accurately. The density contrast assumed is greater than that which typically characterises such intrusions, and the geometries adopted (tapering downwards) contrast with the conical forms generally assumed when such bodies are the primary focus of gravity modelling. This traditional view of the shapes of plutons has been challenged, with alternatives including sheeted and funnel shaped forms (e.g. Vignoresse et al., 1999; Petford and Clemens, 2000; Cruden and McCaffrey, 2001), but the weight of evidence still favours a conical form for the Devonian plutons of northern England. This is supported, for example, by a comparison between the outcrop patterns and gravity anomalies over the Shap and Skiddaw plutons in the Lake District and the details of modelling the North Pennine (Weardale) granite batholith (Kimbell et al., 2006, 2010). In contrast there is evidence for a sheeted, ‘cedar tree’ geometry in the case of the Ordovician components of the Lake District granite batholith (Chadwick et al., 2005; Kimbell et al., 2010). It would be possible to incorporate the granites as an additional component in the model by resetting the initial inversion surface to top basement across their inferred locations and then accommodating the residual anomalies this generates by a granite body optimised upwards from a basal surface. The dangers with this approach are: (i) where basins and granites lie in close proximity, partitioning the gravity response between the two is not straightforward and attempts to do this could actually hamper the analysis of the former; and (ii) granites are identified with varying degrees of certainty in the offshore area and it is important not to pre-judge this interpretation in the case of the features defined with less confidence. The current gravity inversion surface thus incorporates the gravity effects of inferred granites and the comparison between this and the seismic database has been used to discriminate between these and alternative interpretations.

Besides the effects associated with low-density plutons, the observed gravity field will contain relatively short wavelength signatures associated with other density contrasts within the Lower Palaeozoic and crystalline basement and with high density intrusive rocks. It was not practicable to provide a quantitative model of these signatures that could be subtracted prior to inversion, so their influences remain and need to be considered as part of the analysis process.

5 Discussion

Figure 31 is an annotated version of the gravity modelling results (thickness between base Zechstein and the inversion surface) and Figure 32 is an annotated version of the map showing the thickness contours superimposed on a residual magnetic map. These are used to illustrate the following discussion, which is also aided by a series of cross sections showing the relationship between the gravity inversion and the original seismic picks (locations shown in Figure 33 and sections shown in Figures 34-43). Apart from a highly generalised influence on the background field, the gravity inversion surface was derived independently of the top Cementstone and top Kyle Limestone horizons and their comparison provides useful insights. The main features will be discussed from north to south, with inferences drawn from the annotated maps and sections as appropriate.

A low in the gravity inversion surface on the west side of Quad 19 is associated with shallow magnetic anomalies and is considered most likely to be due to an offshore granite. A further low which extends from Quad 19 to Quad 20 represents a possible basin, potentially extending to depths in excess of 4 km (Profile C; Figure 36). There is a general correspondence with a zone of lower magnetic field values (Figure 28), which is compatible with this interpretation. A sharp local magnetic feature on the northern flank of the possible basin might be due to an intrusion into it or magnetic basement that extends to shallower depth than indicated by the model. The initial seismic interpretation did not detect any sub-Zechstein structures in this area, so the possibility of a granitic or Lower Palaeozoic sedimentary source for the anomaly cannot be excluded.

The fault zone that marks the southern margin of the Forth Approaches Basin is delineated by the gravity model, which suggests that is offset sinistrally at two locations on the eastern side of Quad 26 (Figure 32). These offsets are also recorded by magnetic anomalies associated the magnetic sources in the footwall of the bounding fault (Figure 33; see Section 2.2), enhancing the confidence with which they are identified. Profile B shows well intersections in this area that illustrate that a model that satisfies the basement proving in well 26/14-1 on the structural high to the south of the basin underestimates the Upper Palaeozoic sedimentary thickness at nearby well 26/08-1 within the basin. The average pre-Zechstein density measured in the latter well (2.38 Mg/m^3) is lower than that assumed in the modelling, so the mismatch is inferred to be due to the influence of basement density contrasts (relatively high density beneath the basin and/or low density beneath the high). Although the model depth calibration in the Forth Approaches Basin is poor, there are indications of internal structure that would be worth investigating further. In particular, there is an indication that it may be segmented by NNE-trending structures linked to the offsets resolved at its southern margin.

The Devil's Hole Granite forms a low in the gravity inversion surface (Figures 31 and 37). Magnetic anomalies occur over its central part (Figure 32), but not over possible eastward and westward extensions. The current seismic interpretation does not trace intra-Carboniferous/Devonian reflectors into this area, but the proving of Lower Palaeozoic rocks in well 27/3-1 just to the south of the western extension suggests an intrusive source for that.

There is a zone of apparent sedimentary thickening that extends from Quad 26 to the western side of Quad 28. In the north it is bounded by the high drilled by well 26/14-1. There is a southern limit at a gravity gradient which spans the Quad 26-27 boundary. The BIRPS (British

Institutions Reflection Profiling Syndicate) MOBIL-3 seismic reflection profile (Klemperer and Hobbs, 1991; Snyder and Hobbs, 1999) indicates some possible intra-Carboniferous reflectors dipping southwards towards a bounding fault which coincides with the latter feature (100-110 km on Profile B; Figure 35), although the seismic imaging quality is poor and hampered by multiples. A coincident gravity high and magnetic anomaly on the Quad 26/27 boundary about 20 km north of this margin is suggestive of a basic intrusion. The zone of apparent sedimentary thickening is broader in the vicinity of the Quad 28-29 boundary but the limited seismic mapping available provides meagre evidence for a thick Upper Palaeozoic sequence in this area (see the comparisons between top Cementstone horizon at c. 150 km on profile C (Figure 36) and 120 km on profile D (Figure 37)). A thickening of the Devonian sequence is possible, but comparison with results from well 27/10-1 (at about 77 km on profile D) suggests that there is an overestimate of depth to Lower Palaeozoic basement here, even allowing for the influence of the Devil's Hole Granite on the inversion. Comparison with the along-strike Southern Upland area suggests that low density Lower Palaeozoic rocks may contribute to this mismatch. There is a correlation between the grain of the gravity model across Quads 26-28 and that of magnetic anomalies associated with Permo-Carboniferous dykes, most notably a strong feature that extends in an ENE direction from Dunbar across the southern side of Quad 26 (Figure 32; Smythe, 1994). This suggests that cumulative dyke thickness may in places be great enough to influence the gravity field, although a more indirect association related to controlling basement structures may apply. There is also a coincidence between the gravity high in the east and a longer wavelength magnetic anomaly (e.g. at the north-east end of Profile E; Figure 38), suggesting an association there with either magnetic basement or more pervasive Permo-Carboniferous intrusion. The mismatch between gravity model and seismic interpretation in this area could thus be explained by the influence of high density rocks.

The gravity survey data indicate an offshore extension of the Oldhamstocks Basin at the north-east corner of Quad 33, but the coverage is too sparse to provide any detail in that area. Onshore, there is a gravity low which coincides with the Upper Palaeozoic outcrop, but an extension of this over the adjacent Lower Palaeozoic (Riccarton Group) inlier suggests that the latter rocks also contribute. This is compatible with observations over the main Lower Palaeozoic outcrop of the Southern Uplands where gravity gradients have been identified which have be ascribed to low density turbidite units combined with variations in their thickness above a higher density concealed layer (Akhurst et al., 2001; Kimbell et al., 2006). Farther offshore, beneath Profile A (Figure 34), the gravity inversion surface lies well below the locally mapped top Cementstone horizon.

Northward sedimentary thickening occurs across extrapolation of the the Pressen-Flodden-Ford axis up to about 150 km offshore (Figure 31). This axis marks the southern limit of the Tweed Basin in the west (Chadwick and Holliday, 1991) and is coincides with thickening identified in the current seismic interpretation on Profile C in the east (Figure 36), so does most likely represent an Upper Palaeozoic feature. A magnetic high to the south of the axis (Figure 32) could be due to the shallowing of magnetic basement or to a concentration of Permo-Carboniferous magmatism.

A gravity low associated with the Northumberland Trough extends 40-50 km offshore. The model was constrained in this area by an estimated basement depth of 2 km on the CSSP seismic refraction profile where it crosses Profile A (Figure 34; Green, 1984); this lies close to the local top Cementstone pick. The model predicts that basement deepens southwards to 3-4 km before shallowing across the extension of the Ninety Fathom fault system. This is broadly compatible with a projection of the onshore structure of the basin interpreted by Chadwick et al. (1995), although the Ninety Fathom Fault forms a sharper step in the latter interpretation. An apparent coast-parallel, intra-basin high 15-20 km offshore coincides with a data gap, so further survey is required to establish whether it is real. The modelled eastern margin of the basin has a north-south orientation and appears to forms against a block underpinned by the Farne Granite and its probable westward extension (Figure 31). The Farne Granite is relatively magnetic (Figure 32),

but farther south the Teeside Granite is less magnetic than the basement it intrudes, similar to the North Pennine (Weardale) granite batholith (Figure 32; Kimbell et al., 2010).

Seismic surveys identify a basin in the southern part of Quad 29 (Arsenikos et al., 2015). Seismic and gravity models are in agreement at the southern edge of this quad, but the gravity inversion surface lies above the top Kyle Limestone horizon farther north, as indicated by the central part of profile F (Figure 39) and eastern end of Profile G (Figure 40). The gravity model is distorted in this area due to the use of an initial version of the seismic model (Figure 27; Profile G), but relatively high density basement may also have an influence.

The north-eastern margin of the North Dogger Basin is well-resolved by the gravity model (see the eastern ends of profiles H and I; Figures 41 and 42). The south-western part of the basin has a smaller amplitude than indicated by seismic mapping on profile I (see the contrasting geometries at 200-210 km; Figure 42) and J (e.g. 140-160 km; Figure 43).

The Dogger Granite is clearly identifiable as a low in the gravity inversion surface that coincides with a structural high in the seismic interpretation. This granite is responsible for a strong magnetic anomaly (Figure 42) and the map view (Figure 32) indicates a likely extension with a north-south orientation at the southern edge of Quad 36. An east-west oriented low in the inversion surface in the northern part of Quad 44 coincides with a structural high (60-80 km on Profile J; Figure 43) and a magnetic anomaly (Figure 32), so is also identified as a possible granite.

Two relative lows in the gravity inversion surface occur in the vicinity of the Quad 36/37 boundary. The feature to the west has a north-east trend and the feature to the east has a northward trend. The coincidence of the latter with a structural high (c. 160 km on Profile H; Figure 41) suggests that a granite may be present. However the lack of a coincident magnetic anomaly (Figure 32) and the correlation with a modest Upper Palaeozoic sedimentary thickening (Figure 41) reduce the confidence with which this can be identified. The north-east-trending feature coincides with a seismically-defined sedimentary thickening (230-250 km on Profile C; Figure 36), albeit with greater amplitude, but also has a conspicuous magnetic anomaly (Figures 32 and 36). A local Upper Devonian thickening above a low density, presumably Lower Devonian, pluton appears incongruous, and highly magnetic Lower Devonian extrusive rocks at depth within the basin provide a possible alternative explanation. Magnetic Devonian lavas are observed in the vicinity of the Cheviot Granite but the strongest magnetisation is associated with contact metamorphism adjacent to that granite (Lee, 1982 and references therein) and thus does not provide a convincing analogue.

There is a correlation between a deepening of the gravity inversion surface and that of the top Kyle Limestone reflector on the northern and eastern sides of the Silverpit Basin (e.g. the southern end of Profile C (Figure 36) and 60-80 km on Profile I (Figure 42)). The top Kyle Limestone reflector cannot be traced into the deepest parts of the basin predicted by the gravity model (see the southern ends of profiles B and I; Figures 35 and 42), so theoretically an alternative source (e.g. a granite) could apply there, although structural continuity suggests that a deepening of the basin is more likely. The locally very deep basement indicated by the gravity inversion in Quad 42 coincides with an area of probable model distortion and is regarded as suspect. An impediment to the preferred explanation for the Silverpit Basin gravity anomaly is the combination of relatively shallow top Cementstone horizon observed in Quad 42 and the high density (c. 2.70 Mg/m^3) of the Upper Devonian rocks intersected by well 42/10b-2. The latter intersection comprised rocks of the Tayport Formation, which are probably underlain by sandstones of the Buchan Formation and these are likely to be less dense, providing a possible explanation.

Immediately to the west of the thick modelled sedimentary sequence in the Silverpit Basin is an area straddling the Quad 41/42 boundary where the modelled sedimentary thickness is much less than the seismic thickness (e.g. south-west end of Profile H; Figure 45). The coincidence of this anomaly with the Sole Pit axis of Japsen (2000) strongly suggests an association with

overcompaction in the pre-Chalk sequence along that axis, which was not allowed for in the density model. The 'ramp' in the model between the two areas seems very sharp when compared with the limited data available on rock densities across it (e.g. Figure 20a) so this area is recommended for more detailed modelling, particularly in view of the coincidence with the Breagh gas field. Until such modelling is done it is not possible to discount a basement influence. The anomalous zone extends north of the Sole Pit axis identified by Japsen (2000) into the undrilled south-eastern part of Quad 35 (Figure 32), with the 'ramp' lying just to the east of the Quad 35/36 boundary (Figure 31). This extension presents a suitable target for follow-up.

The southern part of the study area is crossed by east-south-east-trending Palaeogene dykes (Figure 32), which parallel the structural trends in the area and may have influenced halokenesis (Underhill, 2009). The present results indicate a change in trend or splay of the Blyth dyke in the south-east corner of the study area which closely follows the structural trend within the Silverpit Basin.

6 Conclusions

This project aimed to identify possible Upper Palaeozoic basins in the Central North Sea where poor seismic coverage and quality had prevented their earlier discovery. This has been attempted by identifying low-density pre-Zechstein bodies by gravity modelling and distinguishing those with a probable sedimentary origin from those associated with Late Caledonian granite plutons. The procedure required the removal of the gravity effect of the Zechstein and younger sequence, and a density model for that sequence was constructed which employed predictions based on compaction effects and burial anomalies in the post-Zechstein units and a relationship between thickness and average density in the Zechstein sequence.

Isolation of the gravity effect of the pre-Zechstein targets required removal of a background field, and this is regarded as the step in the methodology that is most vulnerable to error. An initial long-wavelength background has been defined but this is appropriate for refinement in any further iterations of the modelling.

A number of targets for further investigation have been identified (Figure 44):

(i) A possible basin spanning the Quad 19/20 boundary.
(ii) Further possible basins in a zone extending from Quad 26 to Quad 28. The modelling of these is likely to be distorted by the influence of underlying, relatively low density Lower Palaeozoic rocks, but the feature spanning the Quad 26/27 boundary has some support from legacy seismic data and is the most promising lead in this area.
(iii) Sedimentary thickening to the north of the extrapolation of the Pressen-Flodden-Ford line.
(iv) The enigmatic gravity features straddling the Quad 36/37 boundary.
(v) A 'ramp' in the model in Quads 42 and 36 that appears to relate, at least in part, to lateral density changes associated with the Sole Pit compaction anomaly, and which coincides with the Breagh gas field in the south.
(vi) Although they are not 'undiscovered', the offshore extensions of the Northumberland Trough and Oldhamstocks Basin are not well-imaged by legacy seismic data and would benefit from more detailed investigation.

The gravity modelling results should provide supplementary information in areas where seismic mapping has provided the primary tool (e.g. providing a complementary view of the internal structure of the basins), and the digital deliverables include the gravity inversion surface in both depth and two-way-travel-time to facilitate this.

It is particularly easy to make recommendations for future work, because a key step has already been taken in the form of a new government-funded geophysical survey across the region which

was conducted during 2015. This involved the acquisition of a set of long-offset seismic reflection profiles together with coincident gravity and magnetic surveys. The data are currently being processed and are due for release in the first quarter of 2016. High quality seismic data, combined with substantially enhanced gravity and magnetic coverage, will provide an opportunity for much firmer identification and confirmation of targets. The multiparameter data acquisition will lend itself to detailed seismic/gravity/magnetic profile modelling, which is the key to separating cover sequence and basement signatures.

While this primary focus of future geophysical investigations is self-evident, it is worth noting that such investigations could be aided and supplemented by further rock physical property analysis. Progress has been made on defining predictive models for rock densities but these could be augmented by the incorporation of further well data combined with more detailed seismic interpretation. Figure 1 illustrates that there are wells within the area of interest that have not yet been included in the density study. The results of Japsen (1998, 1999, 2000) have been invaluable but they can be enhanced. The establishment of Central North Sea velocity and density models could underpin a range of future projects, particularly if made generally available. An example of the velocity component of such a resource is provided by the Velmod model for the Dutch sector (Van Dalfsen et al., 2006, 2007). In addition to their obvious applications in depth-conversion and gravity modelling, such property models could form the basis of the investigation of burial anomalies that would help to understand the geodynamic evolution of the region.

Appendix 1 Digital deliverables

The digital deliverables comprise georeferenced geophysical images and grids and contour files of the outputs from the gravity modelling. All these are referred to UTM Zone 31 (ED50).

GEOPHYSICAL IMAGES

cns_grav_ba_csrn.jpg	Bouguer gravity anomaly, illuminated from the north. Reduction density is variable onshore and 2.2 Mg/m^3 offshore. Shown in Figure 4.
cns_grav_ba_resid_csrn.jpg	Residual Bouguer anomaly, illuminated from the north. Calculated by removal of a 10 km upward continuation.
cns_grav_ba_resid_csrs.jpg	Residual Bouguer anomaly, illuminated from the south. Calculated by removal of a 10 km upward continuation. Shown in Figures 5 and 9.
cns_mag_tmi_csrn.jpg	Total magnetic intensity, illuminated from the north. Shown in Figure 6.
cns_mag_rtp_csrn.jpg	Reduced-to-pole magnetic field, illuminated from the north. Shown in Figure 7.
cns_mag_rtp_resid_csrn.jpg	Residual reduced-to-pole magnetic field, illuminated from the north. Calculated by removal of a 10 km upward continuation. Shown in Figures 8, 28 and 32.
cns_mag_pseud_csrn.jpg	Pseudogravity anomaly calculated from the magnetic field. Illuminated from the north.
cns_mag_pseud_resid_csrn.jpg	Residual pseudogravity anomaly, illuminated from the north. 8^{th} degree high-pass Butterworth filter with a central wavelength of 200 km.

The subfolder **extended_north_sea_images** contains the same set of images extended over a region that incorporates both the Central North Sea and Moray Firth – Orcadian Basin study areas. The colour scales used for these are not optimum for the individual study areas but they are useful for identifying regional patterns.

MODEL GRIDS

The model grids all have a 2.5 km grid node spacing, but the structural grids were derived by interpolation from input grids with a 5 km node spacing. The grids are provided in ESRI (ArcGIS), ESRI binary (flt), Zmap, Geosoft, and ASCII (xyz) formats. Layer files are included with the first of these which contain the colour symbology used in displaying these grids in the current report.

ginv_v1_gobs	Observed gravity field (free-air anomalies offshore, Bouguer anomalies onshore) (mGal). Shown in Figure 22.
ginv_v1_gcalz	Calculated gravity effect of sequence down to base Zechstein (mGal). Shown in Figure 23.
ginv_v1_gcalc	Calculated gravity field of full model (mGal). Shown in Figure 29
ginv_v1_bzech	Depth to base Zechstein in the gravity model (m)
ginv_v1_dep	Depth to the gravity inversion surface (m). Shown in Figure 26.

ginv_v1_pzthk	Thickness between base Zechstein and the gravity inversion surface (m). Shown in Figures 27, 31, 33 and 44.
ginv_v1_twt	The gravity inversion surface expressed as two-way travel time (ms; positive downward). This grid only covers the offshore area.
ginv_v1_twtng	The gravity inversion surface expressed as two-way travel time (ms; negative downward). This grid only covers the offshore area.
ginv_v1_bkgrd	Assumed background field (mGal). Shown in Figure 24.
ginv_v1_strip	Gravity field after removal of the gravity effect to base Zechstein and the background field (mGal). Shown in Figure 25.
ginv_v1_gres	Residual gravity anomalies over the full model (observed gravity - calculated gravity - background) (mGal). Shown in Figure 30.

CONTOUR SHAPEFILES

grav_inversion_depth_contours_v1	Contours of ginv_v1_dep at 500 m intervals. Shown in Figure 26.
pre_zechstein_thickness_contours_v1	Contours of ginv_v1_pzthk at 500 m intervals. Shown in Figures 27, 28, 31, 32, 33 and 44. The zero contour has been removed to provide a cleaner display.

Appendix 2 Supplementary rock density information

The supplementary information on rock densities comprises digital files compiled during the analysis of digital density logs.

DENSITY LOGS FOR INDIVIDUAL WELLS

Plots of the density logs for individual wells are provided in the PDF files described below. In these the corrected saturated bulk density values from the log are plotted against depth below seabed and annotated with markers based on the DECC well tops database (i.e. not including refinements resulting from the present project). An example of one of these plots is provided in Figure 10 of this report. Some wells used have been omitted from these collections for confidentiality reasons.

WellPlotsWithModelMarkers.pdf	Plots of density logs from wells used in the study, with the regionally interpreted markers used in the gravity modelling superimposed. TC = top Chalk, BC = base Chalk, TZ = top Zechstein, BZ = base Zechstein, LP = top Carboniferous and older.
WellPlotsWithChronostratMarkers.pdf	Plots of density logs from wells used in the study, with DECC well tops superimposed. Q = top Quaternary, N = top Neogene, G = top Palaeogene, K = top Cretaceous, J = top Jurassic, TU = top Upper Triassic, TL = top Lower Triassic, T = top Triassic (undifferentiated), PU = top Upper Permian, PL = top Lower Permian, P = top Permian (undifferentiated), C = top Carboniferous, D = top Devonian

SUMMARY DENSITIES

For each model layer defined by regional seismic picks, the logged density values were collated and used to produce summary plots shown in the first PDF file listed below. At each well, the average density for each layer was computed, and these values are given in the spreadsheet. Finally, plots were also produced summarising the density values according to the DECC chronostratigraphic intervals, and these are given in the second PDF file listed below.

SummaryPlotsByModelLayer.pdf	Summary density plots for the five model layers defined by regional seismic picks. Data points are coloured by quadrant number.
AverageWellDensitiesPerModelLayer.xlsx	Spreadsheet of average density per model layer for each well used in the study.
SummaryPlotsByInterval.pdf	Summary density plots by chronostratigraphic interval (Q = Quaternary, N = Neogene, G = Palaeogene, K = Cretaceous, J = Jurassic, T = Triassic, PU = Upper Permian, PL = Lower Permian, C = Carboniferous, D = Devonian)

DENSITY MAPS

For each layer, the average value per well was mapped out across the study area using kriging in ArcGIS's Geostatistical Wizard. For layers 1 - 3 ordinary kriging was used, using the 'stable' variogram model, while for layer 5 empirical Bayesian kriging was used. The interpolation of layer 4 was handled using regression kriging in the 'gstat' geostatistical package in R (Pebesma, 2004) using an exponential variogram model. Kriged density maps for layers 1 to 5 are given in the PDF file below.

LayerDensityMaps.pdf	Maps of average layer densities for the five model layers defined by regional seismic picks

BURIAL ANOMALIES

The deviation of measured densities from the normal compaction curves of Sclater and Christie (1980) can be characterised at each well by a burial anomaly, defined as the amount by which the depth must be shifted so as to fit the measured data to the theoretical curves. This is a simplified version of the approach of Japsen (1998, 1999, 2000), who used sonic log data to establish the burial history of formations in the North Sea.

The PDF file below contains a set of plots for the Carboniferous sequence in individual wells, in each of which the normal compaction relationships were fitted to the measured densities by least-squares, adjusting the depth offset required to achieve a fit. Applying this procedure for the compaction relationships ("chalk", "sand", "shaly sand" and "shale") gives four estimates of burial anomaly for each well, from which one was selected based on the known dominant lithology for the interval. It is recognised that these are simple estimates that may be affected by factors including lithological and diagenetic variations. An attempt at a similar approach to the Devonian densities did not provide satisfactory results.

CarboniferousCompactionPlots.pdf	Plots of density log data for the Carboniferous, illustrating the burial anomaly required to fit the normal compaction curves of Sclater & Christie (1980)
CarboniferousBurialAnomalies.xlsx	Spreadsheet of burial anomalies (km) for the Carboniferous computed using curve matching. Negative values indicate apparent uplift.

References

British Geological Survey holds most of the references listed below, and copies may be obtained via the library service subject to copyright legislation (contact libuser@bgs.ac.uk for details). The library catalogue is available at: https://envirolib.apps.nerc.ac.uk/olibcgi.

AKHURST, M C, MCMILLAN, A A, KIMBELL, G S, STONE, P, and MERRIMAN, R J. 2000. Silurian subduction-related assembly of fault-defined tracts at the Laurieston Fault, Southern Uplands accretionary terrane, Scotland, U.K. *Earth and Environmental Science Transactions of the Royal Society of Edinburgh*, Vol. 91, 435-446.

ARSENIKOS, S, QUINN, M, PHARAOH, T C, SANKEY, M, and MONAGHAN, A. 2015. Seismic interpretation and generation of key depth structure surfaces within the Carboniferous and Devonian of the Central North Sea, Quadrants 25-44. *British Geological Survey Commissioned Report* CR/15/118.

BAMFORD, D. 1979. Seismic constraints on the deep geology of the Caledonides of northern Britain. *Geological Society, London, Special Publications*, Vol. 8, 93-96.

BANKA, D, PHARAOH, T C, WILLIAMSON, J P, LEE, M, THYBO, H, WYBRANIEC, S, and CORE, T P P F. 2002. Potential field imaging of Palaeozoic orogenic structure in northern and central Europe. *Tectonophysics*, Vol. 360, 23-45.

BARRON, H F, PHILLIPS, E R, and FLOYD, J D. 2004. The Lamington Conglomerate: further evidence for an ophiolitic source for the Ordovician Marchburn Formation, Northern Belt, Southern Uplands. *Scottish Journal of Geology*, Vol. 40, 7-12.

BARTON, P J. 1992. LISPB revisited - a new look under the Caledonides of northern Britain. Geophysical Journal International, Vol. 110, 371-391.

BARTON, P, and WOOD, R. 1984. Tectonic evolution of the North Sea basin: crustal stretching and subsidence. *Geophysical Journal of the Royal Astronomical Society*, Vol. 79, 987-1022.

BLUCK, B J. 2013. Geotectonic evolution of Midland Scotland from Cambrian to Silurian: a review. *Scottish Journal of Geology*, Vol. 49, 105-116.

BOTT, M H P. 1967. Geophysical investigations of the northern Pennine basement rocks. *Proceedings of the Yorkshire Geological and Polytechnic Society*, Vol. 36, 139-168.

BOTT, M H P, LONG, R E, GREEN, A S P, LEWIS, A H J, SINHA, M C, and STEVENSON, D L. 1985. Crustal structure south of the Iapetus Suture beneath northern England. *Nature*, Vol. 314, 724-727.

CARTWRIGHT, J, STEWART, S, and CLARK, J. 2001. Salt dissolution and salt-related deformation of the Forth Approaches Basin, UK North Sea. *Marine and Petroleum Geology*, Vol. 18, 757-778.

CHADWICK, R A, and HOLLIDAY, D W. 1991. Deep crustal structure and Carboniferous basin development within the Iapetus convergence zone, northern England. *Journal of the Geological Society*, Vol. 148, 41-53.

CHADWICK, R A, HOLLIDAY, D W, HOLLOWAY, S and HULBERT, A G. 1995. The structure and evolution of the Northumberland-Solway Basin and adjacent areas. *Subsurface Memoir of the British Geological Survey*.

CRUDEN, A R, and MCCAFFREY, K J W. 2001. Growth of plutons by floor subsidence: implications for rates of emplacement, intrusion spacing and melt extraction mechanisms. *Physics and Chemistry of the Earth (A)*, Vol. 26, 303-315.

DONATO, J A. 1993. A buried granite batholith and the origin of the Sole Pit Basin, UK Southern North Sea. *Journal of the Geological Society*, Vol. 150, 255-258.

DONATO, J A, MARTINDALE, W, and TULLY, M C. 1983. Buried granites within the Mid North Sea High. *Journal of the Geological Society*, Vol. 140, 825-837.

DONATO, J A, and MEGSON, J B. 1990. A buried granite batholith beneath the East Midland Shelf of the Southern North Sea Basin. *Journal of the Geological Society*, Vol. 147, 133-140.

FLOYD, J D. 1999. Geology of the country around Carrick and Loch Doon. *Memoir of the British Geological Survey*, Sheet 8 (Scotland).

FLOYD, J D, and KIMBELL, G S. 1995. Magnetic and tectonostratigraphic correlation at a terrane boundary - the Tappins Group of the Southern Uplands. *Geological Magazine*, Vol. 132, 515-521.

FREEMAN, B, KLEMPERER, S L, and HOBBS, R W. 1988. The deep structure of northern England and the Iapetus Suture zone from BIRPS deep seismic reflection profiles. *Journal of the Geological Society*, Vol. 145, 727-740.

GRAHAM, A G C, LONERGAN, L, and STOKER, M S. 2010. Depositional environments and chronology of Late Weichselian glaciation and deglaciation in the central North Sea. *Boreas*, Vol. 39, 471-491.

GRAHAM, A G C, STOKER, M S, LONERGAN, L, BRADWELL, T, and STEWART, M S. 2011. The Pleistocene Glaciations of the North Sea Basin. 261-278 in *Quaternary glaciations - extent and chronology. A closer look*. Developments in Quaternary Science, Vol. 15. (Amsterdam, The Netherlands: Elsevier.)

GRANBY ENTERPRISES LIMITED and TGS-NOPEC GEOPHYSICAL COMPANY (UK) LIMITED. 2008. Promote License P1315, End of License Report, https://itportal.decc.gov.uk/web_files/relinqs/p1315.pdf.

GREEN, A S P. 1984. The crustal structure beneath northern England and adjacent sea areas. Unpublished PhD thesis, Durham University. Available at Durham E-Theses Online: http://etheses.dur.ac.uk/7845/.

JAPSEN, P. 1998. Regional velocity-depth anomalies, North Sea Chalk: A record of overpressure and neogene uplift and erosion. *AAPG Bulletin*, Vol. 82, 2031-2074.

JAPSEN, P. 1999. Overpressured Cenozoic shale mapped from velocity anomalies relative to a baseline for marine shale, North Sea. *Petroleum Geoscience*, Vol. 5, 321-336.

JAPSEN, P. 2000. Investigation of multi-phase erosion using reconstructed shale trends based on sonic data. Sole Pit axis, North Sea. *Global and Planetary Change*, Vol. 24, 189-210.

KIMBELL, G S, CHADWICK, R A, HOLLIDAY, D W, and WERNGREN, O C. 1989. The structure and evolution of the Northumberland Trough from new seismic reflection data and its bearing on modes of continental extension. *Journal of the Geological Society, London*, Vol. 146, 775-787.

KIMBELL, G S, and QUIRK, D G. 1999. Crustal magnetic structure of the Irish Sea region: evidence for a major basement boundary beneath the Isle of Man. *Geological Society, London, Special Publications*, Vol. 160, 227-238.

KIMBELL, G S, GATLIFF, R W, RITCHIE, J D, WALKER, A S D, and WILLIAMSON, J P. 2004. Regional three-dimensional gravity modelling of the NE Atlantic margin. *Basin Research*, Vol. 16, 259-278.

KIMBELL, G S, CARRUTHERS, R M, WALKER, A S D, and WILLIAMSON, J P. 2006. *Regional Geophysics of Southern Scotland and Northern England*. Version 1.0 on CD-ROM. (Keyworth, Nottingham: British Geological Survey.)

KIMBELL, G S, YOUNG, B, MILLWARD, D, and CROWLEY, Q G. 2010. The North Pennine batholith (Weardale Granite) of northern England: new data on its age and form. *Proceedings of the Yorkshire Geological Society*, Vol. 58, 107-128.

KLEMPERER, S L and HOBBS, R W. 1991. *The BIRPS Atlas. Deep seismic reflection profiles around the British Isles*. (Cambridge: Cambridge University Press.)

LAGIOS, E. 1983. A gravity study of the eastern Berwickshire Devonian basins, SE Scotland. *Scottish Journal of Geology*, Vol. 19, 189-203.

LAGIOS, E, and HIPKIN, R G. 1979. The Tweeddale Granite - a newly discovered batholith in the Southern Uplands. *Nature*, Vol. 280, 672-675.

LEE, M K. 1982. The regional geophysics of the Cheviot area. *British Geological Survey Technical Report* WE/EN/82/002.

LYNGSIE, S B, and THYBO, H. 2007. A new tectonic model for the Laurentia-Avalonia-Baltica sutures in the North Sea: A case study along MONA LISA profile 3. *Tectonophysics*, Vol. 429, 201-227.

LYNGSIE, S B, THYBO, H, and RASMUSSEN, T M. 2006. Regional geological and tectonic structures of the North Sea area from potential field modelling. *Tectonophysics*, Vol. 413, 147-170.

MCCAUGHEY, M, BARTON, P J, and SINGH, C S. 2000. Joint traveltime inversion of wide-angle seismic data and a deep reflection profile from the central North Sea. *Geophysical Journal International*, Vol. 141, 100-114.

MILTON-WORSSELL, R, SMITH, K, MCGRANDLE, A, WATSON, J, and CAMERON, D. 2010. The search for a Carboniferous petroleum system beneath the Central North Sea. 57-75 in *Petroleum Geology—From mature basins to new frontiers. Proceedings of the 7th Petroleum Geology Conference*. VINING, B, and PICKERING, S (editors). (London: The Geological Society.)

PEBESMA, E J. 2004. Multivariable geostatistics in S: the gstat package. *Computers and Geosciences*, Vol. 30, 683-691.

PETFORD, N, and CLEMMENS, J D. 2000. Granites are not diapiric! *Geology Today*. September-October issue, 180-184.

PHARAOH, T C, BREWER, T S, and WEBB, P C. 1993. Subduction-related magmatism of late Ordovician age in eastern England. *Geological Magazine*, Vol. 130, 647-656.

ROLLIN, K E. 2009. Regional Geophysics of Northern Scotland. Version 1.0 on CD-ROM. (Keyworth, Nottingham: British Geological Survey.)

SCHECK, M, BAYER, U, OTTO, V, LAMARCHE, J, BANKA, D, and PHARAOH, T. 2002. The Elbe Fault System in North Central Europe—a basement controlled zone of crustal weakness. *Tectonophysics*, Vol. 360, 281-299.

SCLATER, J G, and CHRISTIE, P A F. 1980. Continental stretching: An explanation of the Post-Mid-Cretaceous subsidence of the central North Sea Basin. *Journal of Geophysical Research: Solid Earth*, Vol. 85, 3711-3739.

SINGH, S C, HAGUE, P J, and MCCAUGHEY, M. 1998. Study of the crystalline crust from a two-ship normal-incidence and wide-angle experiment. *Tectonophysics*, Vol. 286, 79-91.

SMYTHE, D K. 1994. Geophysical evidence for ultrawide dykes of the late Carboniferous quartz-dolerite swarm of northern Britain. *Geophysical Journal International*, Vol. 119, 20-30.

SNYDER, D and HOBBS, R. 1999. *The BIRPS Atlas II, A Second Decade of Deep Seismic Reflection Profiling*. (London: The Geological Society.)

SOPER, N J, ENGLAND, R W, SNYDER, D B, and RYAN, P D. 1992. The Iapetus suture zone in England, Scotland and eastern Ireland: a reconciliation of geological and deep seismic data. *Journal of the Geological Society*, Vol. 149, 697-700.

STONE, P, and MCMILLAN, A A. 2013. Regional geochemical patterns in SE Scotland: source lithology, inheritance and glacial overprinting. *Scottish Journal of Geology*, Vol. 49, 33-40.

UNDERHILL, J R. 2009. Role of intrusion-induced salt mobility in controlling the formation of the enigmatic 'Silverpit Crater', UK Southern North Sea. *Petroleum Geoscience*, Vol. 15, 197-216.

VAN DALFSEN, W, DOORNENBAL, J C, DORTLAND, S, and GUNNICK, J L. 2006. A comprehensive seismic velocity model for the Netherlands based on lithostratigraphic layers. *Netherlands Journal of Geosciences (Geologie en Mijnbouw)*, Vol. 85, No. 4, 277-292.

VAN DALFSEN, W, VAN GESSEL, S F, and DOORNENBAL, J C. 2007. *Velmod-2*. TNO Report 2007-U-R1272C. Available online at: http://www.nlog.nl/resources/VELMOD2/Dalfsen%20et%20al.%20(2007).pdf.

VIGNORESSE, J-L, TIKOFF, B, and AMÉGLIO, L. 1999. Modification of the regional stress field by magma intrusion and formation of tabular granitic plutons. *Tectonophysics*, Vol. 302, 203-224.

WILLIAMSON, J P, PHARAOH, T C, BANKA, D, THYBO, H, LAIGLE, M, and LEE, M K. 2002. Potential field modelling of the Baltica-Avalonia (Thor-Tomquist) suture beneath the southern North Sea. *Tectonophysics*, Vol. 360, 47-60.

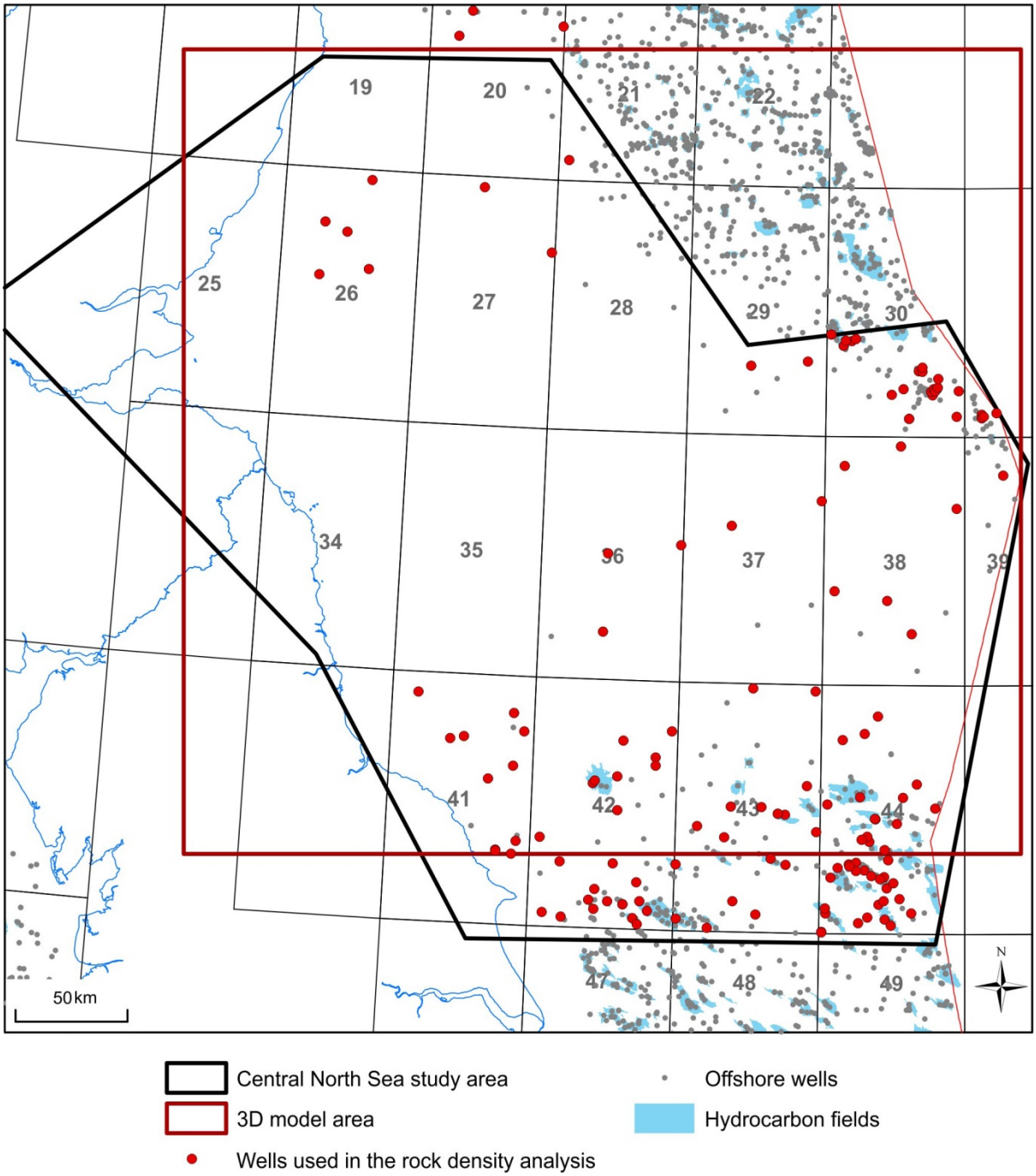

Figure 1 Area covered by the study

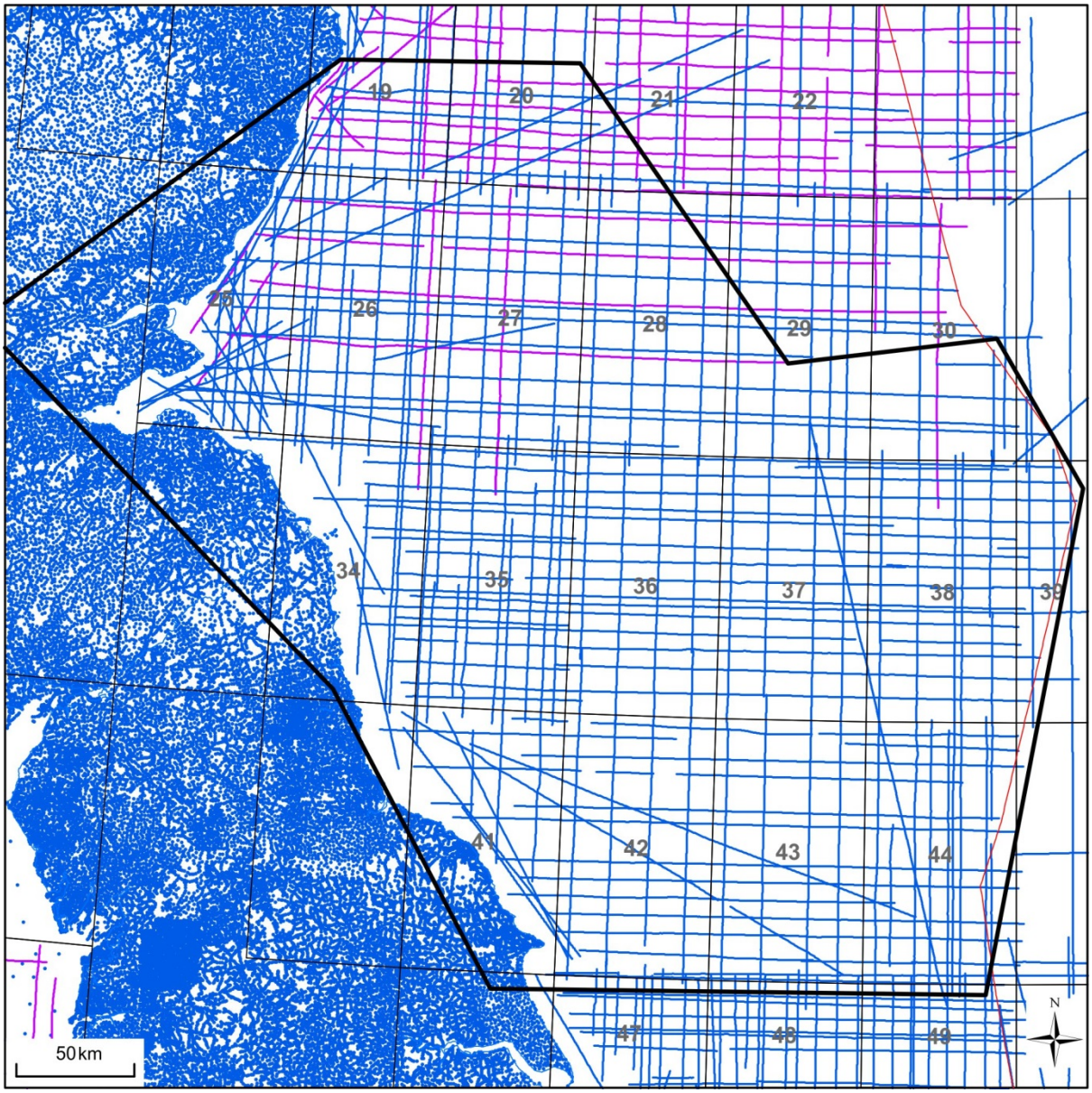

Figure 2 Locations of gravity observations from the BGS database. Blue lines and dots are marine tracklines (digitally acquired) and land/seabed gravity stations respectively. Purple lines are marine surveys that were acquired in analogue form and subsequently digitised.

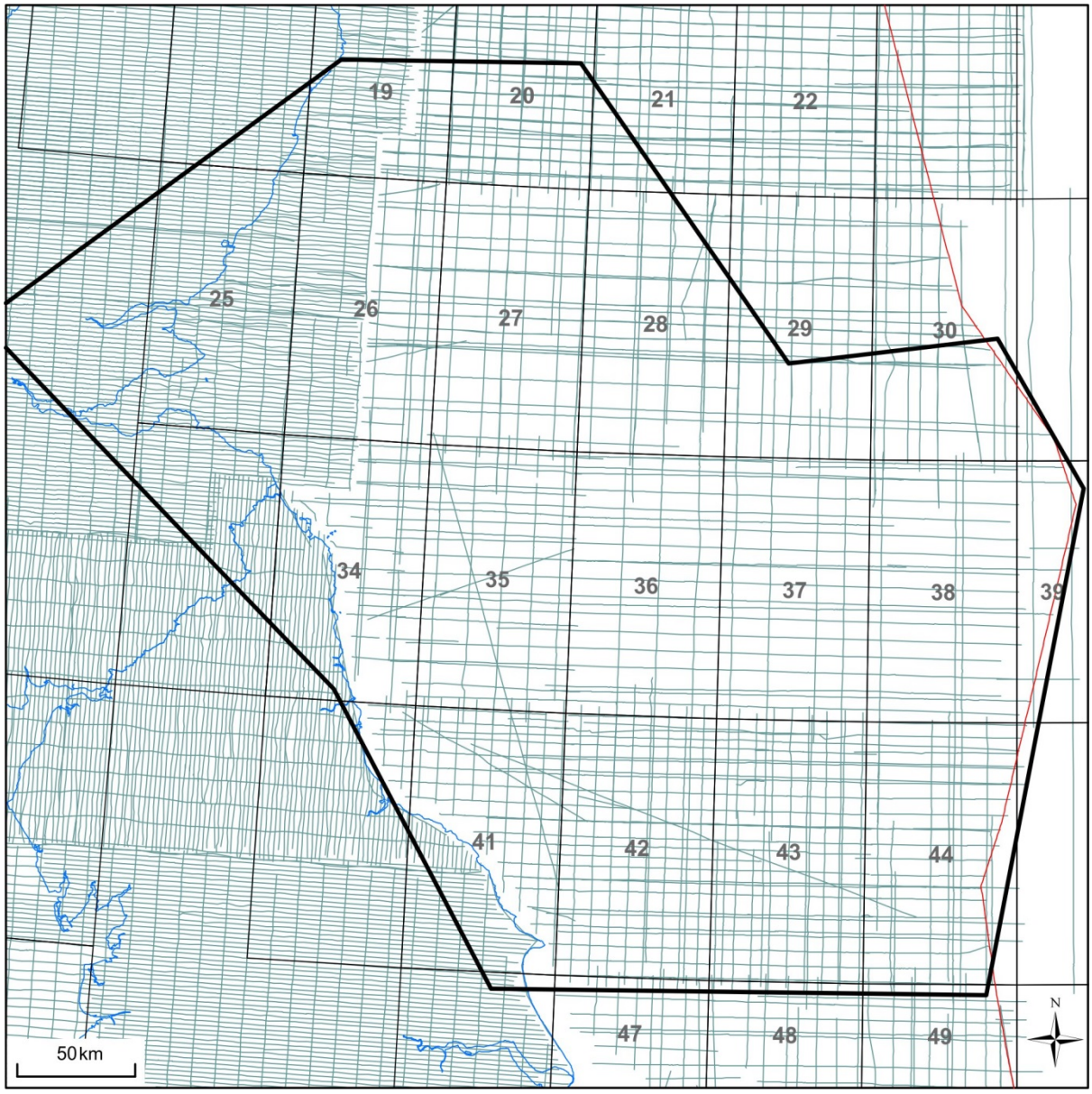

Figure 3 Magnetic survey lines from the BGS database (aeromagnetic surveys in the west and marine magnetic surveys in the east)

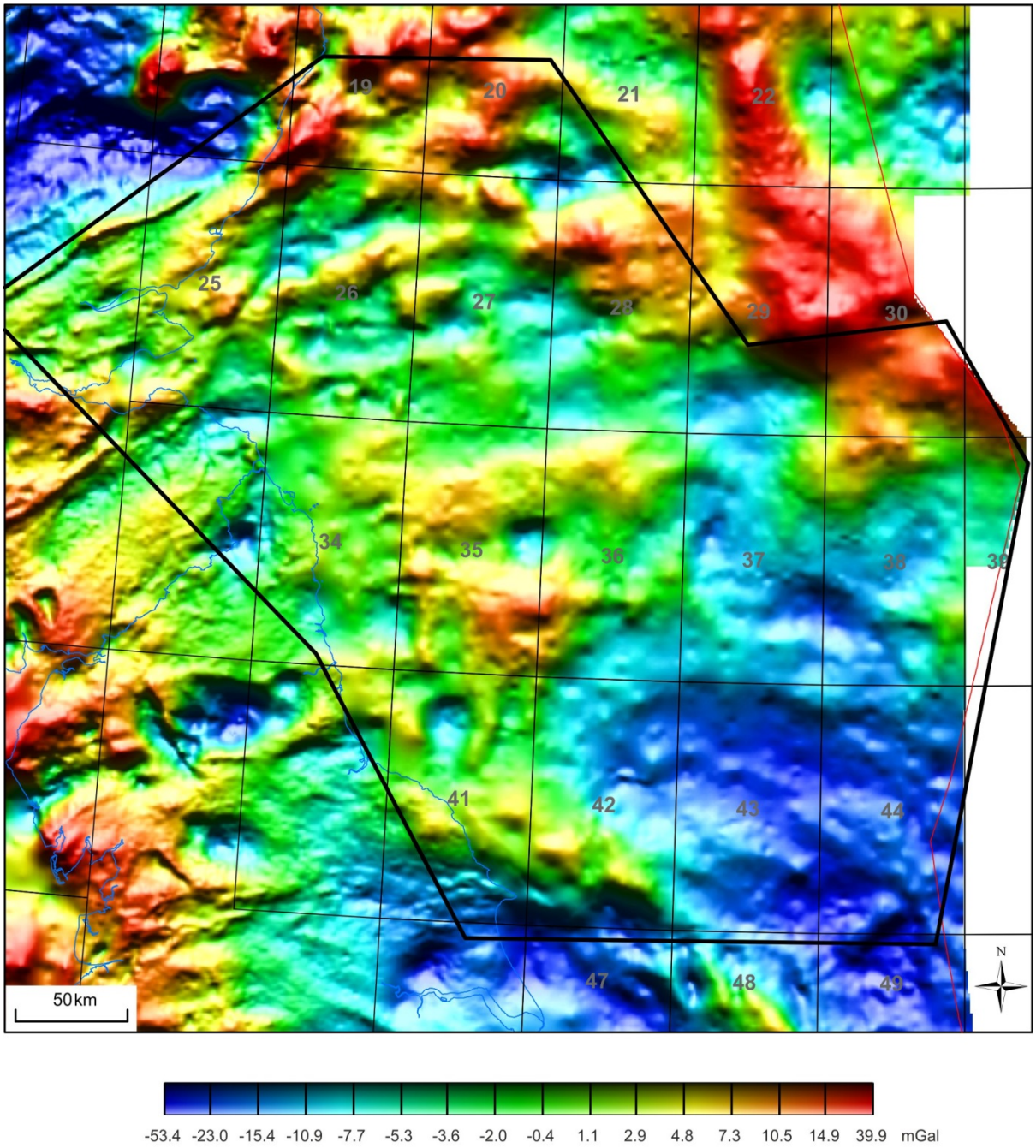

Figure 4 Bouguer gravity anomaly image with equal colour area and illumination from the north. Bouguer reduction density is 2.2 Mg/m^3 in the offshore area and variable (based on surface geology) in the onshore area.

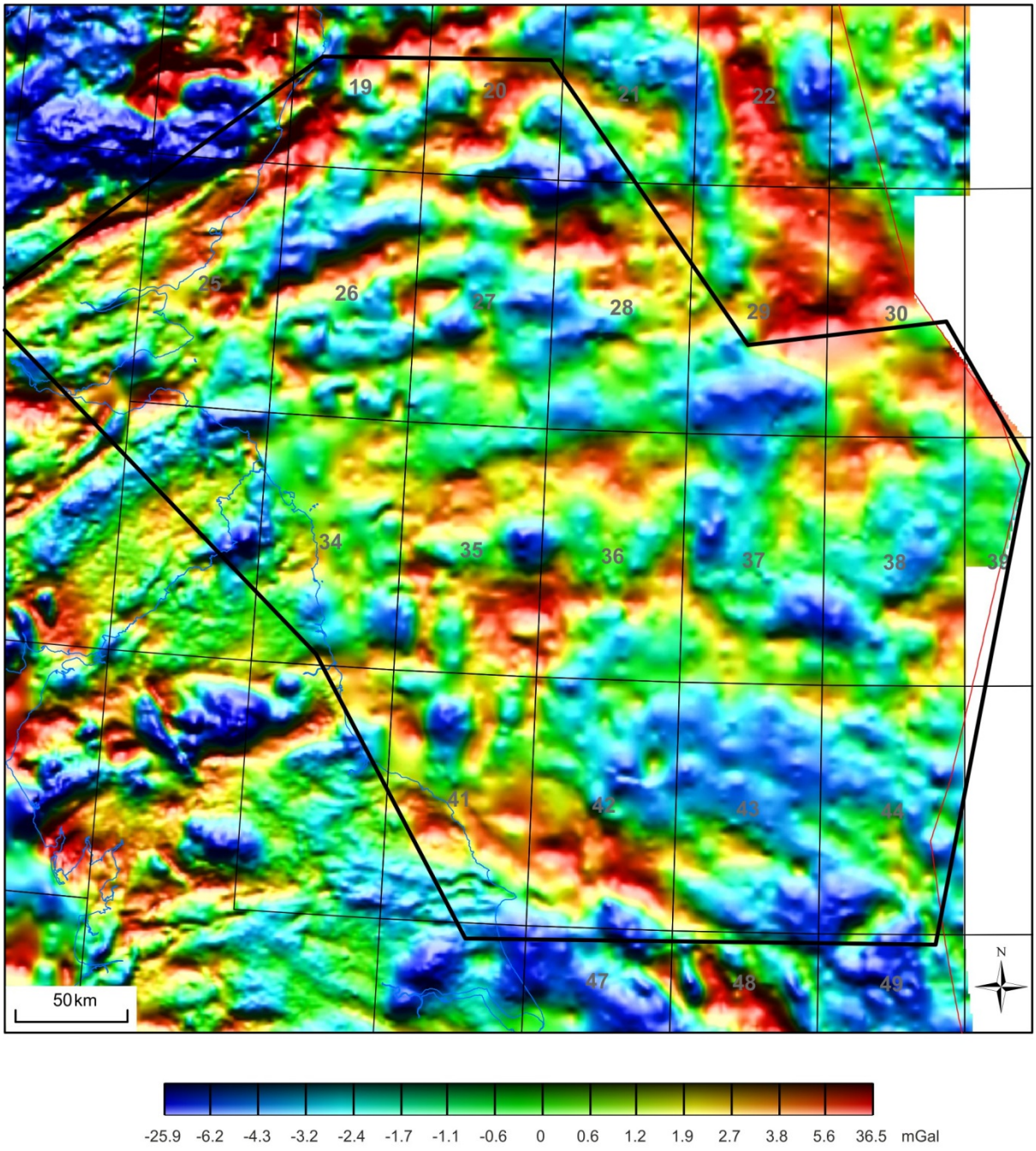

Figure 5 Residual Bouguer gravity anomaly, calculated by removal of a 10 km upward continuation. Equal colour area with illumination from the south.

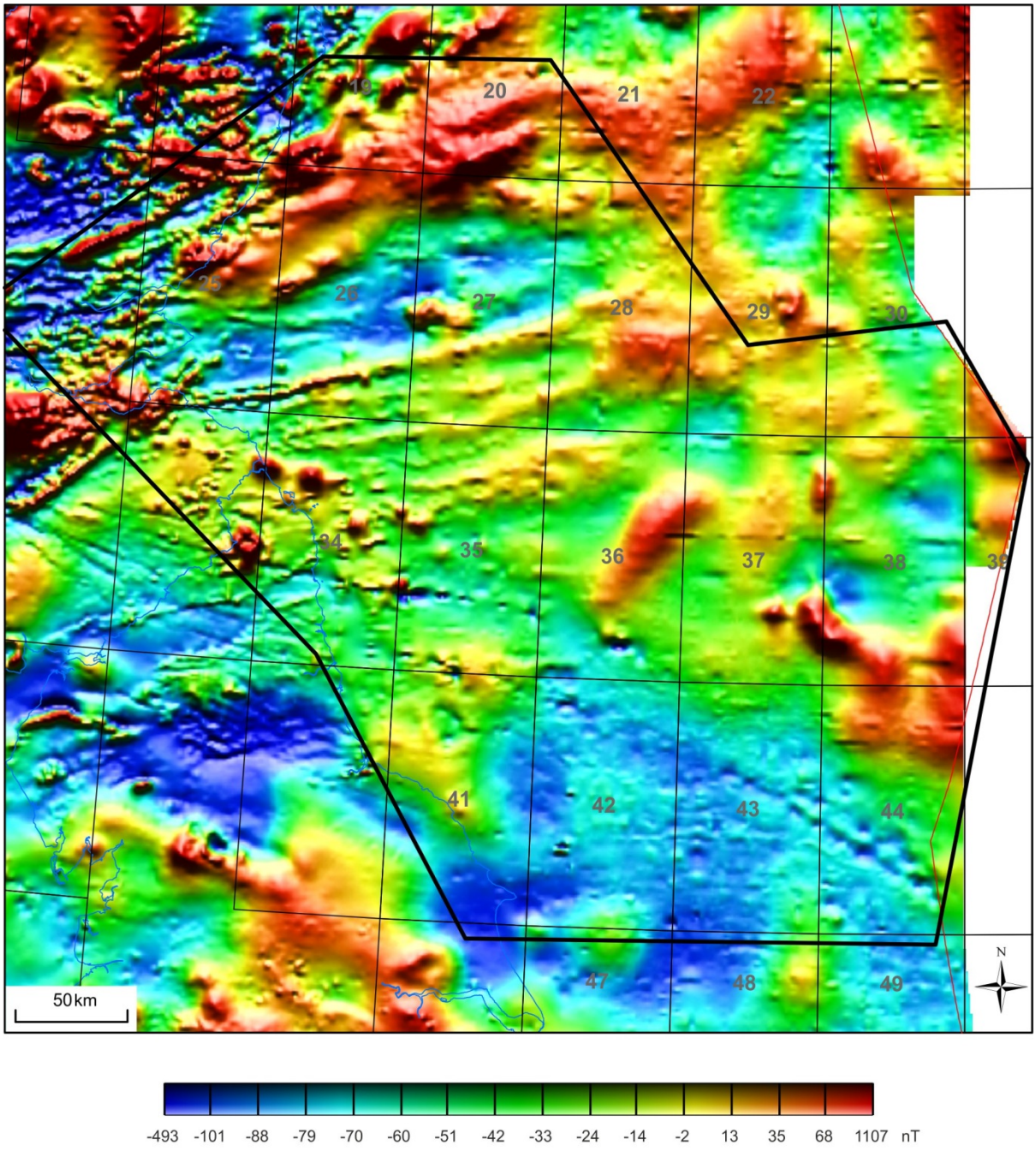

Figure 6 Total magnetic intensity, imaged using equal colour area and illumination from the north.

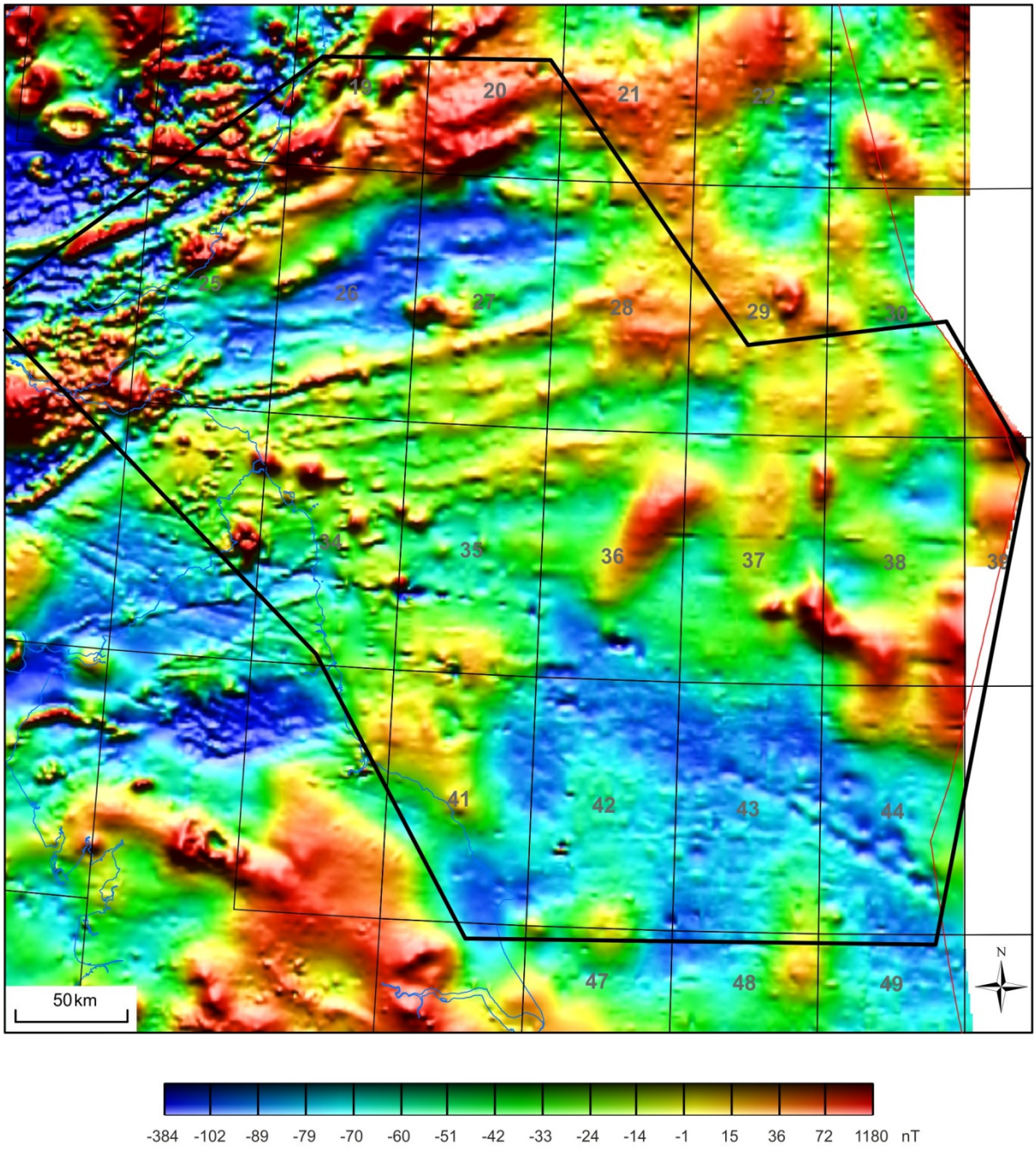

Figure 7 Reduced-to-pole magnetic field, imaged using equal colour area and illumination from the north.

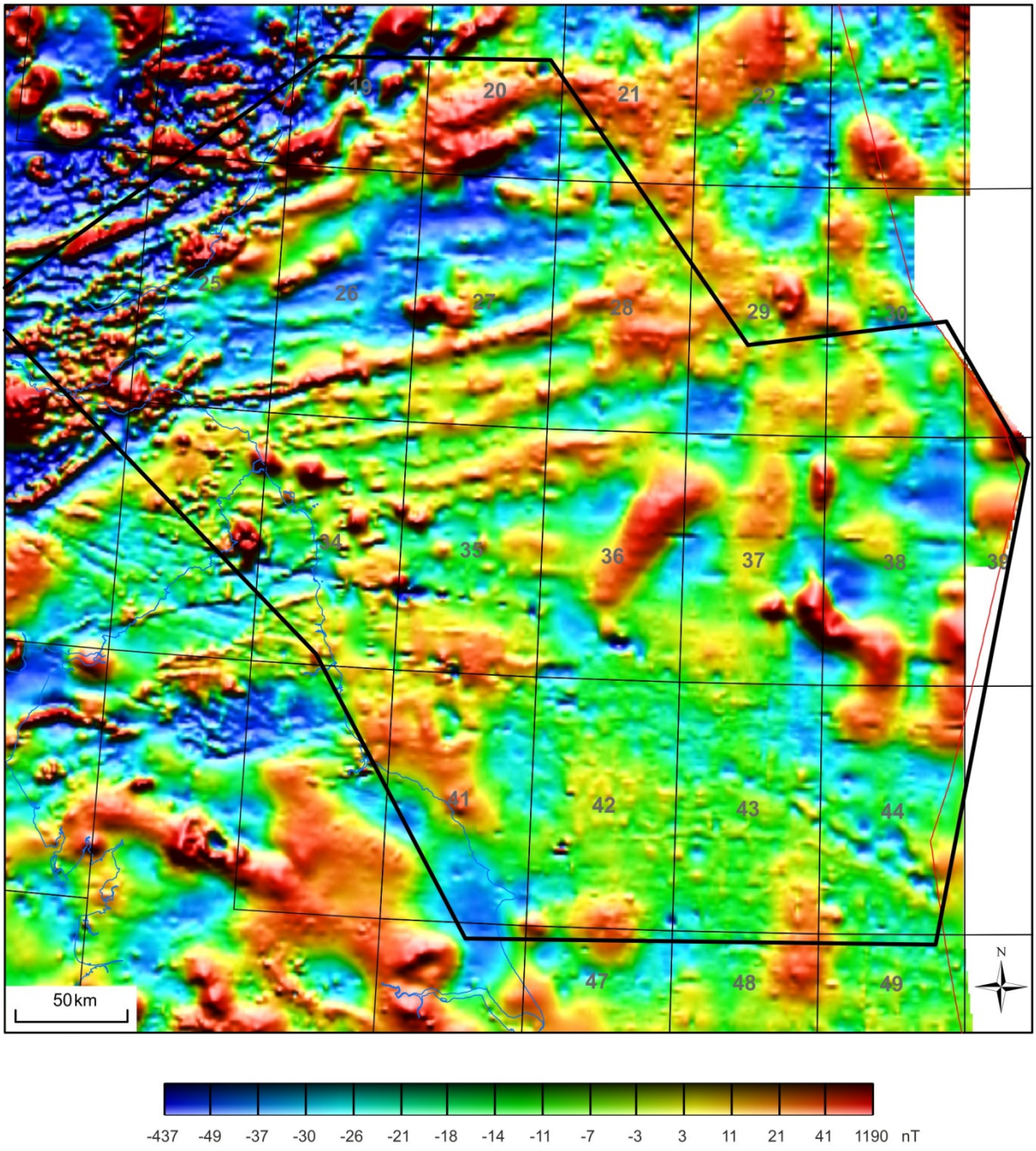

Figure 8 Residual reduced-to-pole magnetic field, calculated by removal of a 10 km upward continuation. Equal colour area with illumination from the north.

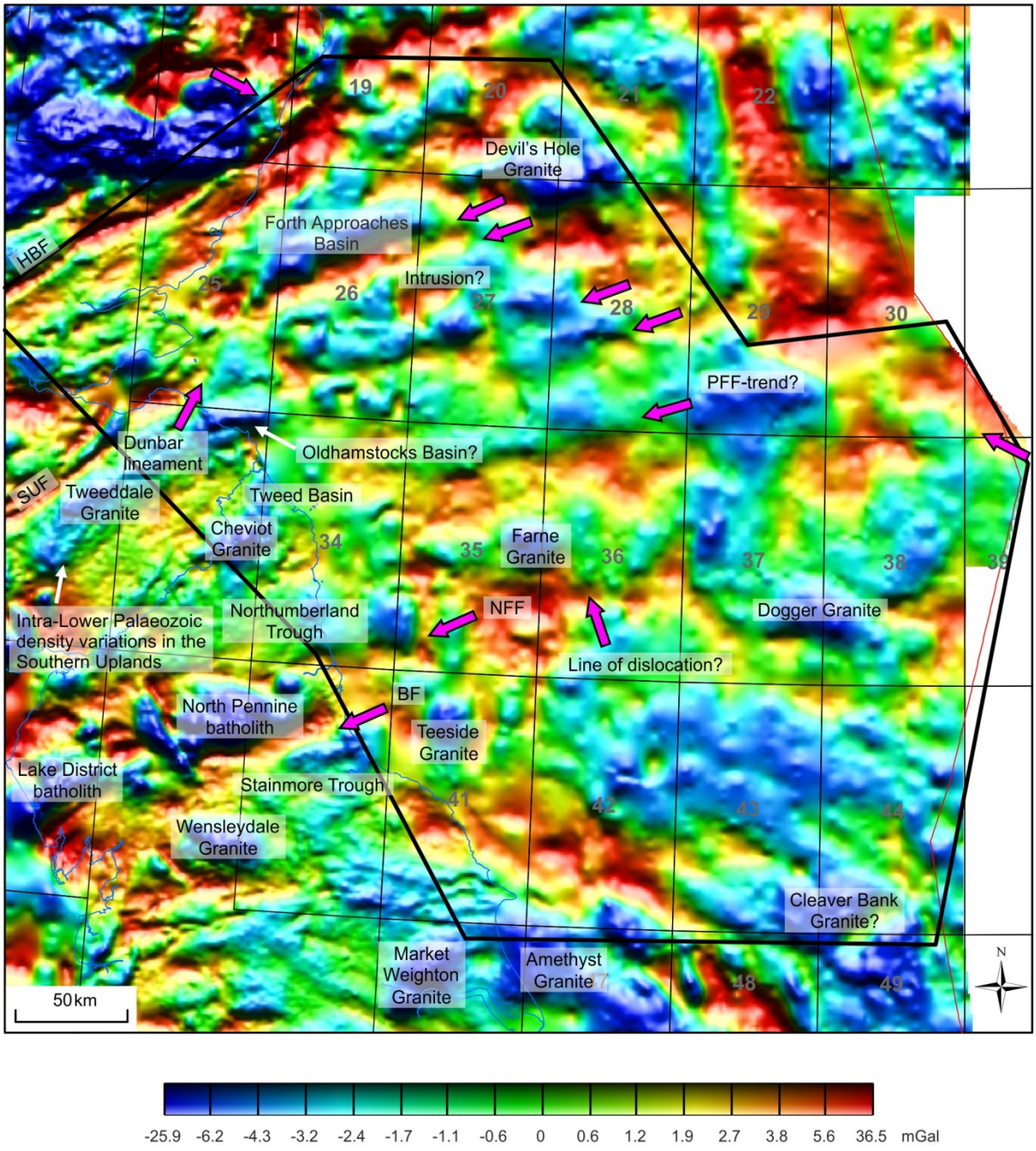

Figure 9 Annotated residual gravity image (Figure 5). Magenta arrows indicate selected gravity lineaments.

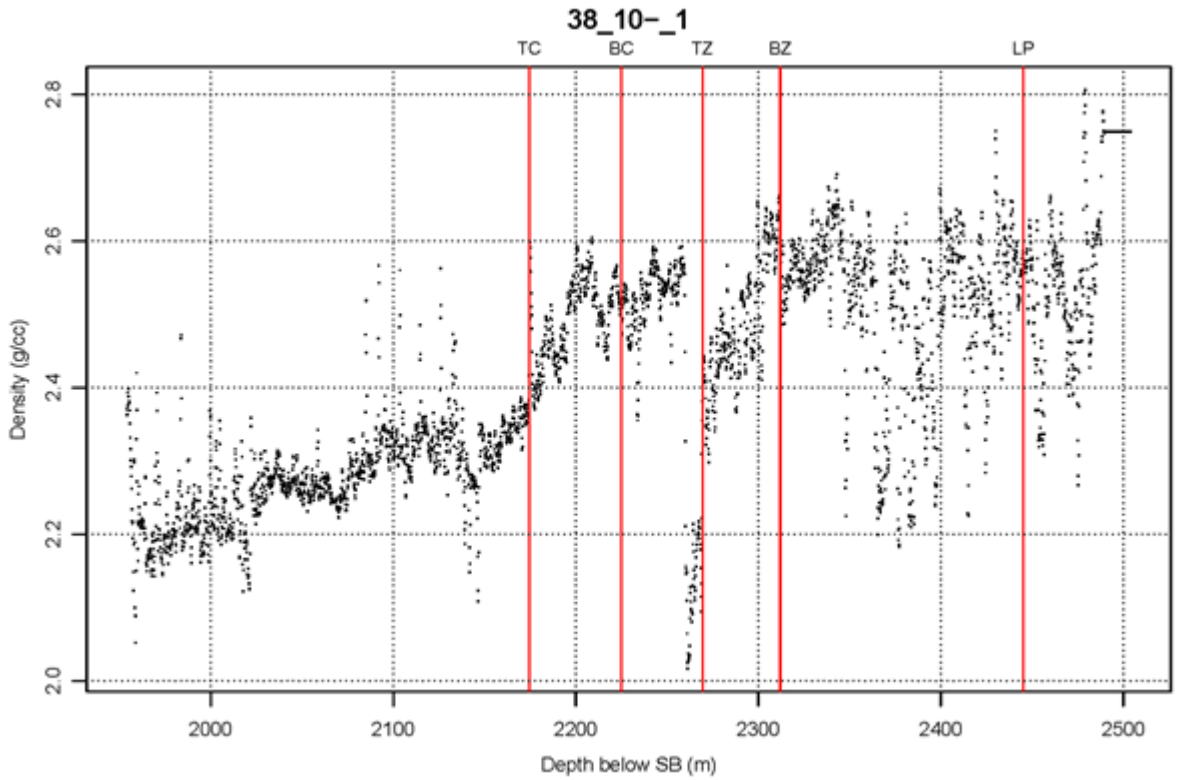

Figure 10 Example plot for well 38/10-1 showing interpreted seismic boundaries: TC = top Chalk, BC = base Chalk, TZ = top Zechstein, BZ = base Zechstein. LP (top Carboniferous and older) it is shown on wells where present but is not a horizon in the gravity model

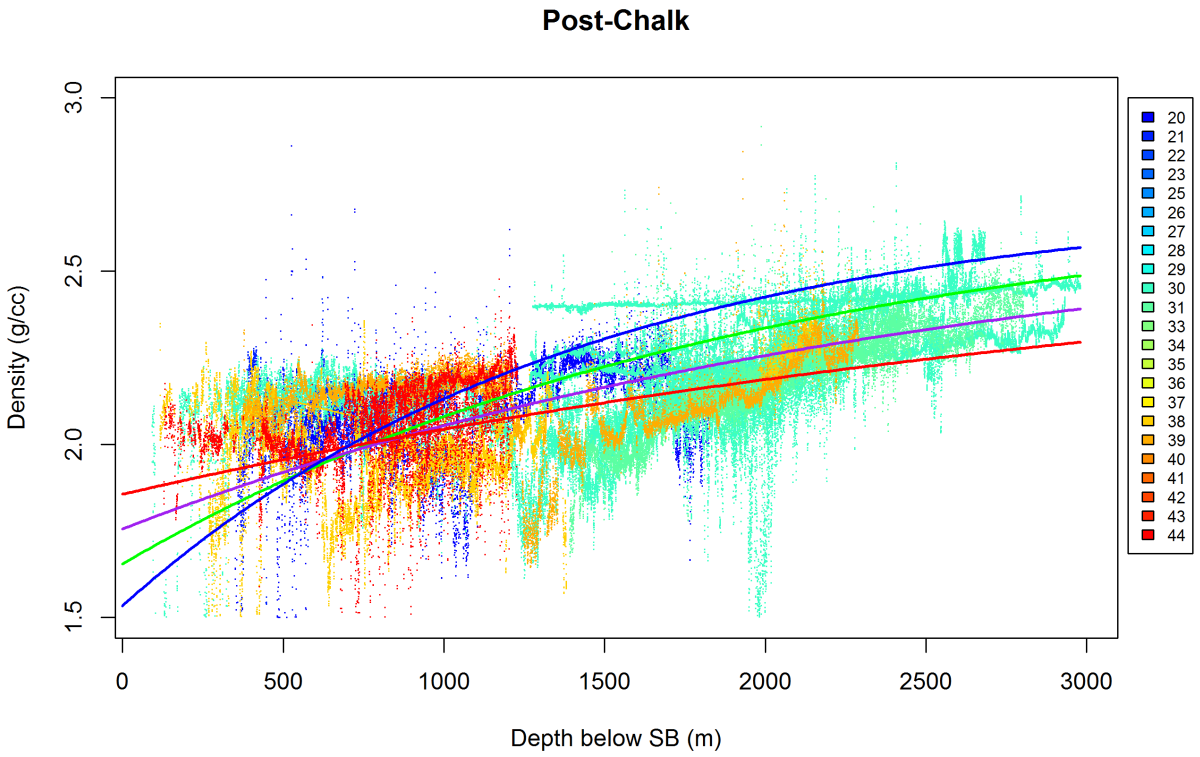

Figure 11 Compilation of densities from logs through the post-Chalk sequence. Smooth curves are the normal compaction trends of Sclater & Christie (1980) for shale (green), sand (red), shaly sand (purple) and chalk (blue). The data are colour-coded according to Quad, as indicated in the legend.

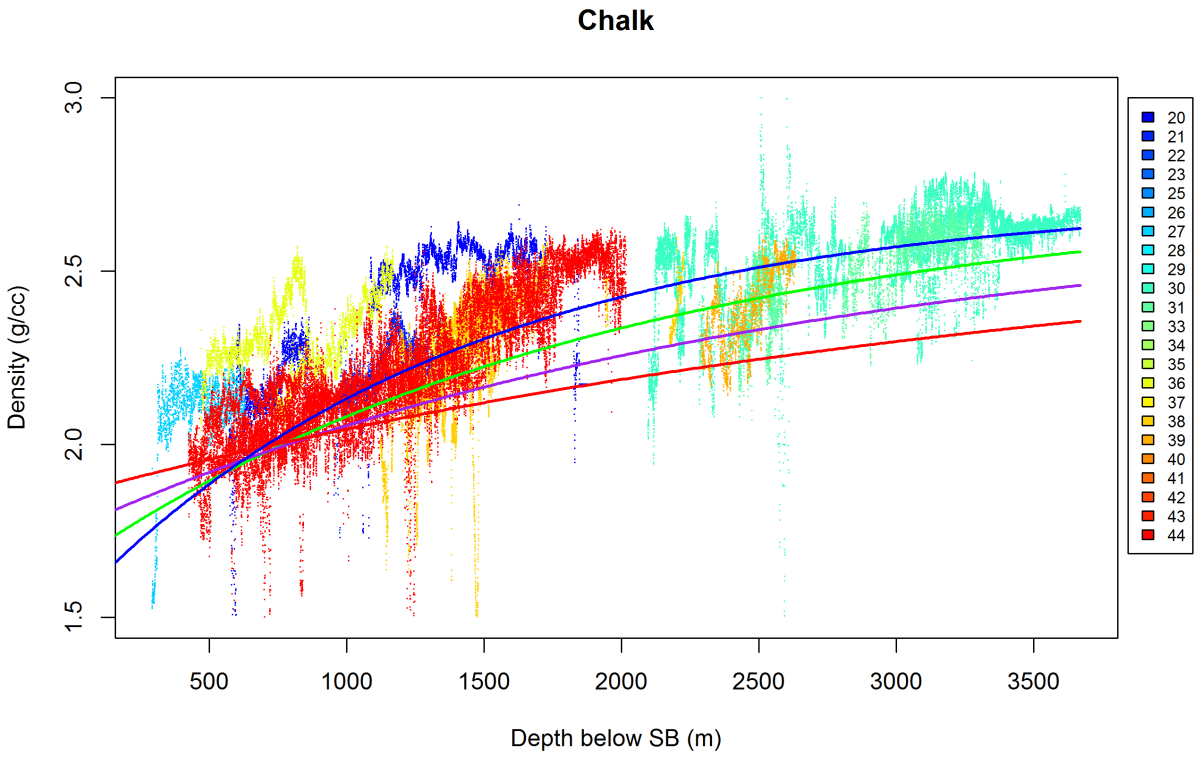

Figure 12 Compilation of densities from logs through the Chalk. Smooth curves are the normal compaction trends of Sclater & Christie (1980) for shale (green), sand (red), shaly sand (purple) and chalk (blue). The data are colour-coded according to Quad, as indicated in the legend.

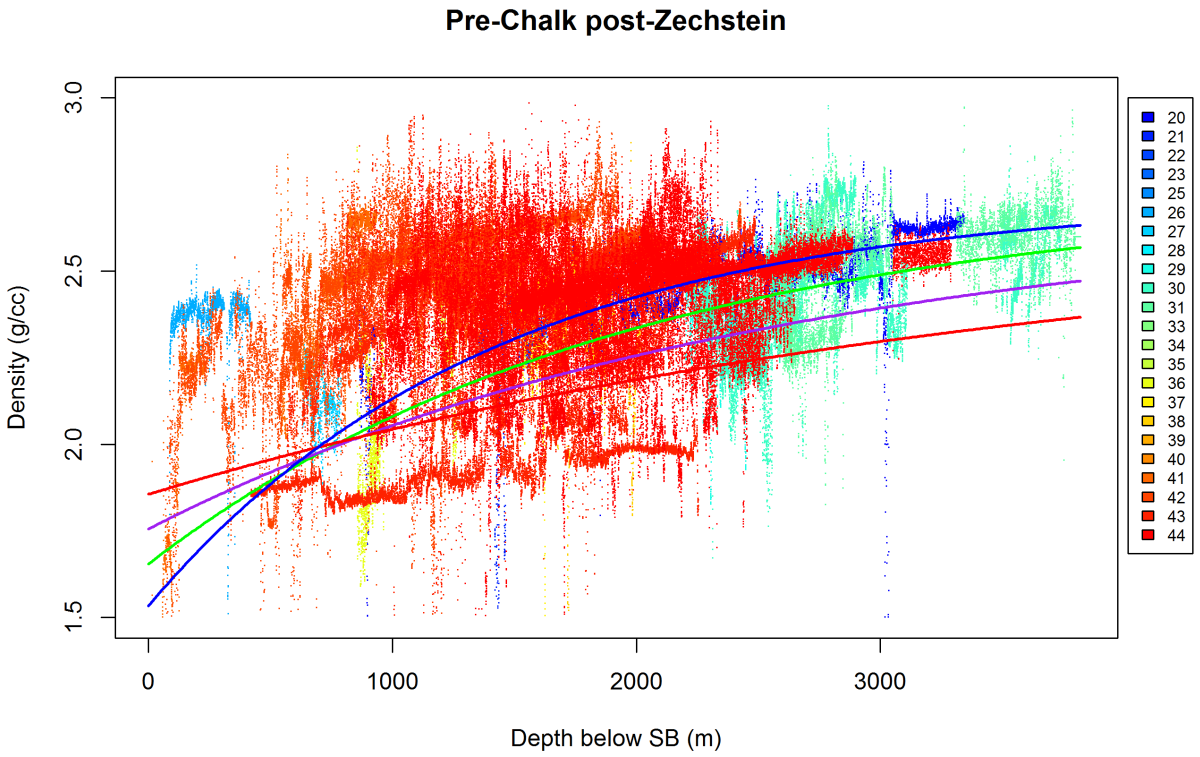

Figure 13 Compilation of densities from logs through the pre-Chalk – post-Zechstein sequence. Smooth curves are the normal compaction trends of Sclater & Christie (1980) for shale (green), sand (red), shaly sand (purple) and chalk (blue). The data are colour-coded according to Quad, as indicated in the legend.

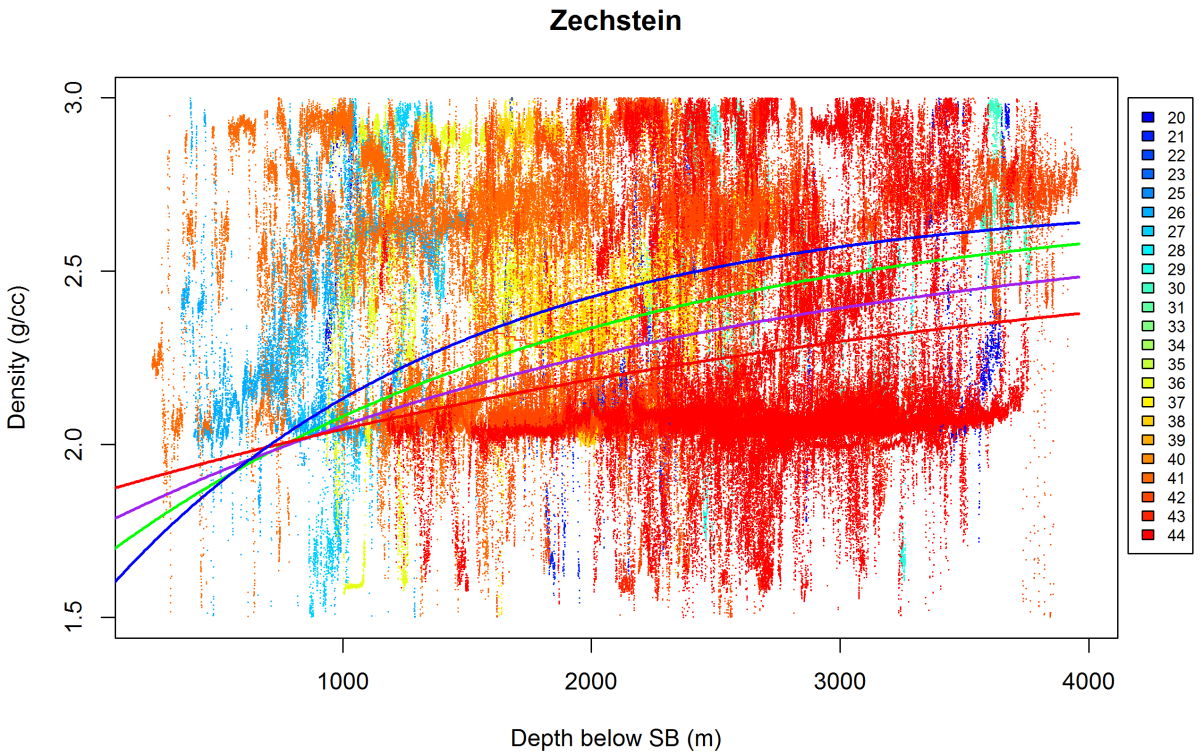

Figure 14 Compilation of densities from logs through the Zechstein Group. Smooth curves are the normal compaction trends of Sclater & Christie (1980) for shale (green), sand (red), shaly sand (purple) and chalk (blue). The data are colour-coded according to Quad, as indicated in the legend.

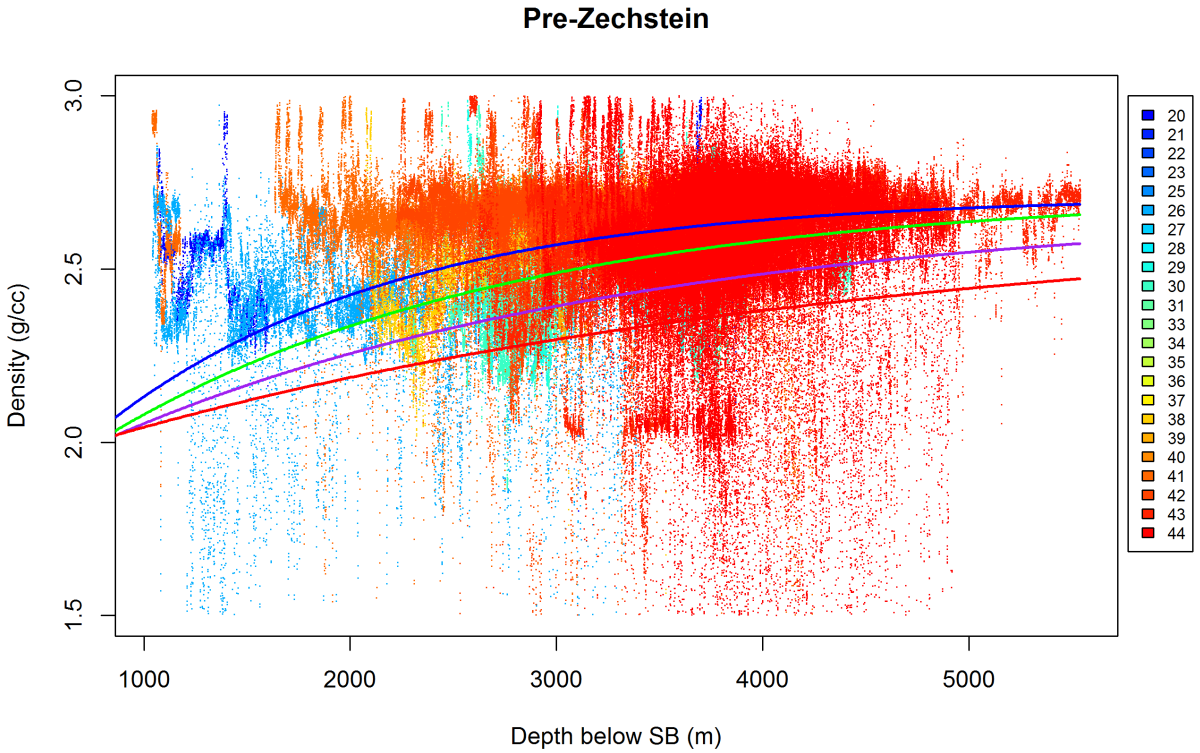

Figure 15 Compilation of densities from logs through the pre-Zechstein sequence. Smooth curves are the normal compaction trends of Sclater & Christie (1980) for shale (green), sand (red), shaly sand (purple) and chalk (blue). The data are colour-coded according to Quad, as indicated in the legend.

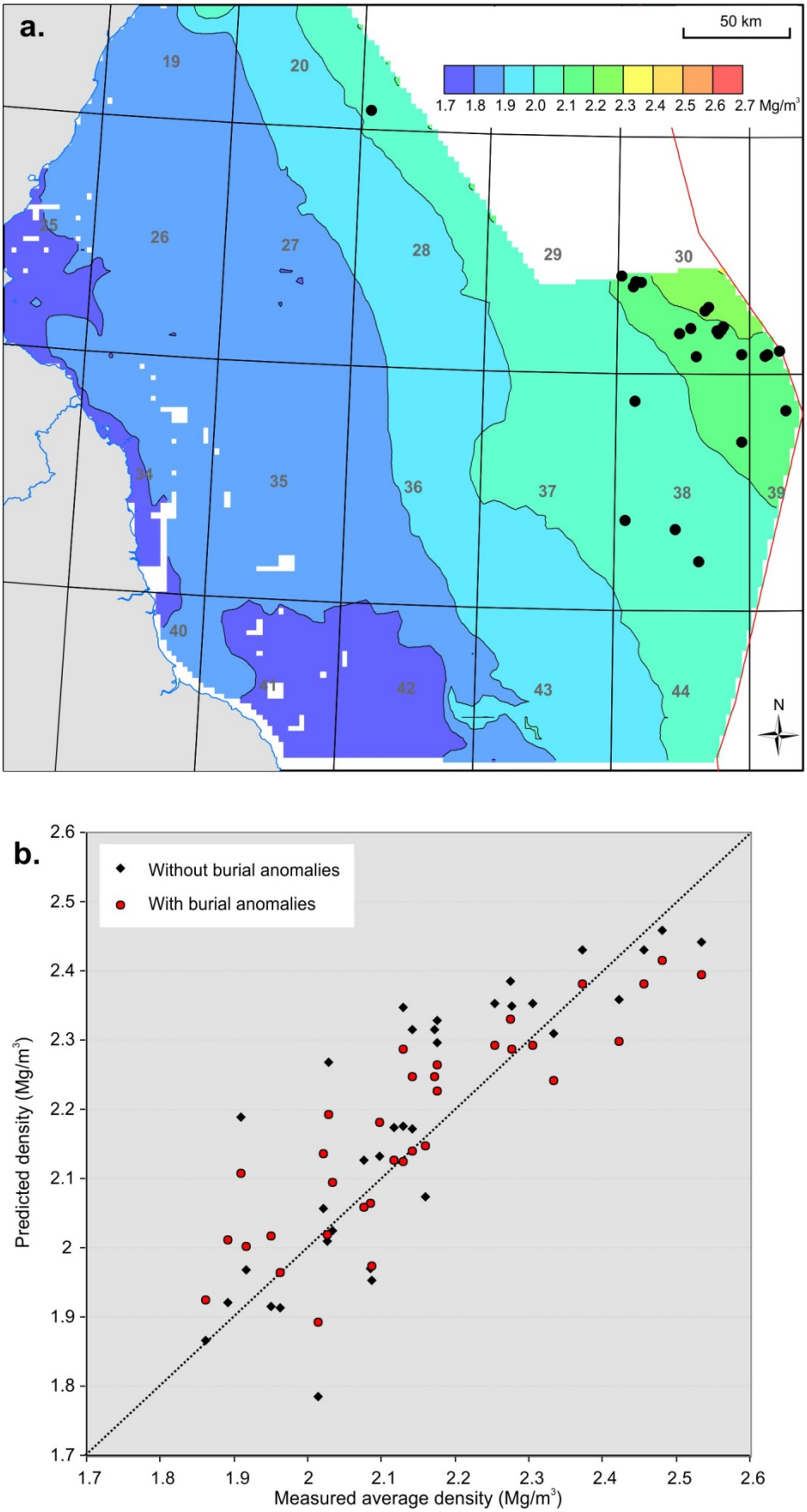

Figure 16 (a) Density model for the post-Chalk layer. (b) Comparison between measured and predicted average densities at the well locations shown with black dots in (a).

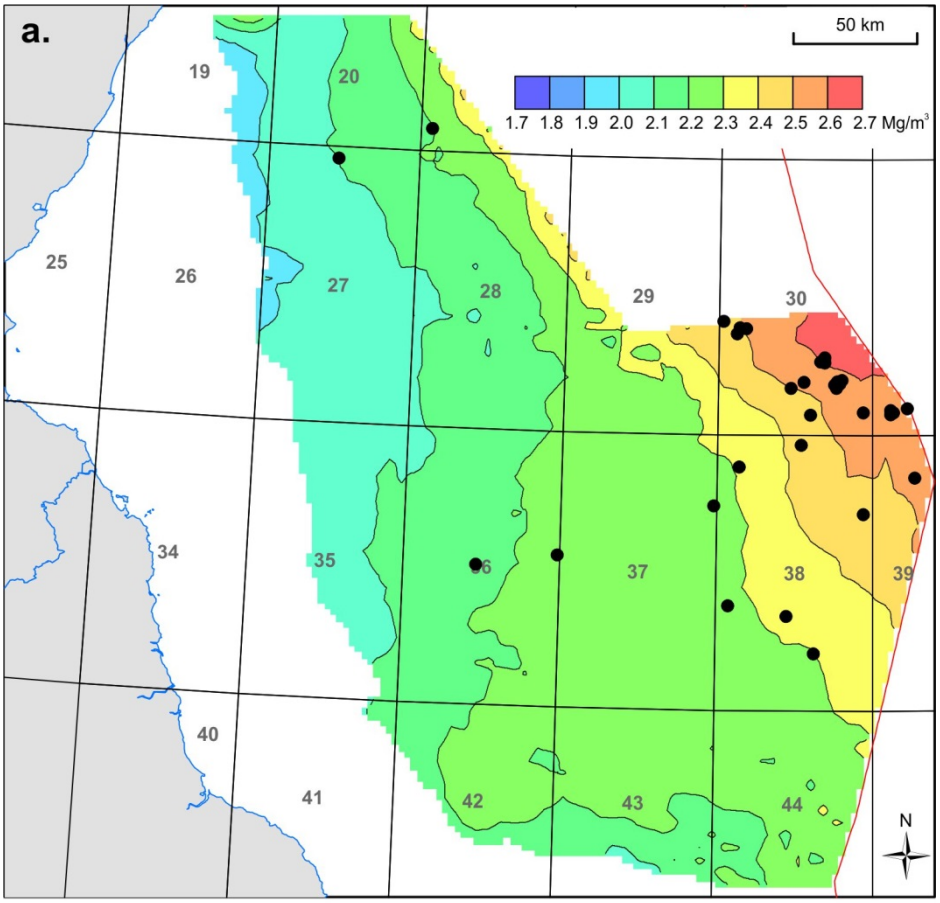

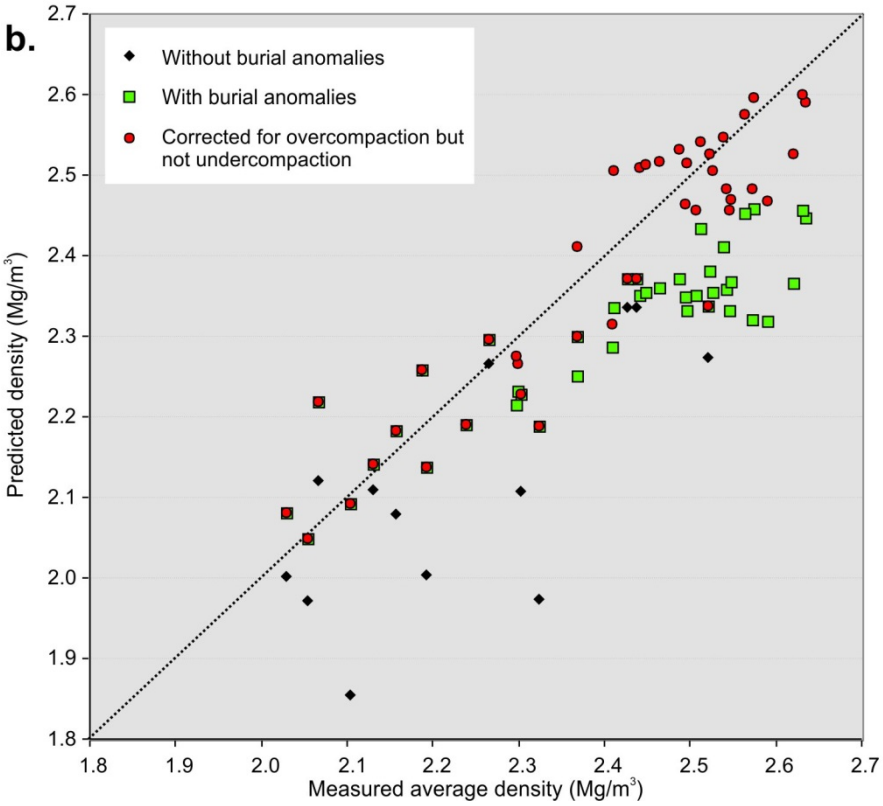

Figure 17 (a) Density model for the Chalk layer. (b) Comparison between measured and predicted average densities at the well locations shown with black dots in (a).

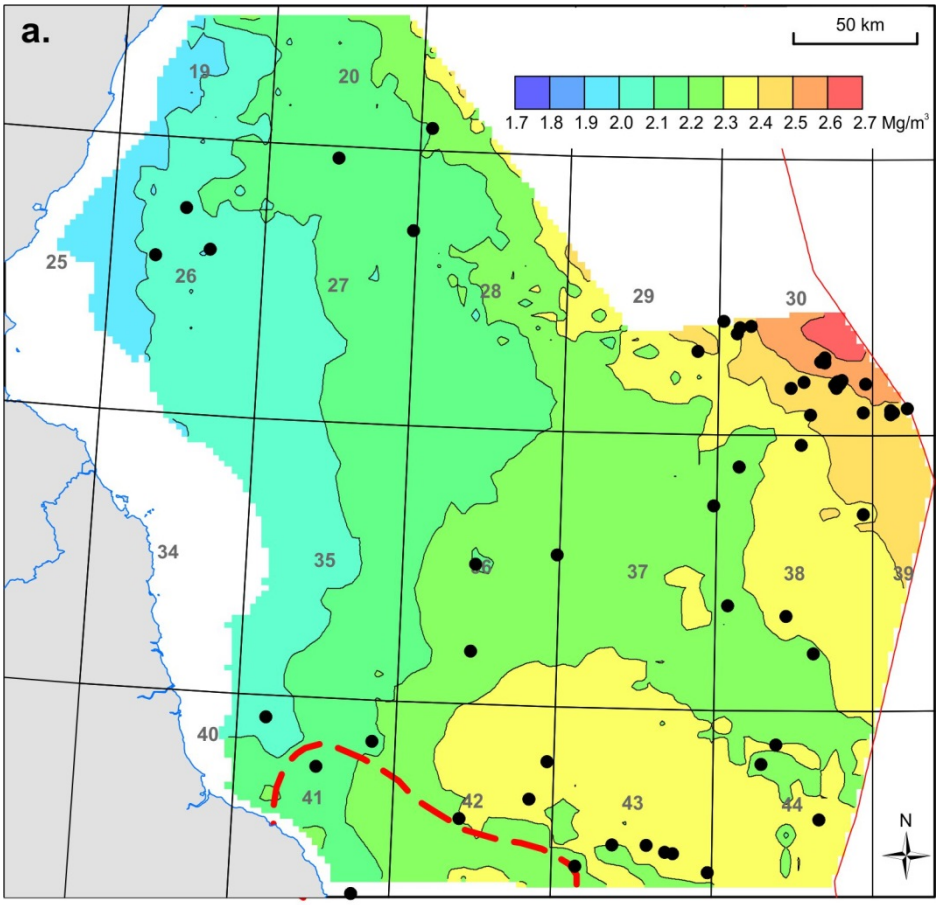

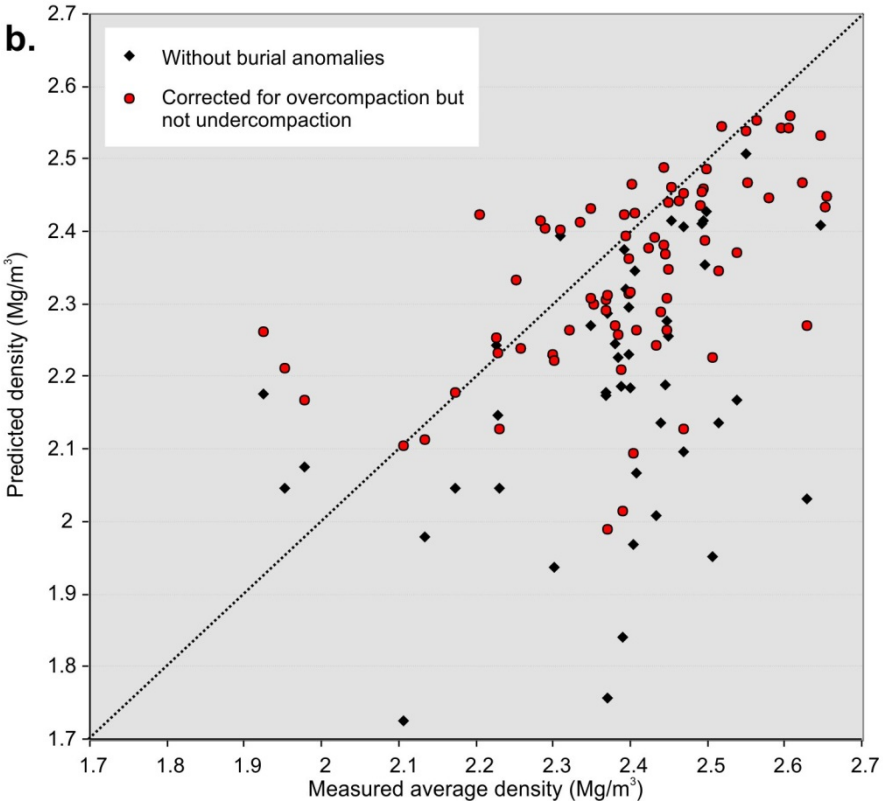

Figure 18 (a) Density model for the pre-Chalk – post-Zechstein layer. The red dashed line indicates the zone of excess pre-Chalk compaction (Sole-Pit axis) identified by Japsen (2000). (b) Comparison between measured and predicted average densities at the well locations shown with black dots in (a).

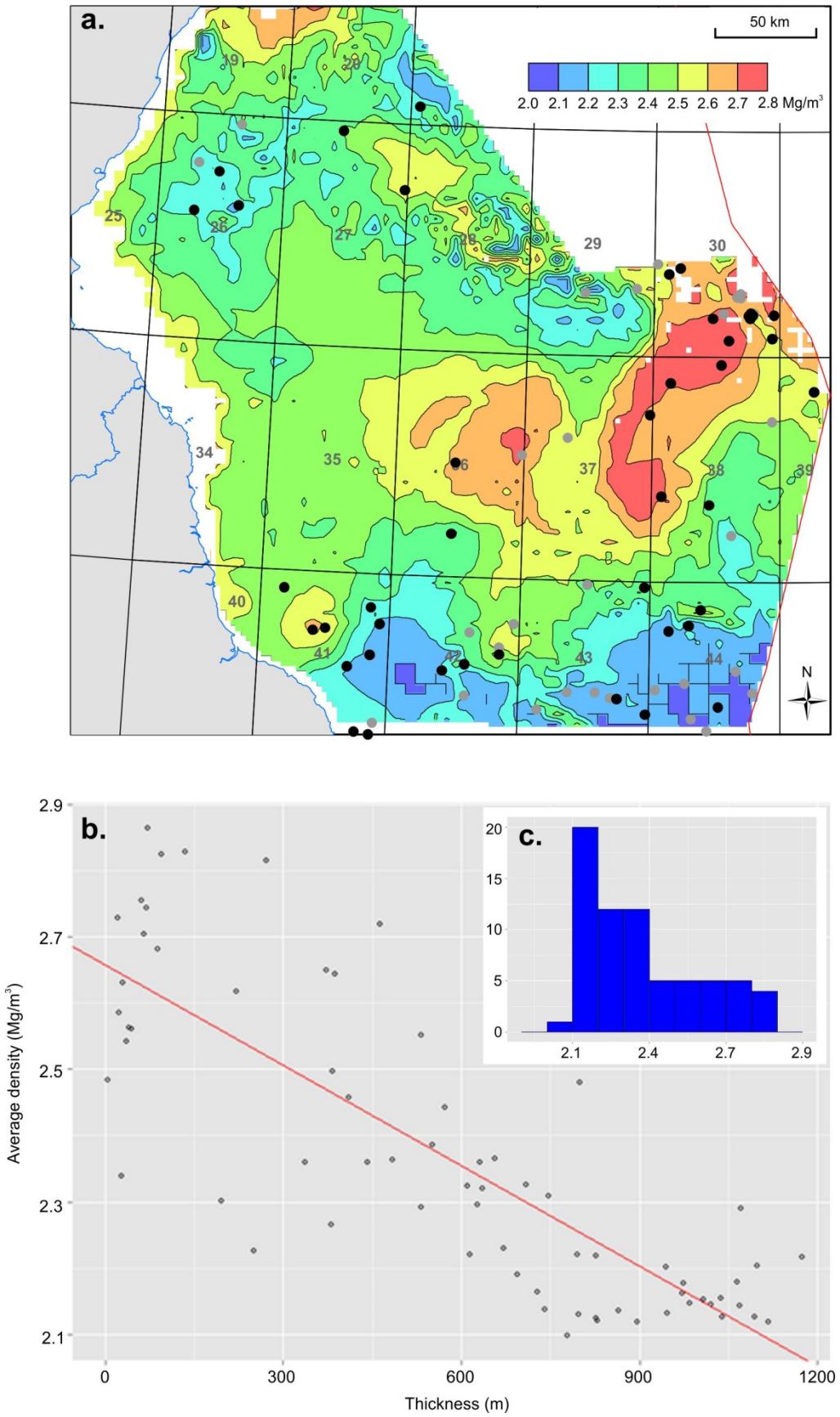

Figure 19 (a) Density model for the Zechstein sequence derived by regression kriging with measured densities at wells (black dots) as the primary variable and the relationship between thickness and average density (shown in b) as external drift. Grey dots on the map are wells with density logs that sampled less than 60% of the Zechstein thickness, which were excluded from the modelling (see text). (c) A histogram of the observed average densities.

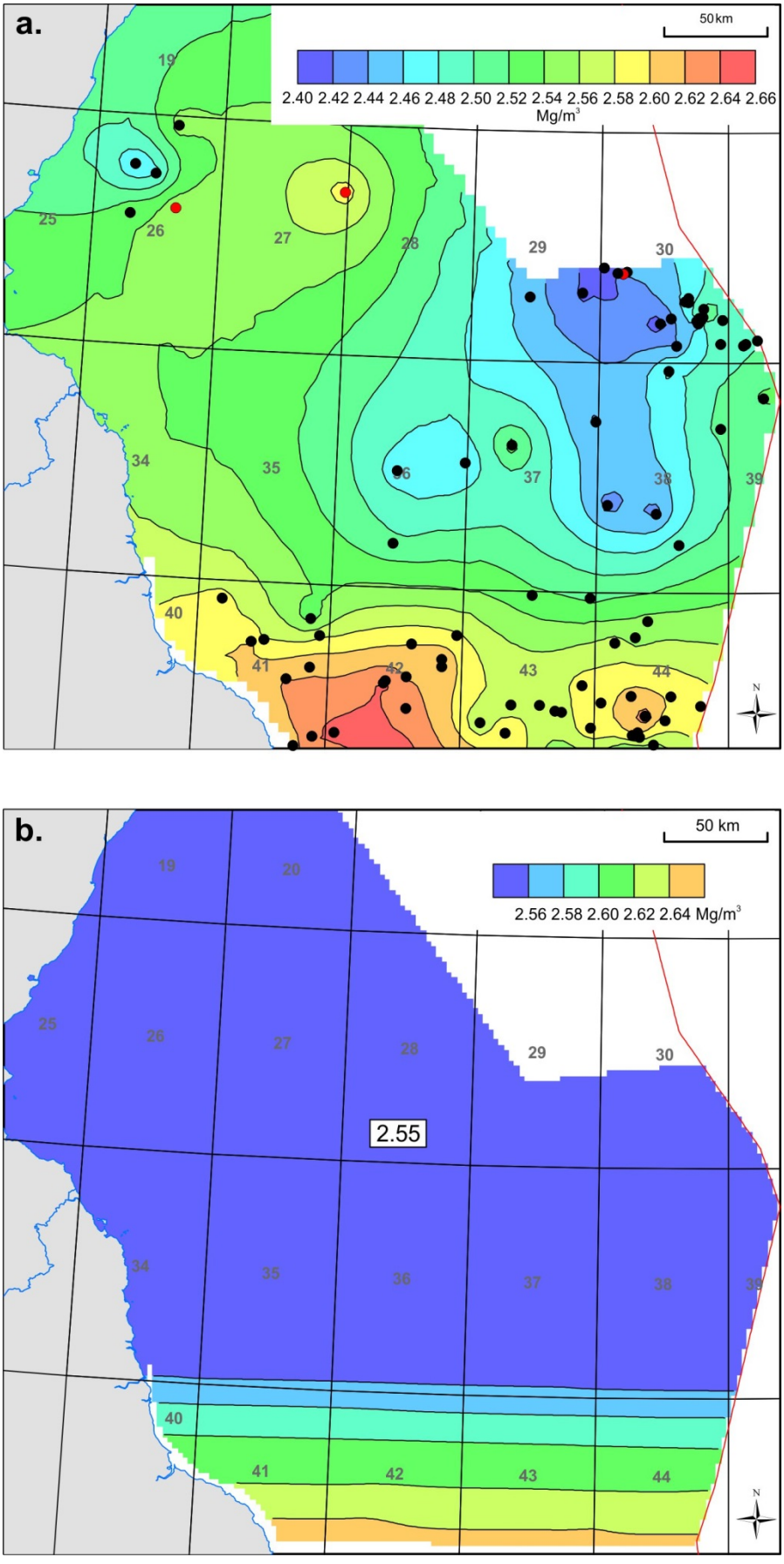

Figure 20 (a) Average density of the part of the pre-Zechstein sequence sampled by the wells shown (interpolation is by kriging). The red symbols indicate the inclusion of Lower Palaeozoic rocks. (b) The highly simplified average density model for the full thickness of the pre-Zechstein Upper Palaeozoic sequence employed in the gravity inversion.

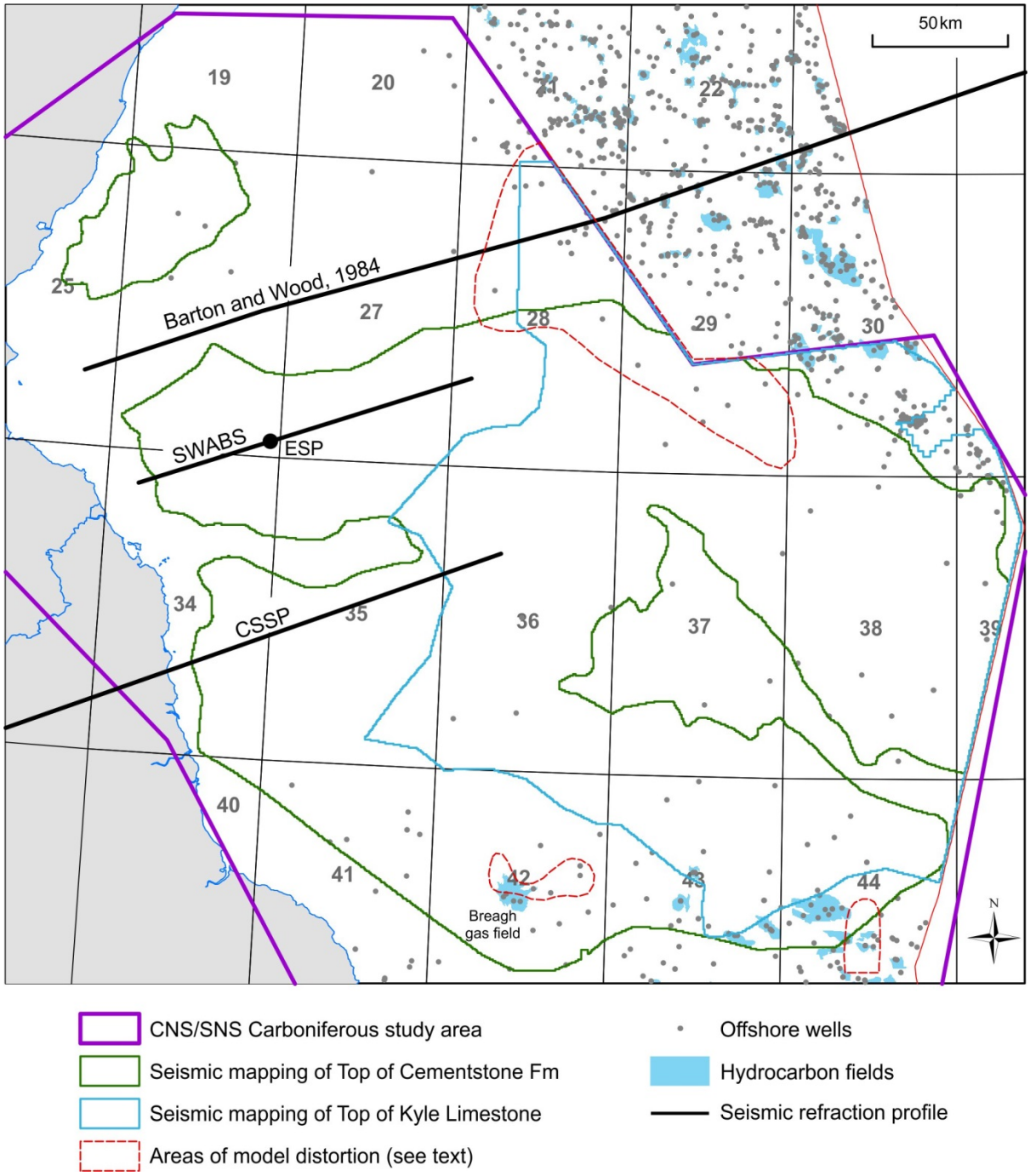

Figure 21 Map of the area covered by the 3D model showing the locations of seismic refraction experiments and mapping of the deeper intra Carboniferous and Devonian reflectors.

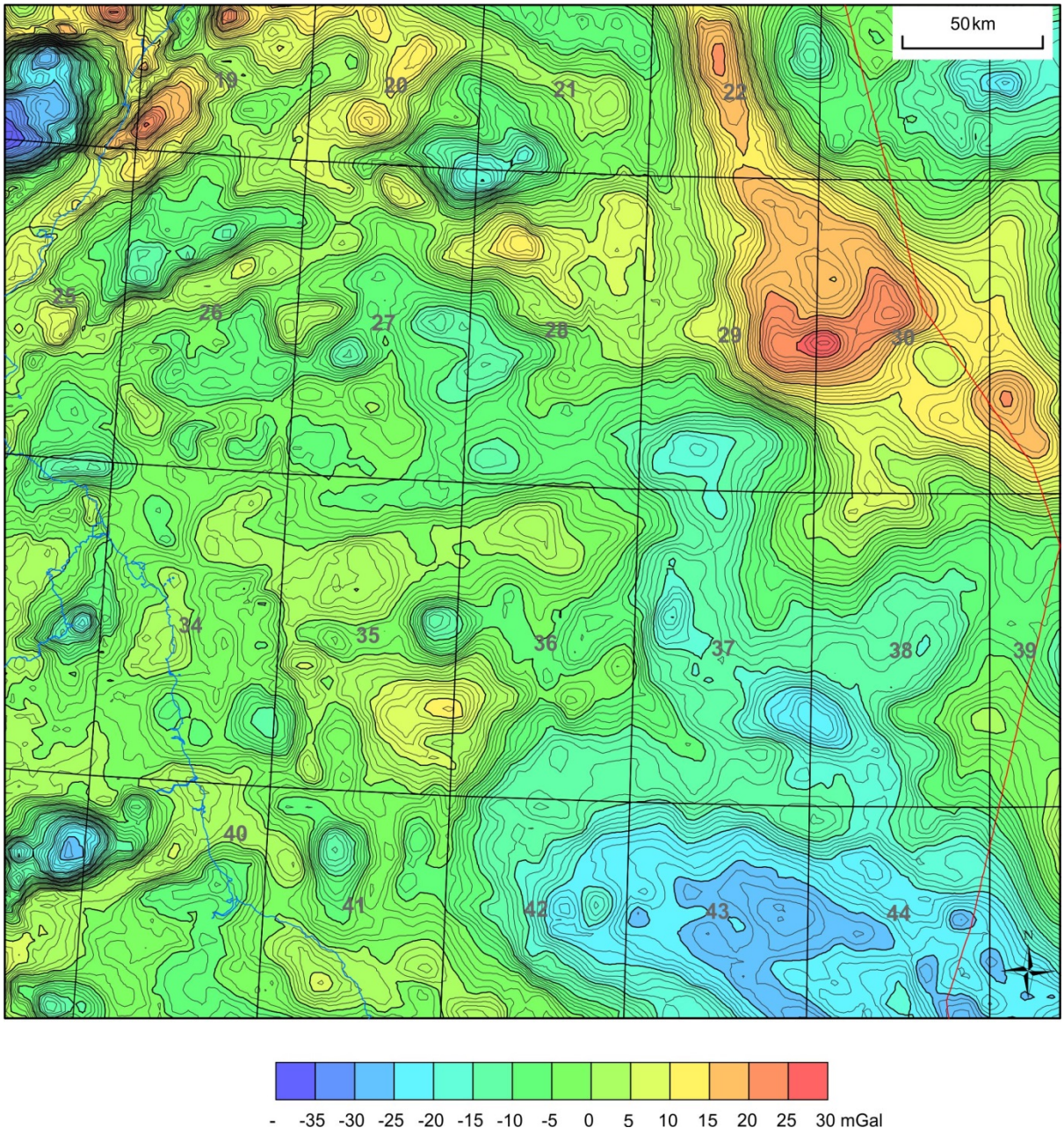

Figure 22 Observed gravity field over the modelled area (free-air anomalies offshore and Bouguer anomalies with a variable reduction density onshore).

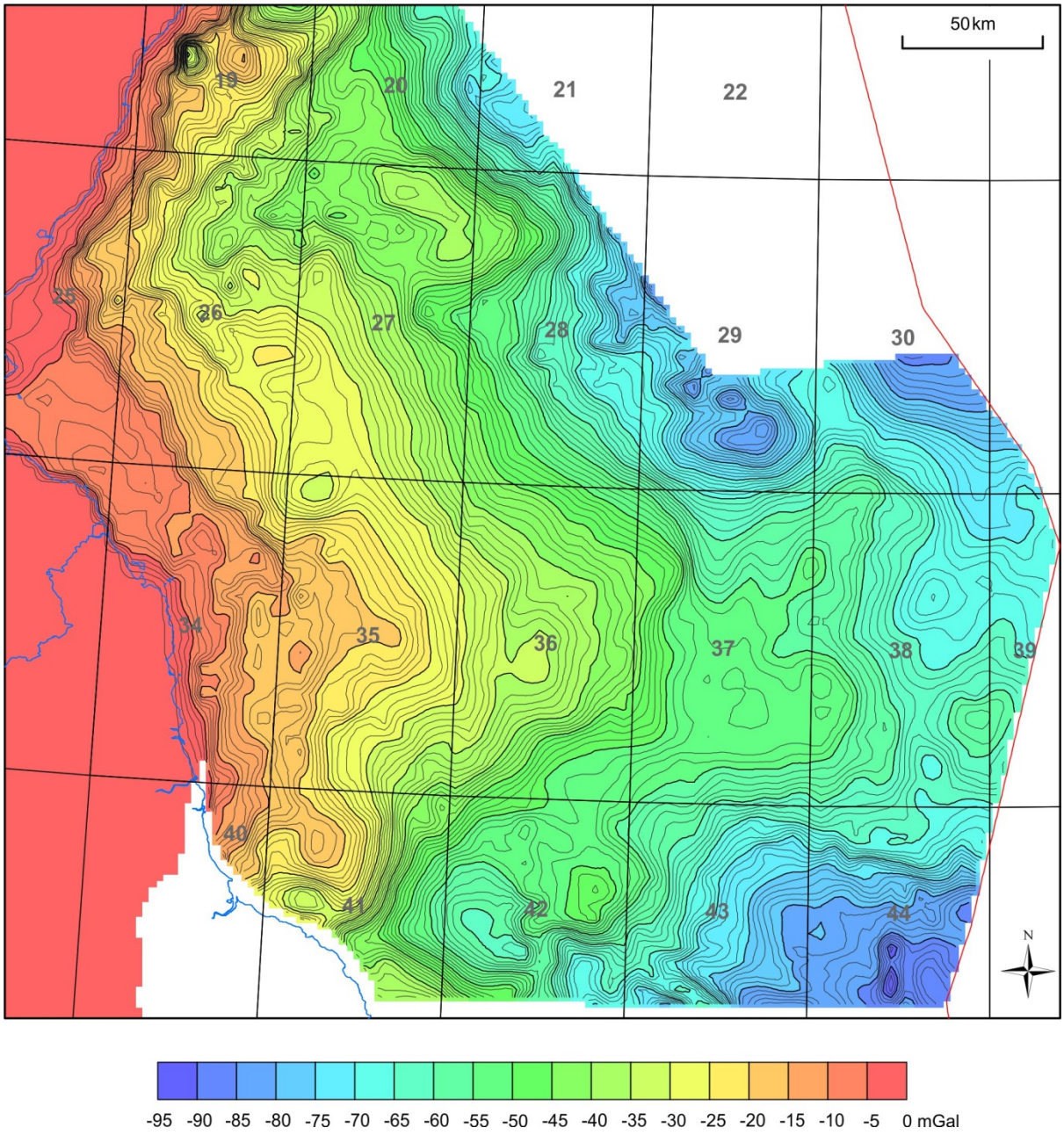

Figure 23 Forward calculation of the gravity effect of the sequence between sea level and base Zechstein.

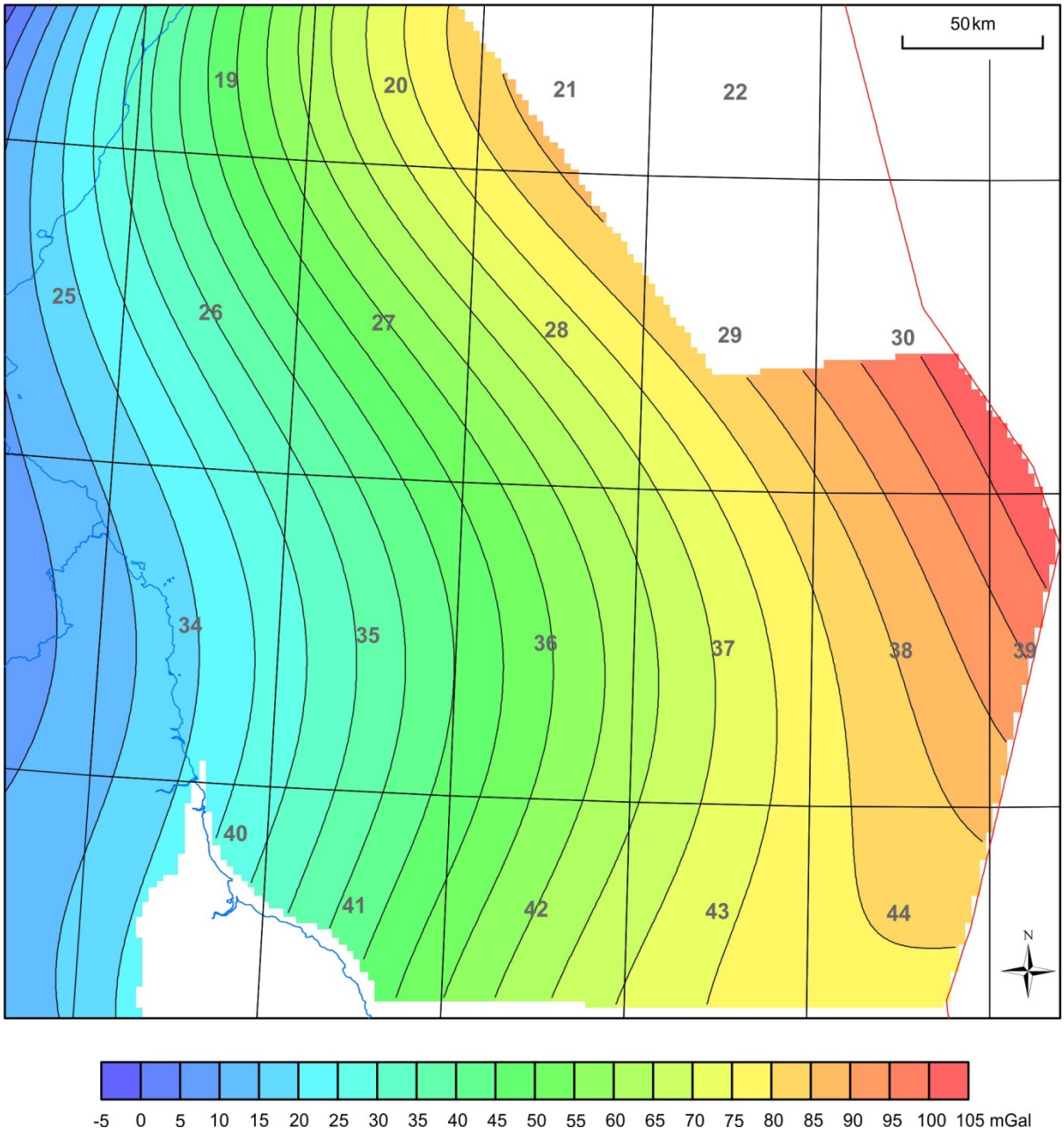

Figure 24 Assumed background gravity field (see text for details)

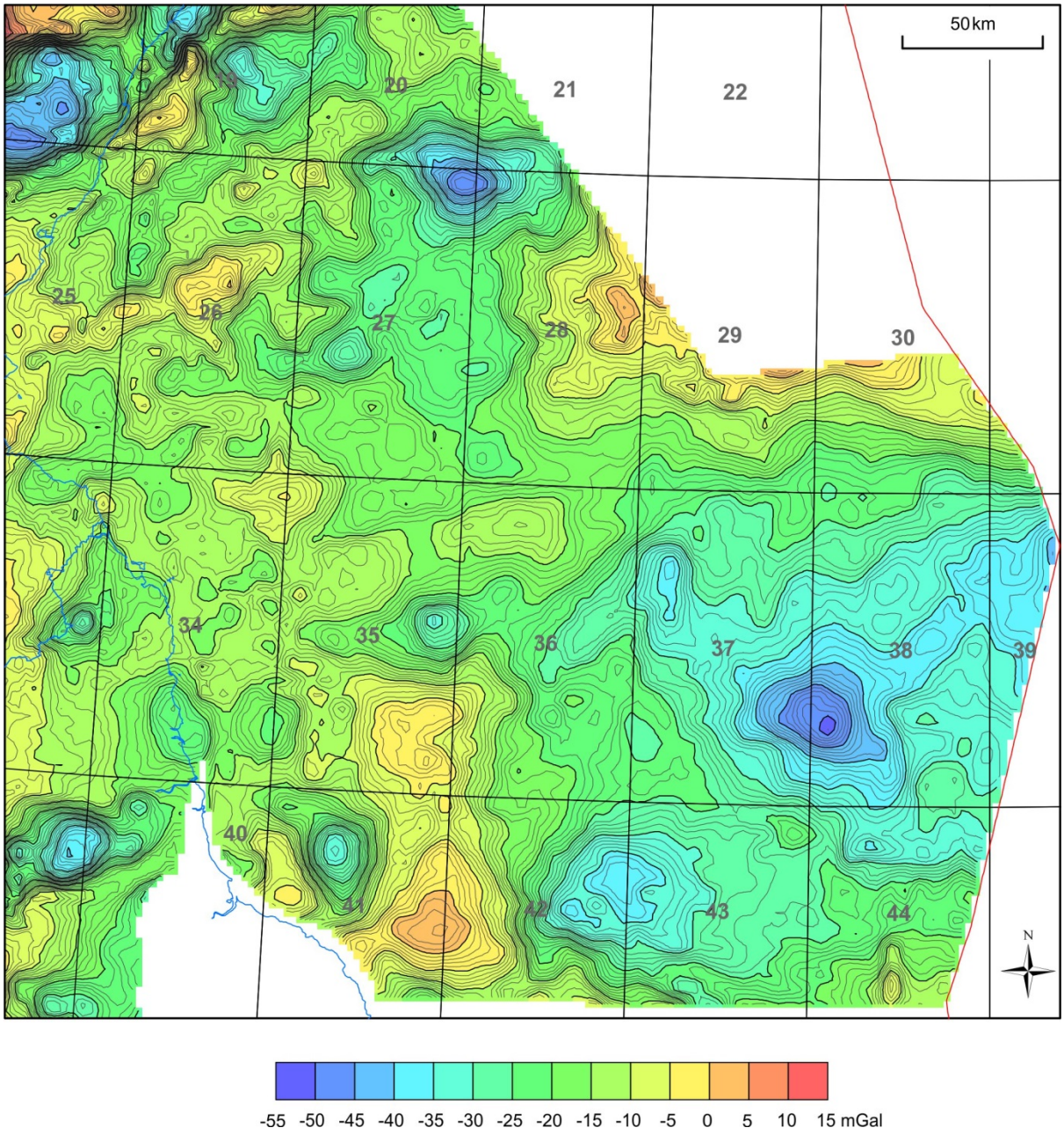

Figure 25 Residual gravity field calculated by subtraction of the forward calculation to base Zechstein (Figure 23) and the background field (Figure 24) from the observed field (Figure 22).

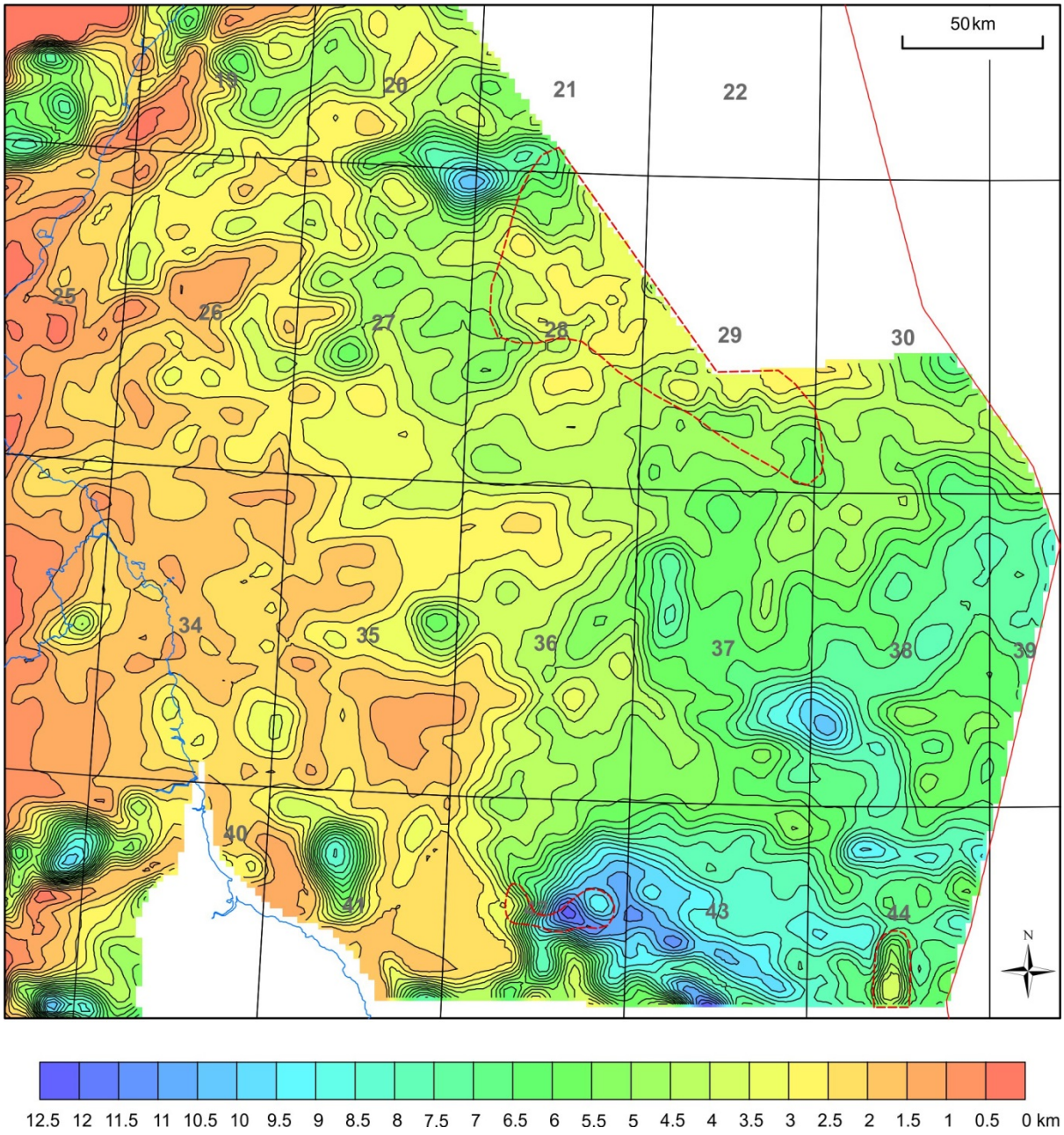

Figure 26 Depth to the surface derived by gravity inversion. Red dashed line indicates areas of model distortion (see text).

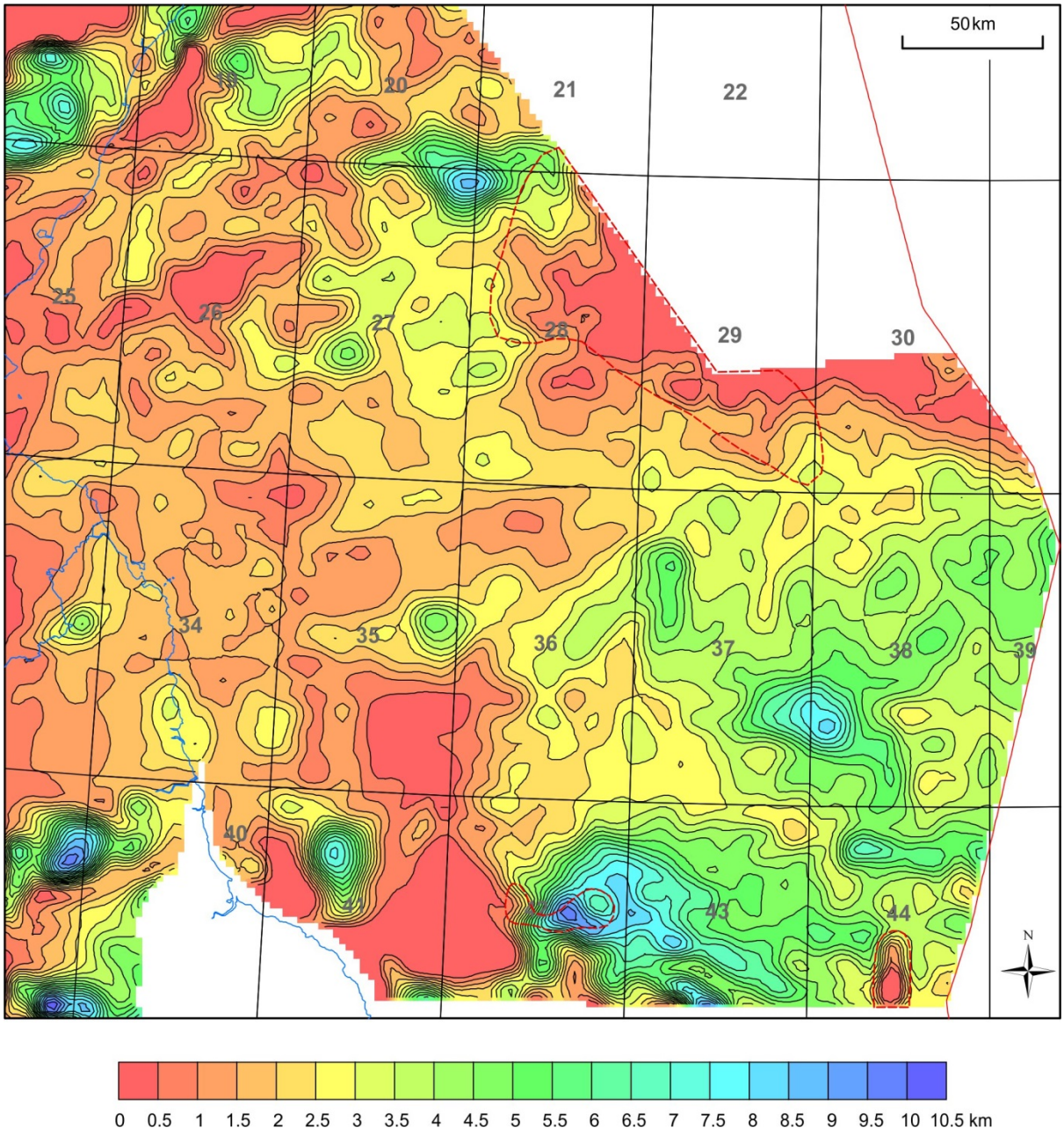

Figure 27 Thickness of the layer between base Zechstein and the gravity inversion surface. Red dashed line indicates areas of model distortion (see text).

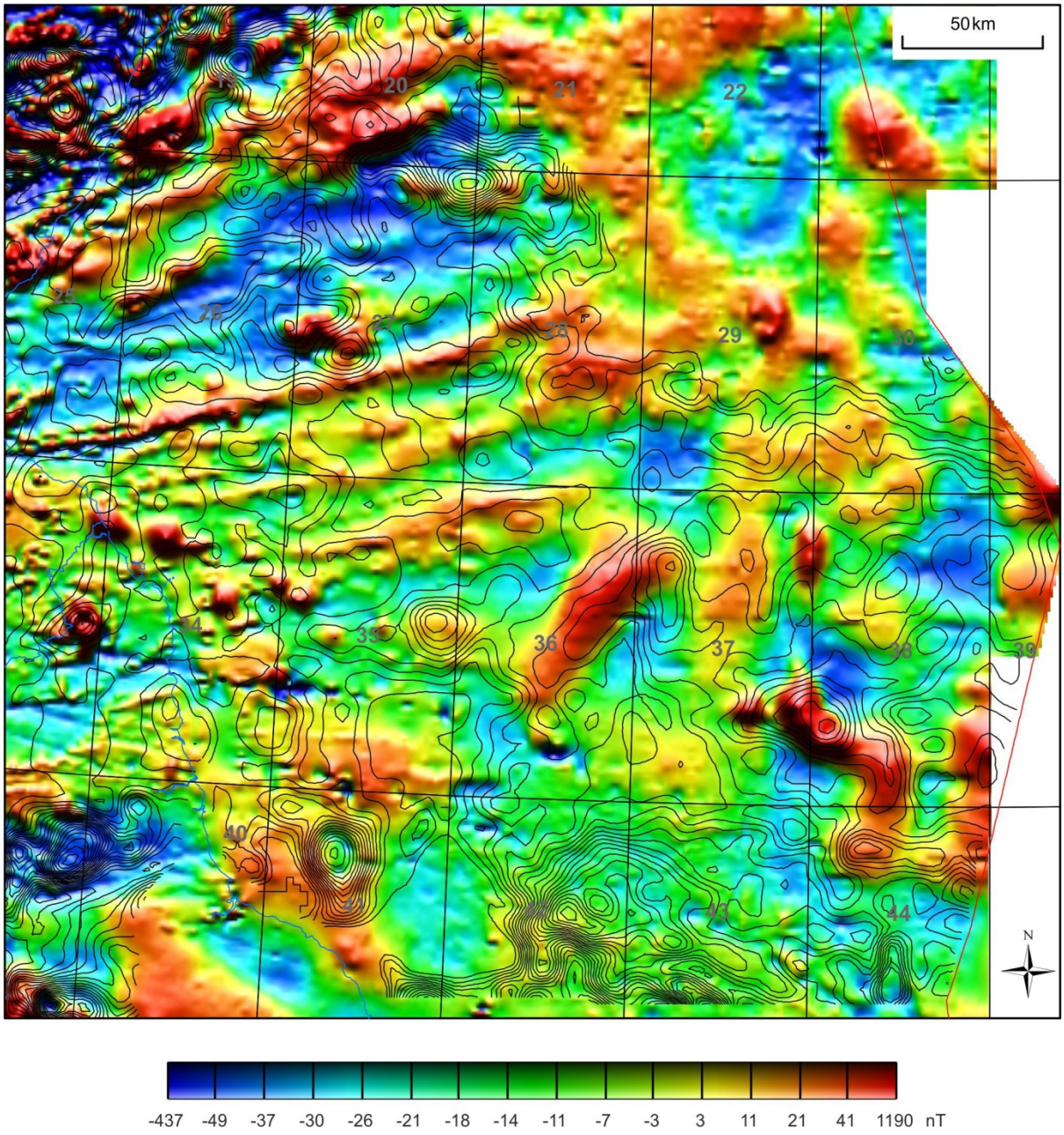

Figure 28 Thickness contours from the gravity inversion superimposed on an image of the residual reduced-to-pole magnetic anomaly (Figure 8)

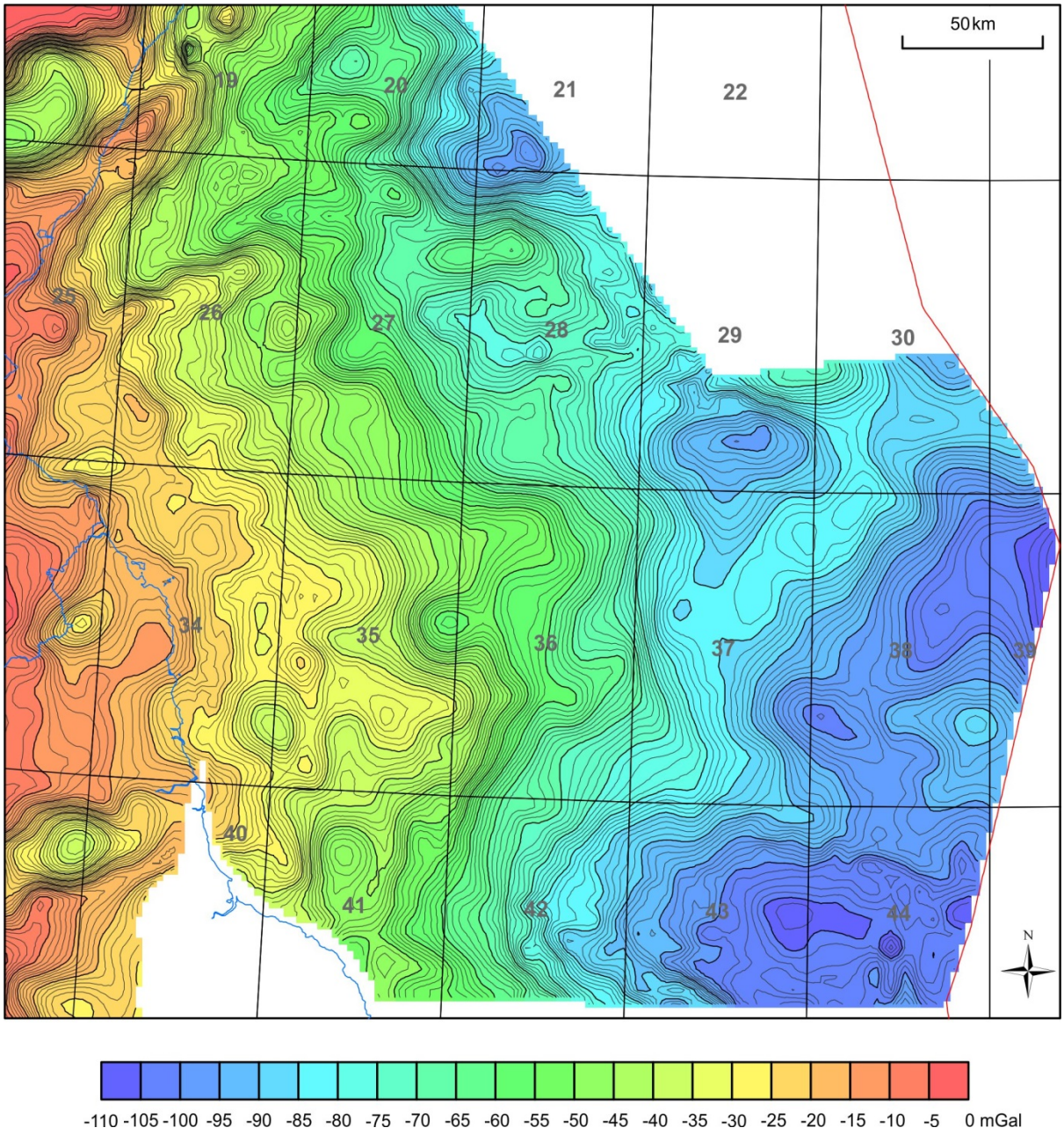

Figure 29 Forward gravity calculation over the full model.

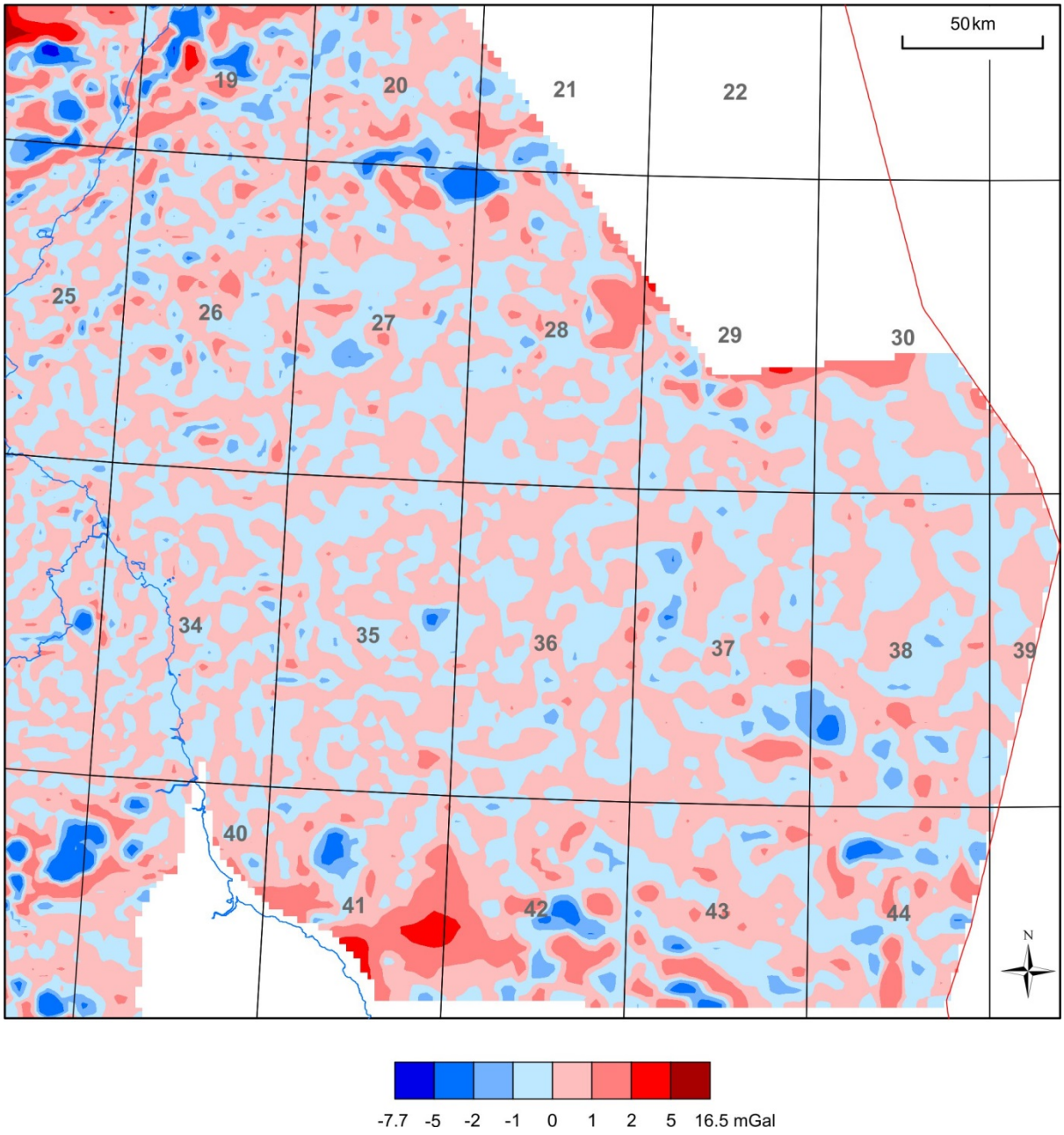

Figure 30 Residual gravity anomalies after subtracting the forward gravity calculation (Figure 29) and the background field (Figure 24) from the observed field (Figure 22)

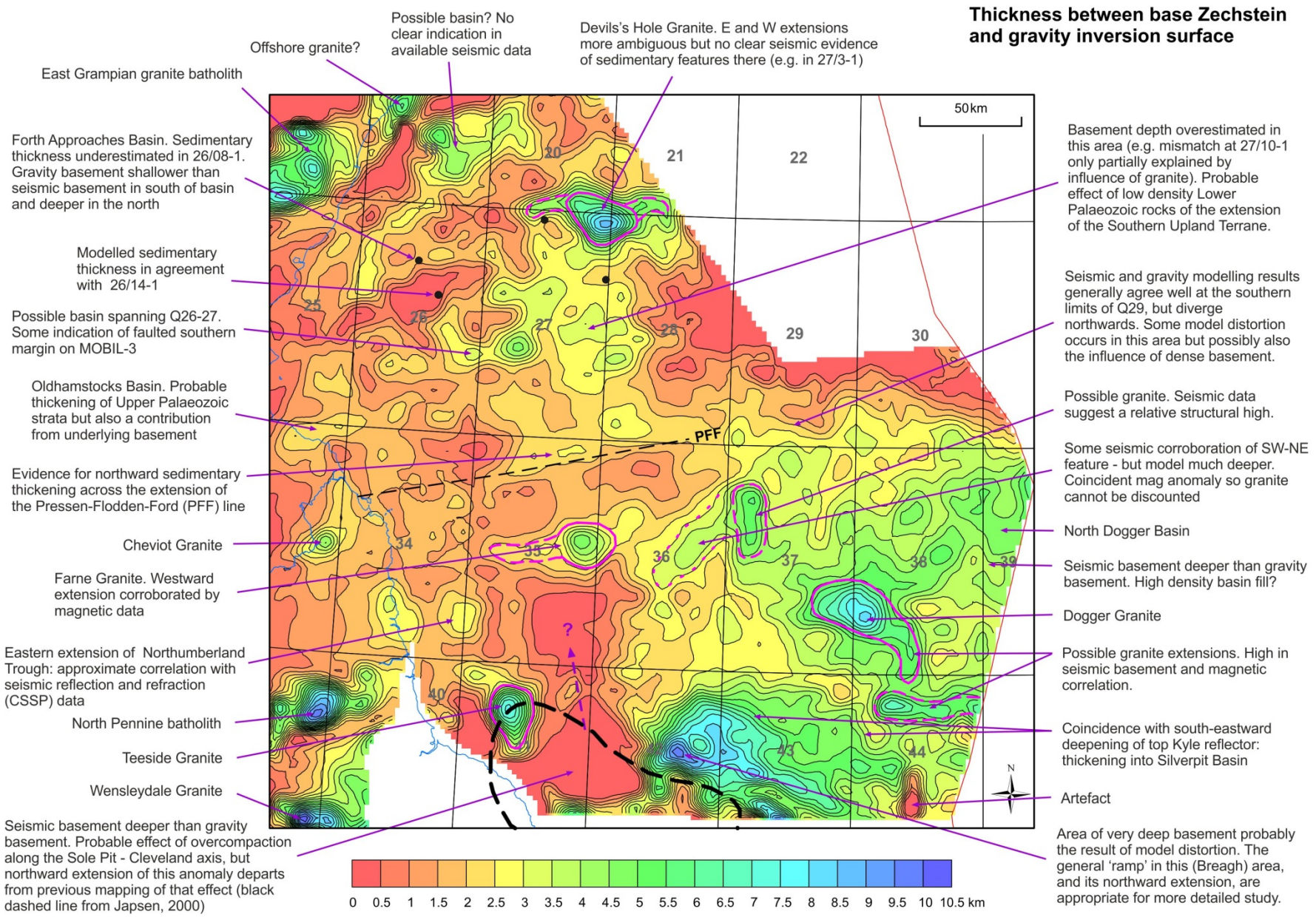

Figure 31 Annotated gravity model (thickness between base Zechstein and gravity inversion surface)

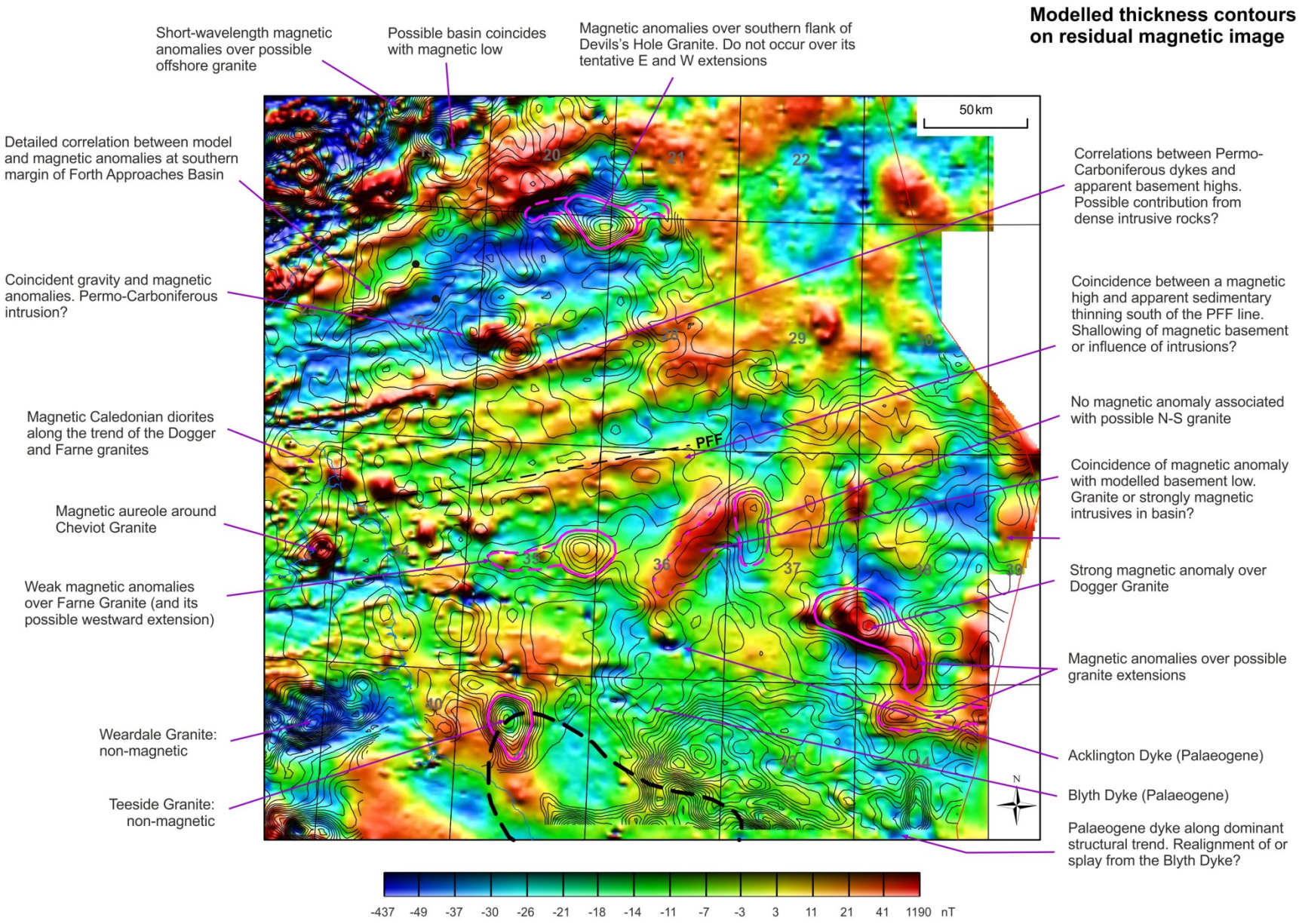

Figure 32 Annotated display of gravity inversion contours (from Figure 31) superimposed on an image of the residual reduced-to-pole magnetic field

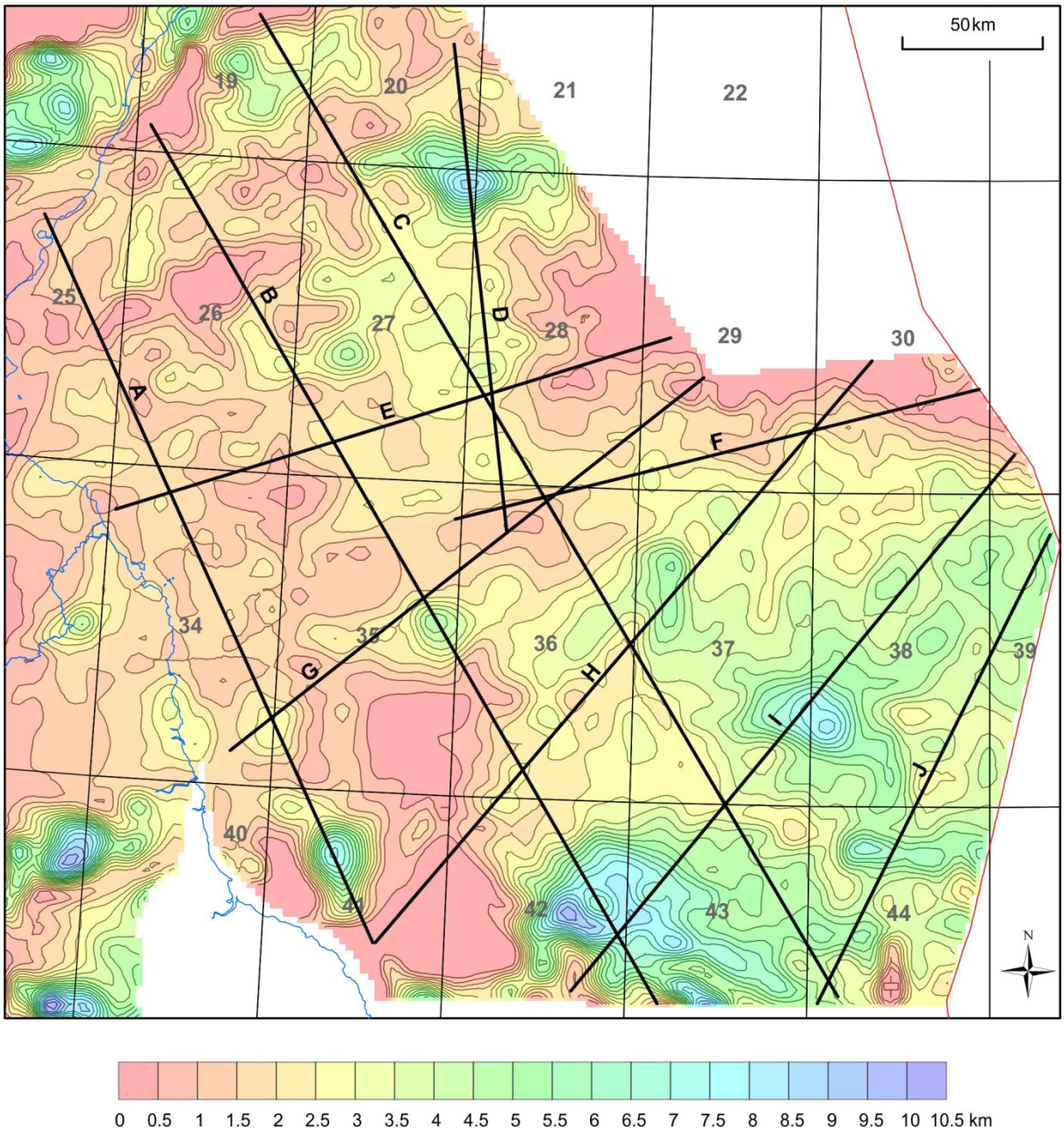

Figure 33 Locations of profiles used to illustrate the modelling results. The background image is the modelled thickness between base Zechstein and the gravity inversion surface (Figure 27).

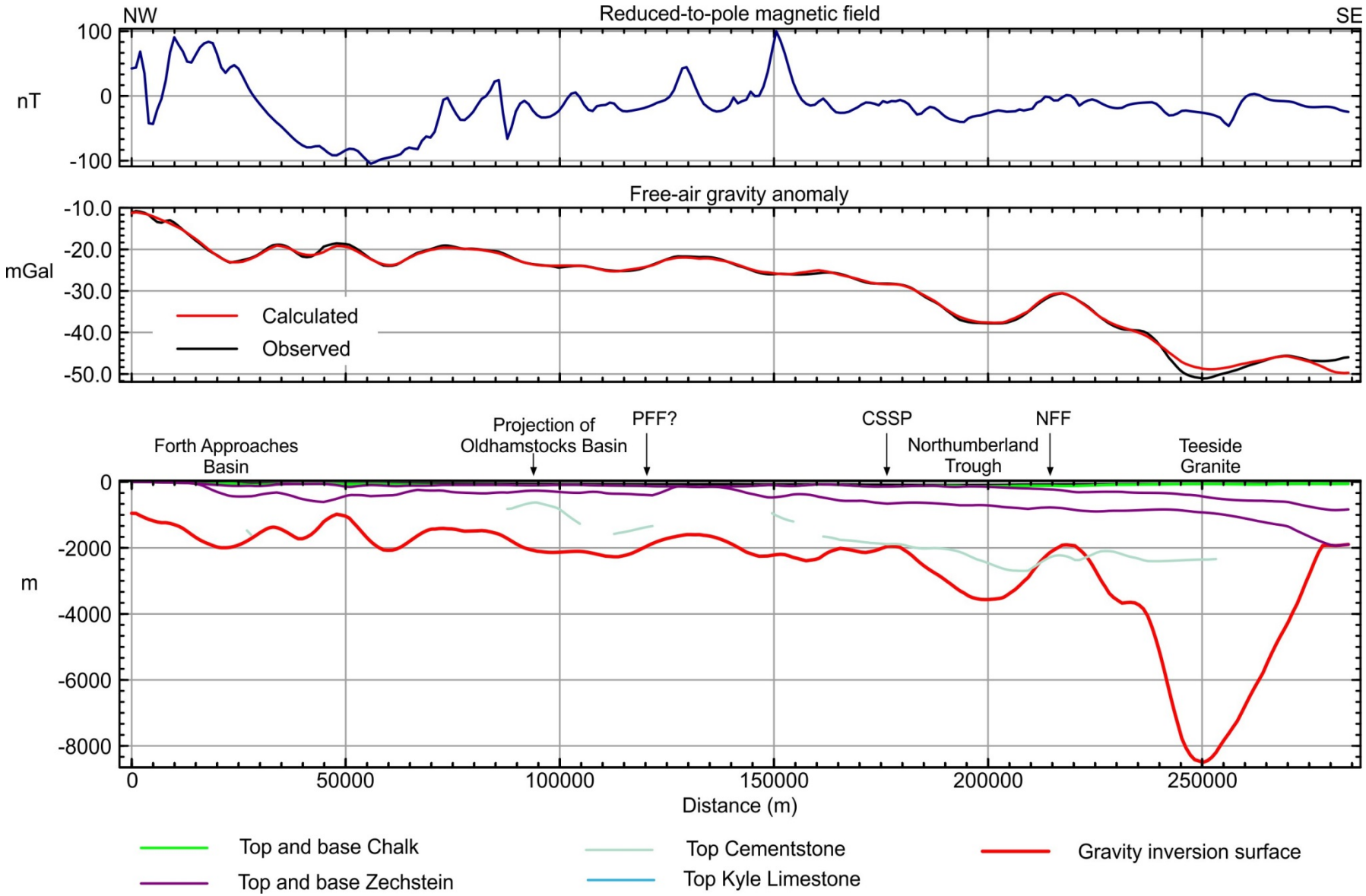

Figure 34 Profile A. Gravity inversion surface compared with seismic horizons (bottom panel), observed (minus background) and calculated gravity fields (middle panel) and observed reduced-to-pole magnetic anomalies (top panel)

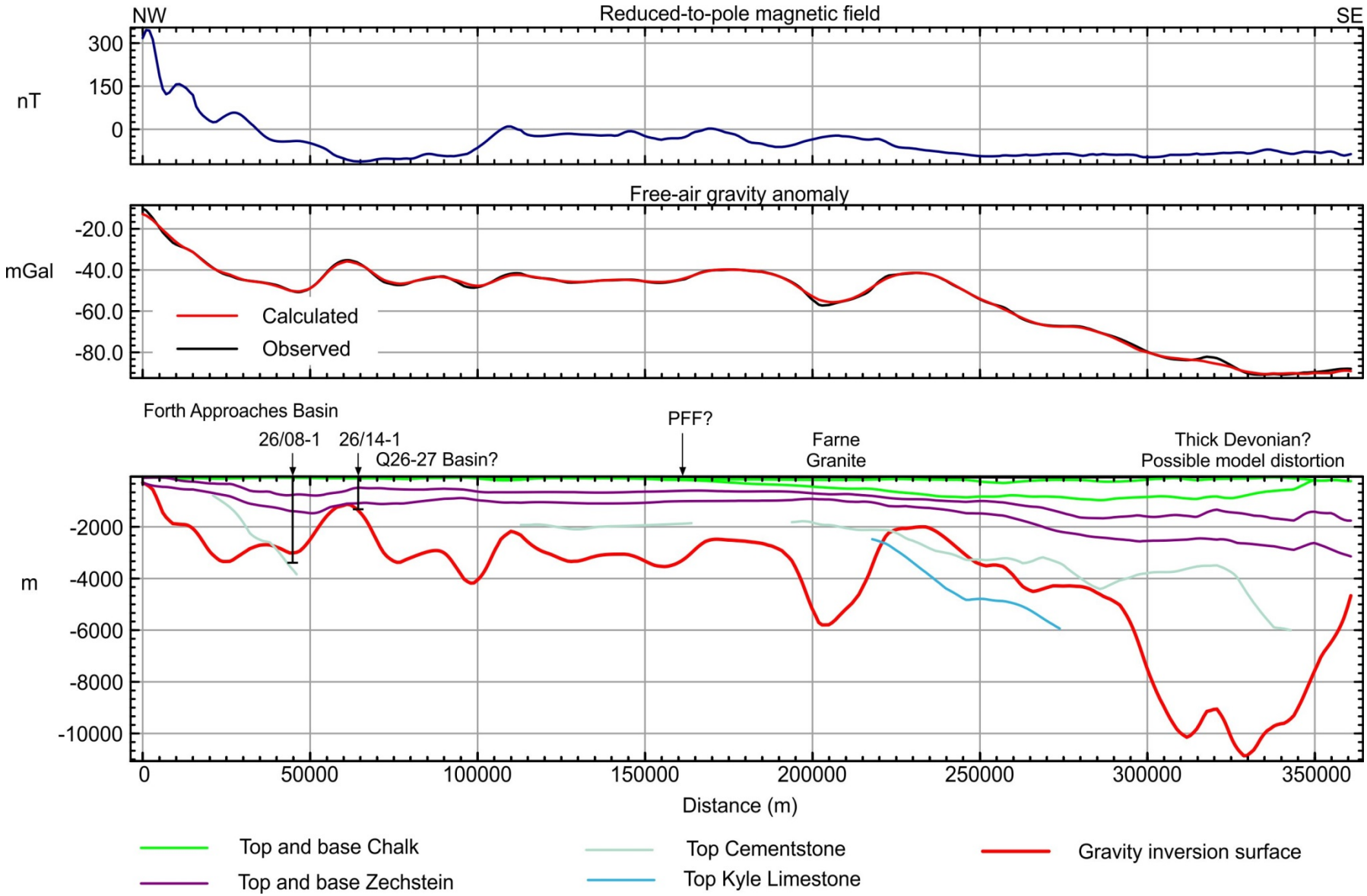

Figure 35 Profile B. Gravity inversion surface compared with seismic horizons (bottom panel), observed (minus background) and calculated gravity fields (middle panel) and observed reduced-to-pole magnetic anomalies (top panel)

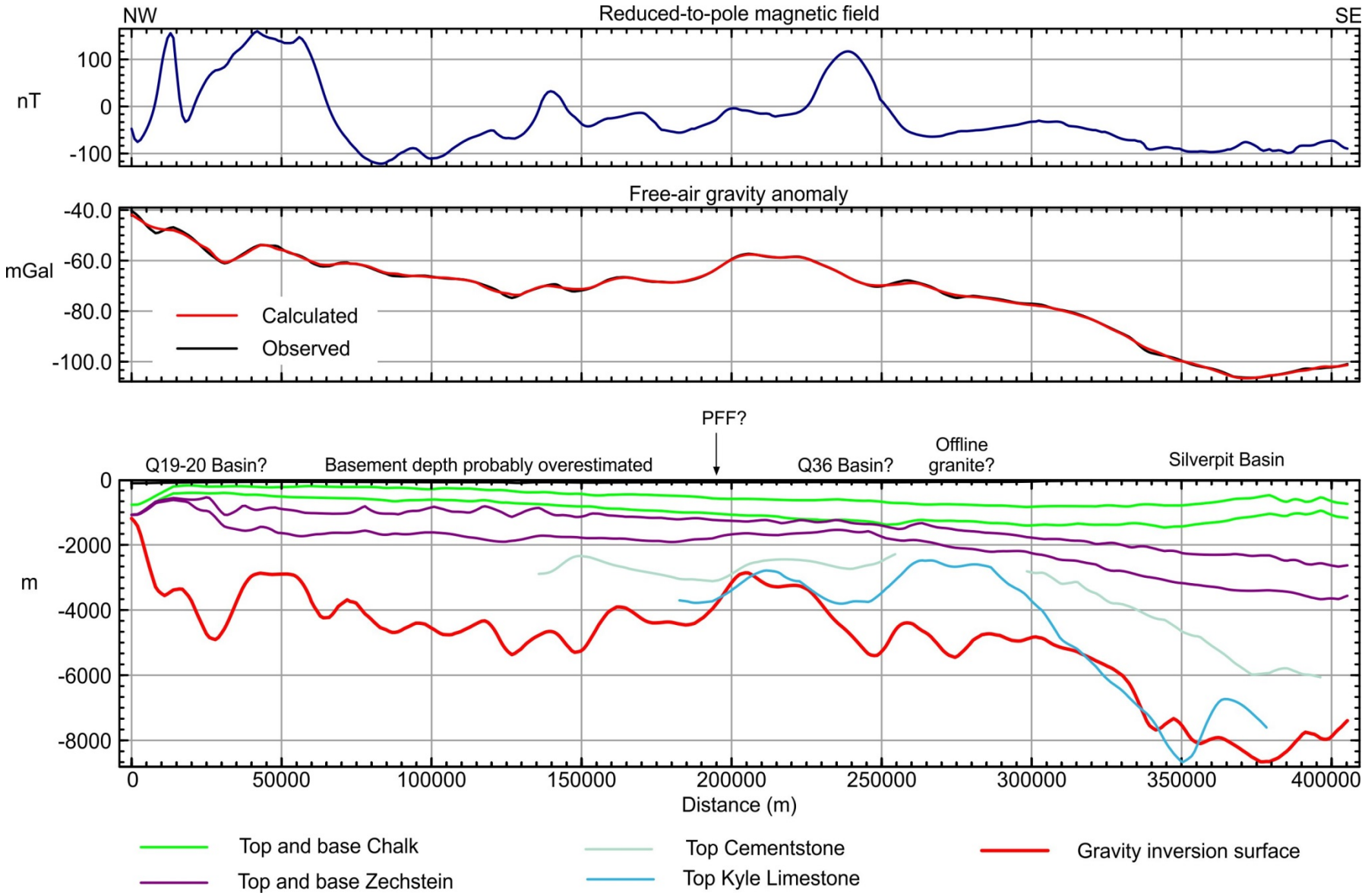

Figure 36 Profile C. Gravity inversion surface compared with seismic horizons (bottom panel), observed (minus background) and calculated gravity fields (middle panel) and observed reduced-to-pole magnetic anomalies (top panel)

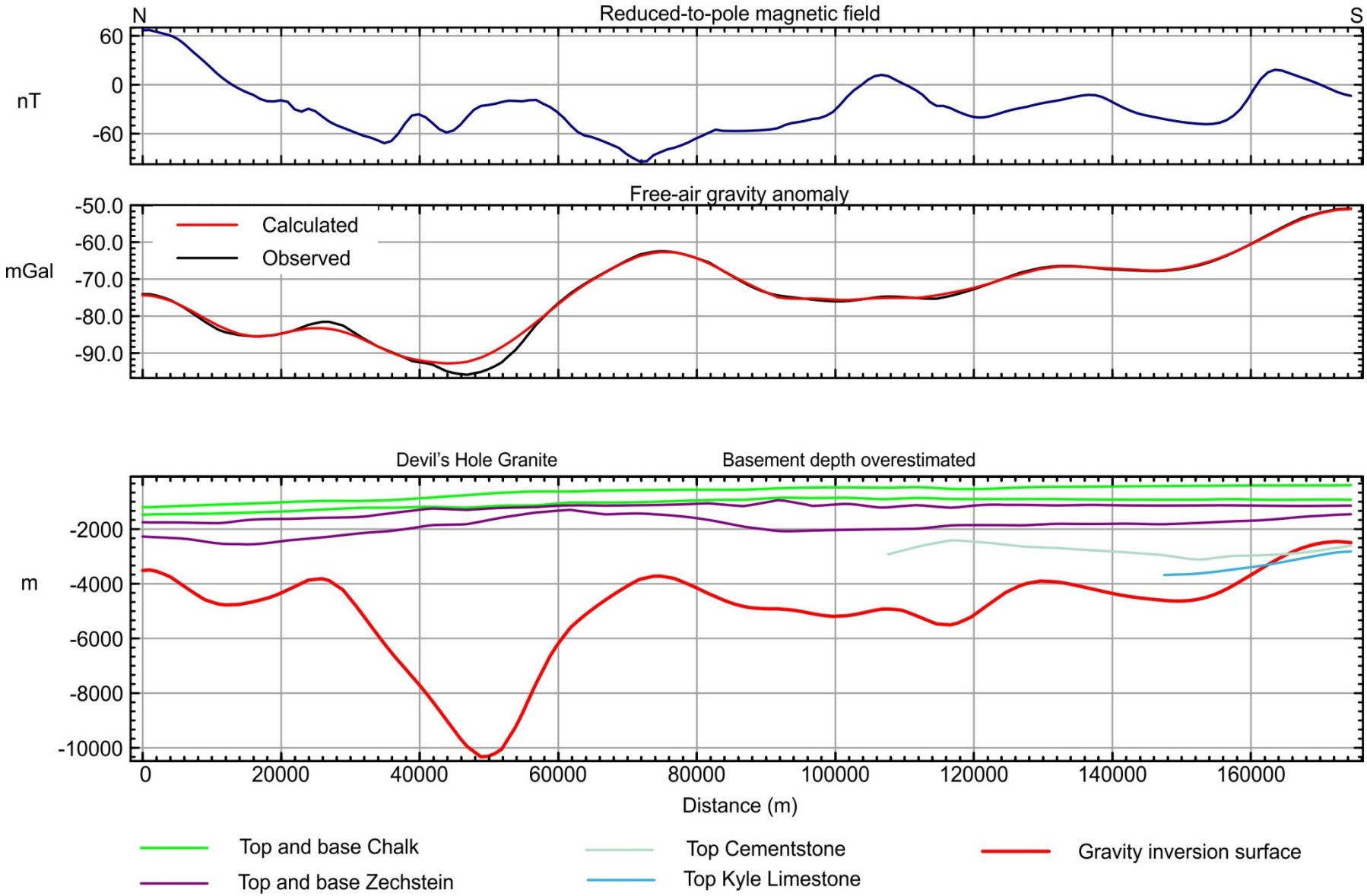

Figure 37 Profile D. Gravity inversion surface compared with seismic horizons (bottom panel), observed (minus background) and calculated gravity fields (middle panel) and observed reduced-to-pole magnetic anomalies (top panel)

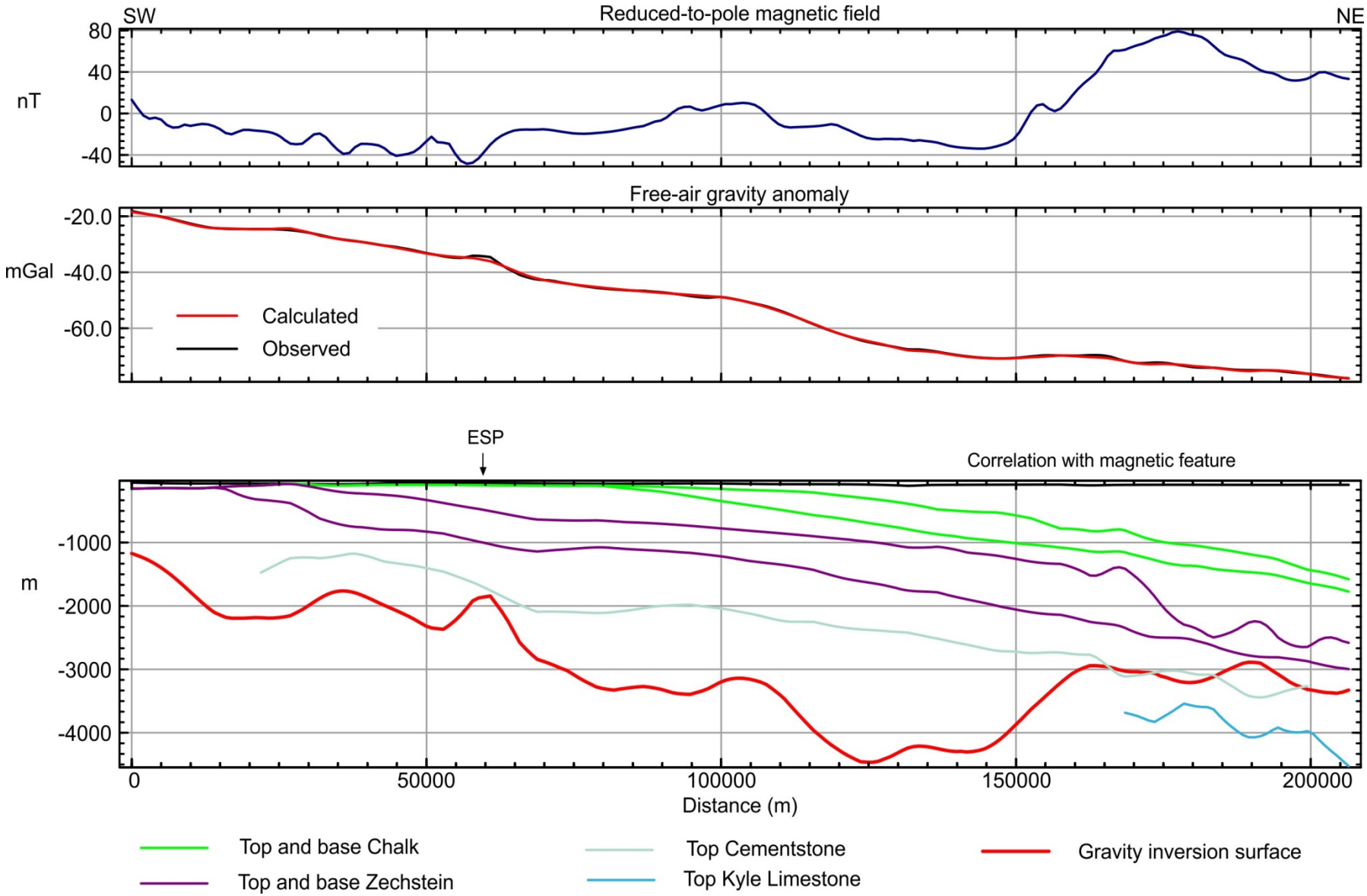

Figure 38 Profile E. Gravity inversion surface compared with seismic horizons (bottom panel), observed (minus background) and calculated gravity fields (middle panel) and observed reduced-to-pole magnetic anomalies (top panel)

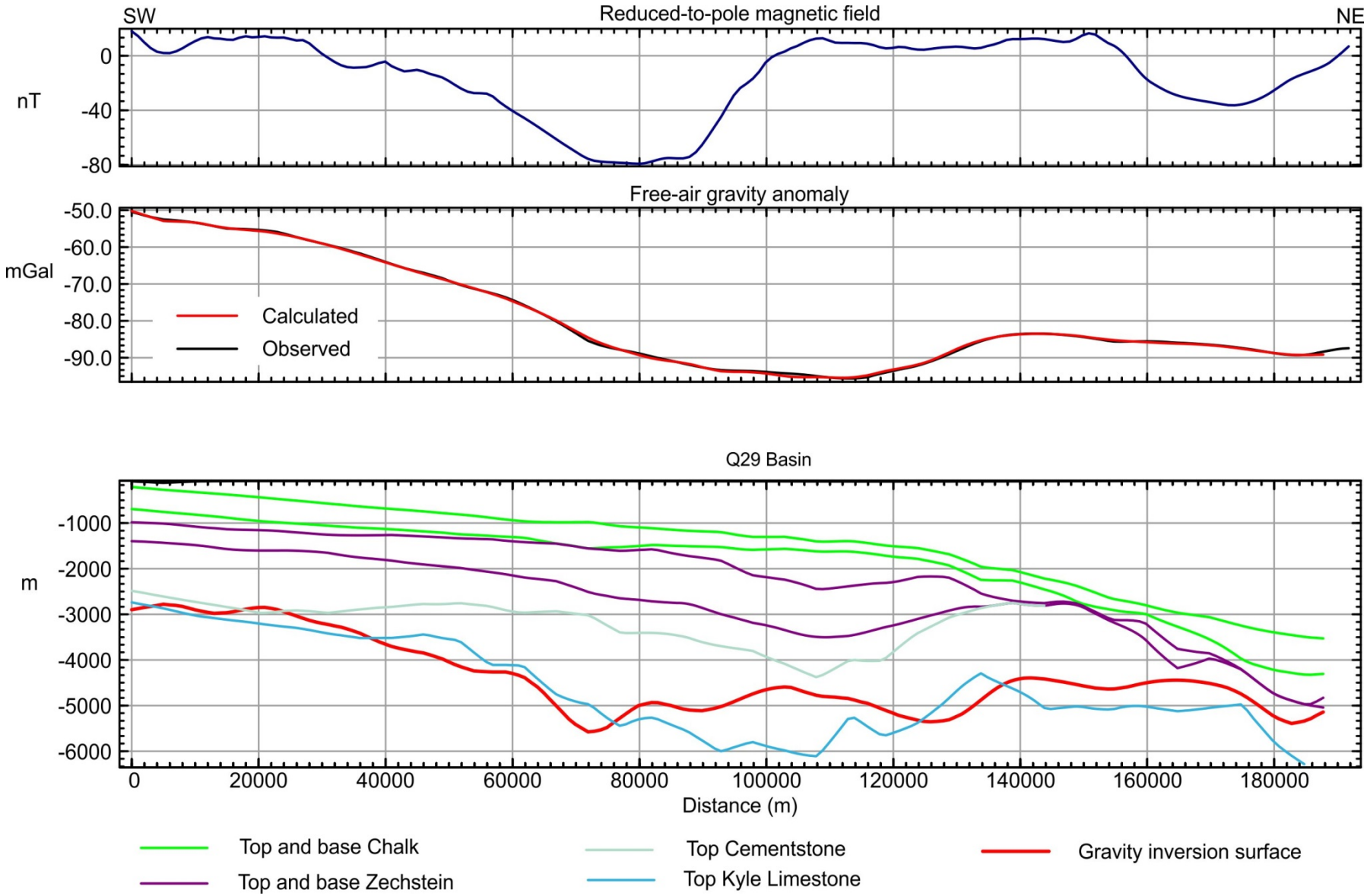

Figure 39 Profile F. Gravity inversion surface compared with seismic horizons (bottom panel), observed (minus background) and calculated gravity fields (middle panel) and observed reduced-to-pole magnetic anomalies (top panel)

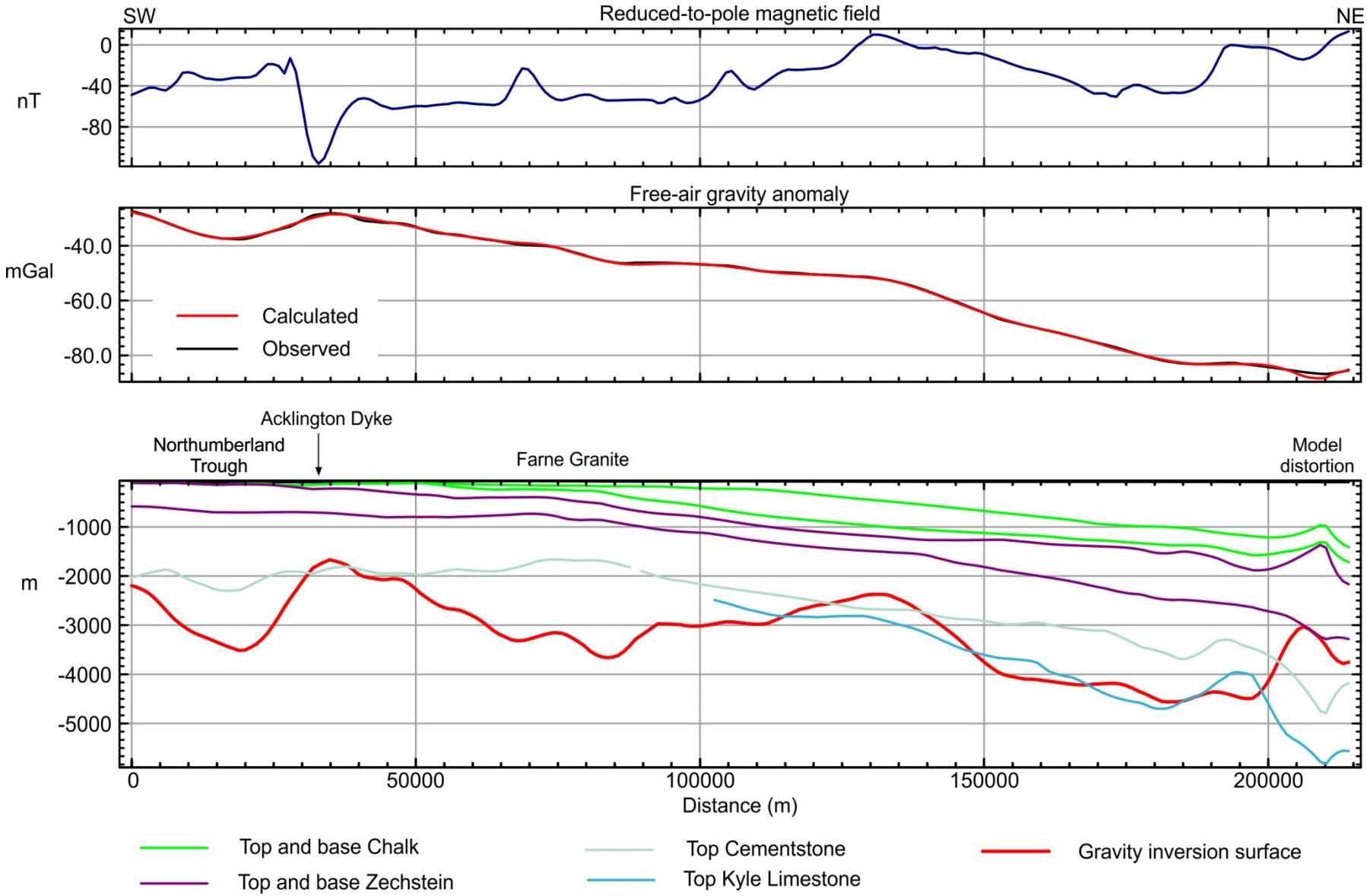

Figure 40 Profile G. Gravity inversion surface compared with seismic horizons (bottom panel), observed (minus background) and calculated gravity fields (middle panel) and observed reduced-to-pole magnetic anomalies (top panel)

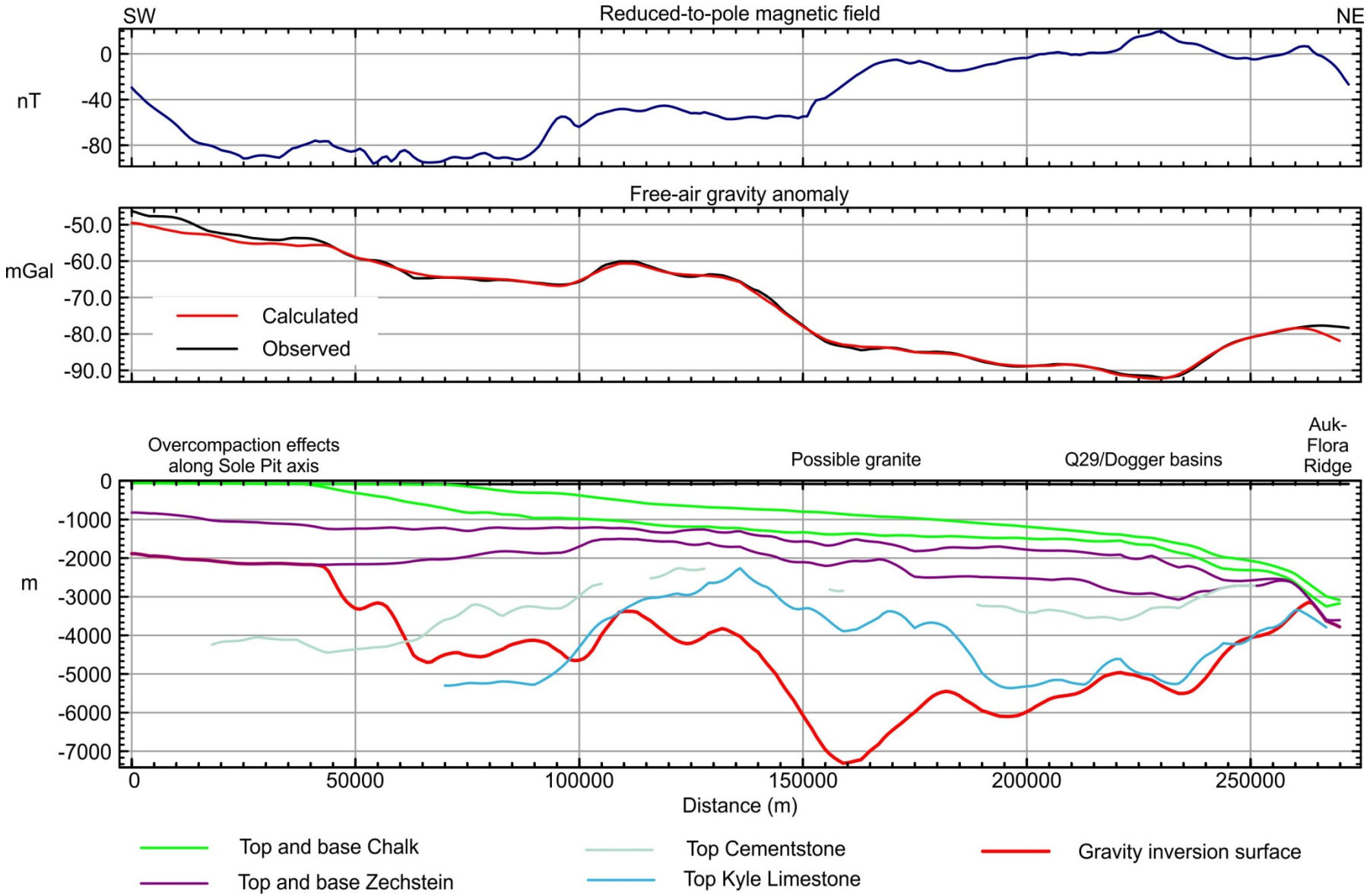

Figure 41 Profile H. Gravity inversion surface compared with seismic horizons (bottom panel), observed (minus background) and calculated gravity fields (middle panel) and observed reduced-to-pole magnetic anomalies (top panel)

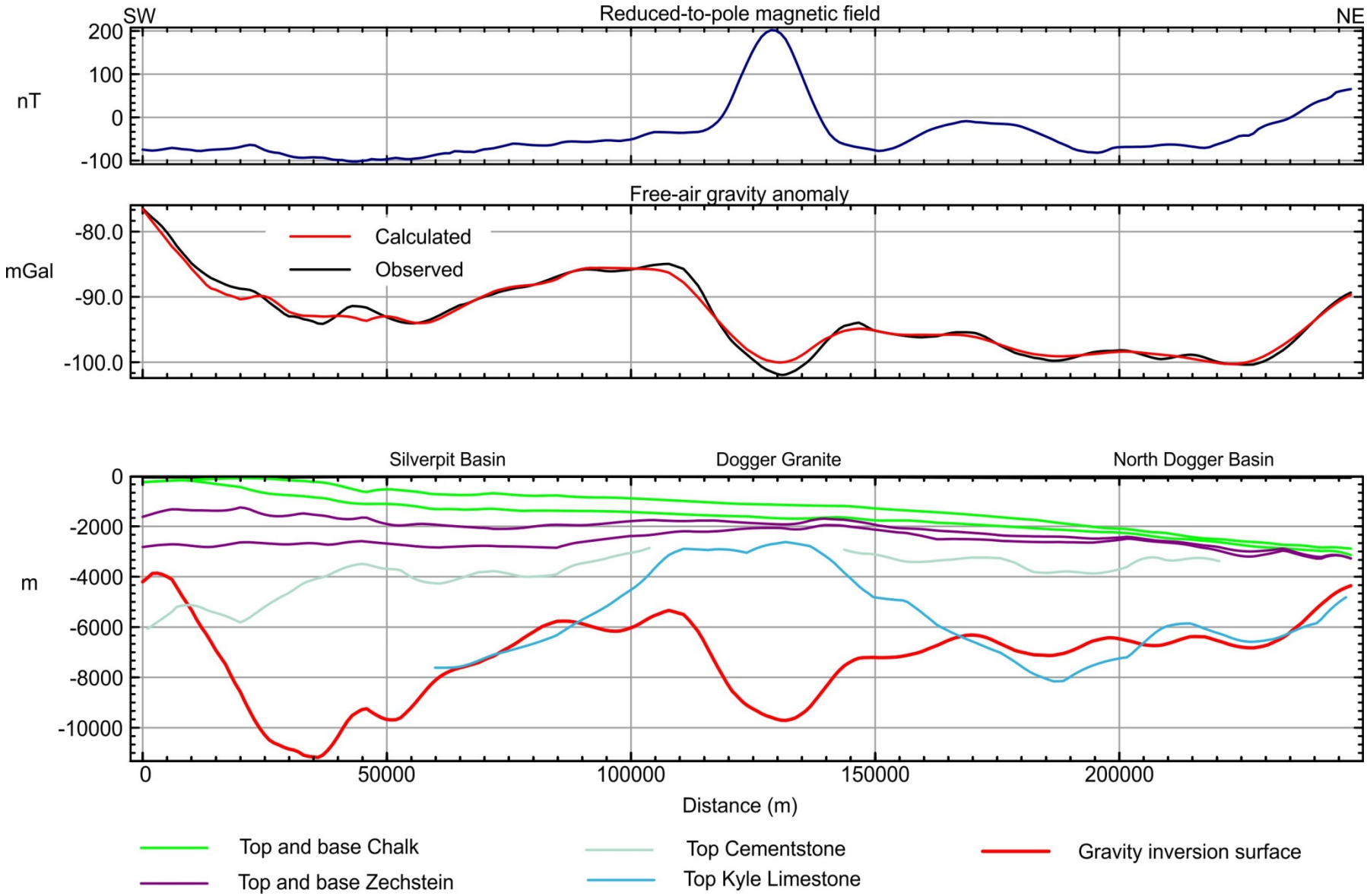

Figure 42 Profile I. Gravity inversion surface compared with seismic horizons (bottom panel), observed (minus background) and calculated gravity fields (middle panel) and observed reduced-to-pole magnetic anomalies (top panel)

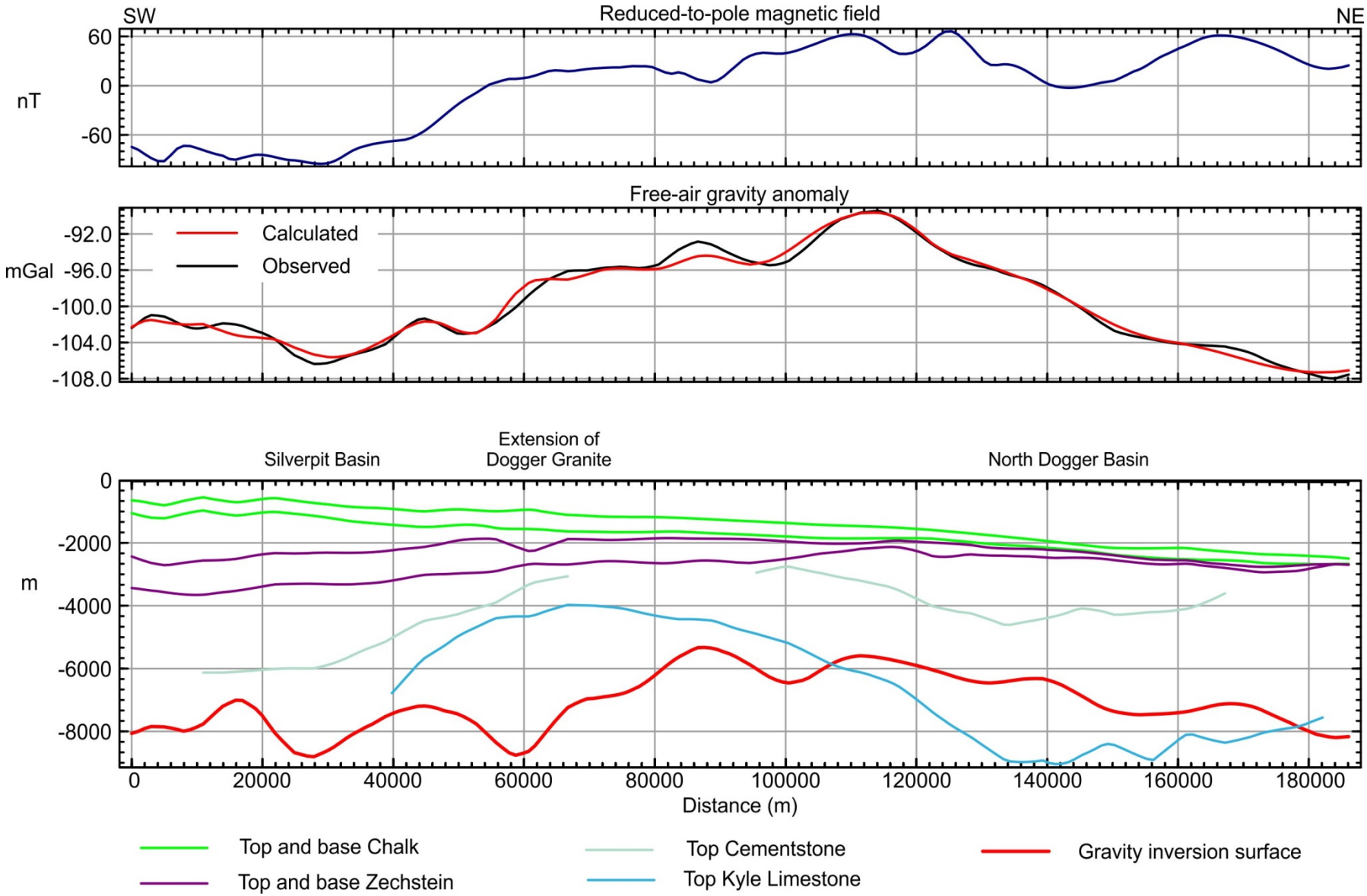

Figure 43 Profile J. Gravity inversion surface compared with seismic horizons (bottom panel), observed (minus background) and calculated gravity fields (middle panel) and observed reduced-to-pole magnetic anomalies (top panel)

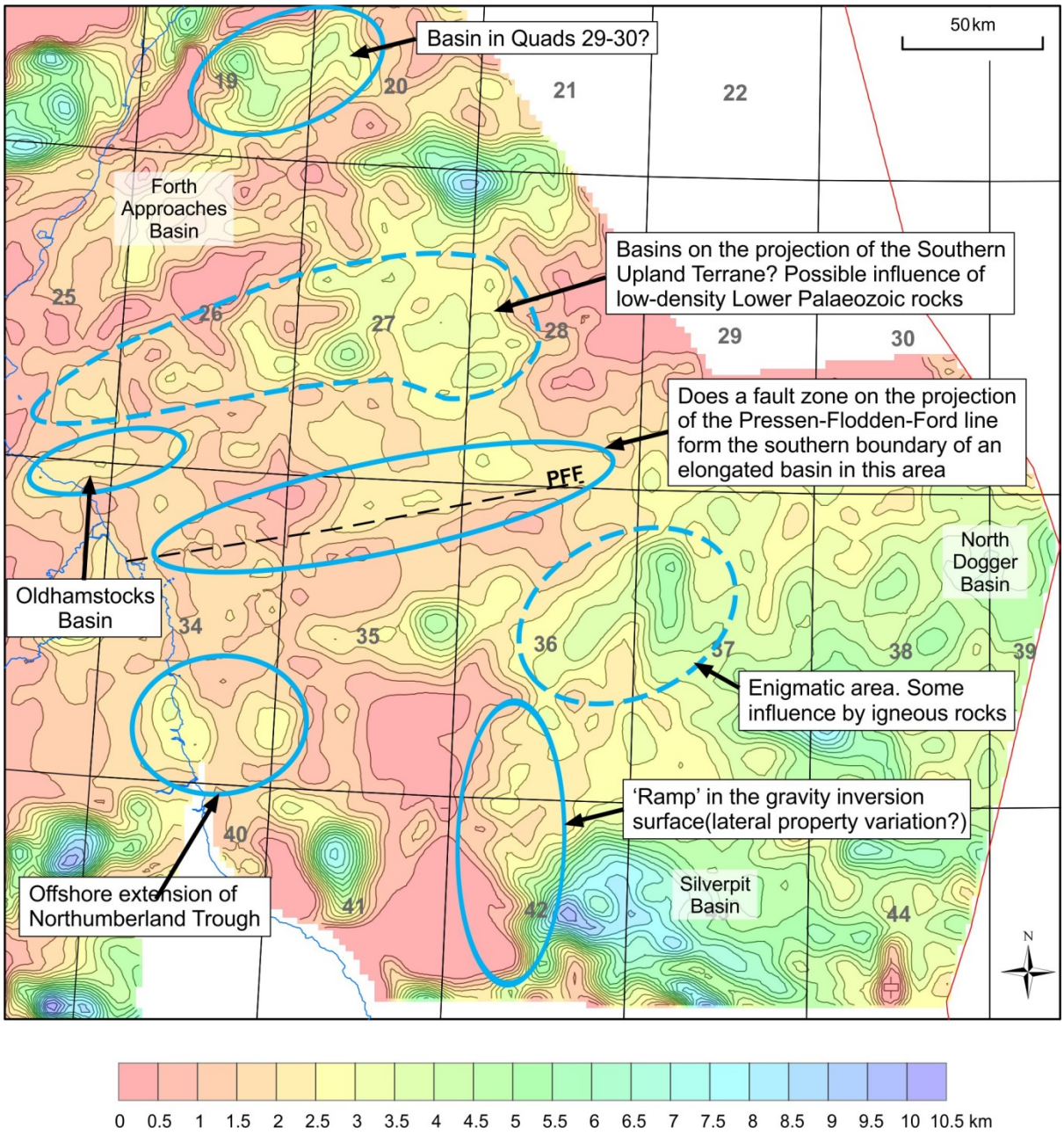

Figure 44 Targets for further investigation (mainly areas of possible sedimentary thickening not resolved or poorly imaged in the initial seismic database). The background image is the modelled thickness between base Zechstein and the gravity inversion surface (Figure 27).